A novel treatment strategy for preterm birth: Intra-vaginal progesterone-loaded fibrous patches

Muhammet Emin Cam[a,b,c,*], Ayse Nur Hazar-Yavuz[c], Sumeyye Cesur[b,d], Ozan Ozkan[e], Hussain Alenezi[a,f], Hilal Turkoglu Sasmazel[e], Mehmet Sayip Eroglu[g,h], Francis Brako[a,i], Jubair Ahmed[a], Levent Kabasakal[c], Guogang Ren[j], Oguzhan Gunduz[b,d], Mohan Edirisinghe[a,*]

[a]Department of Mechanical Engineering, University College London, Torrington Place, London WC1E 7JE, UK

[b]Center for Nanotechnology and Biomaterials Application and Research, Marmara University, Istanbul 34722, Turkey

[c]Department of Pharmacology, Faculty of Pharmacy, Marmara University, Istanbul 34668, Turkey

[d]Department of Metallurgy and Material Engineering, Faculty of Technology, Marmara University, Istanbul 34722, Turkey

[e]Department of Metallurgical and Materials Engineering, Faculty of Engineering, Atilim University, 06836 Ankara, Turkey

[f]Department of Manufacturing Engineering, College of Technological Studies, PAAET, 13092 Kuwait City, Kuwait

[g]Department of Chemical Engineering, Marmara University, Faculty of Engineering, Goztepe Campus, 34722 Kadikoy/Istanbul, Turkey

[h]TUBITAK-UME, Chemistry Group Laboratories, 41470 Gebze/Kocaeli, Turkey

[i]School of Pharmacy, University College London, 29-39 Brunswick Square, London WC1N 1AX, UK

[j]Mechanical and Mechatronics Engineering Division, School of Engineering and Technology, University of Hertfordshire, UK

*Corresponding authors:

E-mail: m.cam@ucl.ac.uk and m.edirisinghe@ucl.ac.uk

ABSTRACT

Progesterone-loaded poly(lactic) acid fibrous polymeric patches were produced using electrospinning and pressurized gyration for intra-vaginal application to prevent preterm birth. The patches were intravaginally inserted into rats in the final week of their pregnancy, equivalent to the third trimester of human pregnancy. Maintenance tocolysis with progesterone-loaded patches was elucidated by recording the contractile response of uterine smooth muscle to noradrenaline in pregnant rats. Both progesterone-loaded patches indicated similar results from release and thermal studies, however, patches obtained by electrospinning had smaller average diameters and more uniform dispersion compared to pressurized gyration. Patches obtained by pressurized gyration had better results in production yield and tensile strength than electrospinning; thereby pressurized gyration is better suited for scaled-up production. The patches did not affect cell attachment, viability, and proliferation on Vero cells negatively. Consequently, progesterone-loaded patches are a novel and successful treatment strategy for preventing preterm birth.

Keywords: Progesterone; pressurized gyration; electrospinning; fibers; polymeric patch; preterm birth

1. Introduction

Preterm birth, also commonly referred to as premature birth, is the birth of a baby who has completed less than 37 weeks of gestation, it is a leading cause of infant mortality under the age of five and it is one of the most crucial research areas in need of new treatment strategies (Kindinger et al., 2017). Around 15 million babies suffer from preterm birth and the number is increasing. Annual health costs associated with surviving babies in the US exceed $ 25 billion per year and climbing (McCormick et al., 2011).

Preterm birth is a syndrome attributed to heterogeneous influences such as a decrease in the action of progesterone (P4), infection, multiple gestations, and cervical disease (Goldenberg et al., 2008). P4, which is a steroid hormone, is a primary prescribed treatment for pre-term births and plays a crucial role in female reproduction with regulatory actions throughout the female reproduction cycle but the mechanism of action is not clear (Graham and Clarke, 1997). P4 may work by activating the anti-inflammatory and pro-relaxation pathways in the uterus, thereby reducing uterine contractility and preventing the onset of premature birth. The rate of preterm birth had declined widely due to P4 treatment in women who are at high risk for preterm birth due to a history of preterm birth or a short cervical length (Nold et al., 2013).

P4 is a poorly water-soluble drug (Cam et al., 2019b) traditionally available in tablet and also gelatinized capsule, vaginal gel, vaginal insert, and injection forms. All forms are daily given except the injection form, which is weekly given. P4 administered orally can cause sleepiness, headaches, back pain, abdominal cramps, constipation, breast tenderness, nausea, dizziness, edema, hypotension, dysphoria, fatigue and may induce a hypercoagulant state. Thus, one of the very significant advantages of P4 given via the vaginal route is its high bioavailability in the uterus as the first pass through the liver is avoided. Although vaginal irritation can be uncomfortable, this route allows for fewer systemic side effects (Goletiani et al., 2007).

Fibrous patches are recognized to be the most prominent micro/nanostructured materials that are presently used in various applications such as bioengineering, healthcare and environmental applications (Cam et al., 2020a). In addition, fibrous patches have very significant advantages such as high permeability, high surface area to volume ratio, low weight, high density of pores and low fiber diameter (Balamurugan et al., 2011). The fibrous patches produced with natural and synthetic polymers have been found to be promising for developing drug delivery systems using several methods. One of the most common and preferred techniques to produce fibrous patches is via electrospinning (Huang et al., 2020; Qin et al., 2019). Moreover, a variety of techniques have been available recently to produce fibrous patches for biomedical applications, one such method is pressurized gyration (Alenezi et al., 2019). Previously, patches for hormone delivery, with some advantages such as controlled release and efficient drug loading, have been produced by electrospinning and pressurized gyration (Brako et al., 2018; Mofidfar and Prausnitz, 2019). In this study, it is aimed to produce a

controlled release form of P4 to overcome low bioavailability, side effects, and high frequency of dosage.

Electrospinning is an effective method for making continuous polymeric micro/nanofibrous patches (Figure 1). Electrospinning is attractive owing primarily to its cost-effectiveness, reproducibility, simplicity and ability to spin a wide range of polymers whilst ensuring the opportunity for direct encapsulation of medicines into the electrospun fibrous patches. Several variable parameters such as polymer solution feed rate, solution composition and applied voltage affect the characteristics of the electrospun fibrous patches (Cam et al., 2019a; Cam et al., 2020b).

An original pressure driven technique for the production of fibrous patches has been established to incorporate concurrent use of pressure, flow, and rotation. The solvent-based production technique, pressurized gyration, simultaneously exploits centrifugal spinning and solution blow spinning to produce fibrous patches (Figure 1). Pressurized gyration offers an alternative option to electric-field driven technologies such as electrospinning. The advantages of pressurized gyration include the ability to spin charge-absent polymers and a high production yield. Pressurized gyration has a much larger production capacity compared to other generation methods such as electrospinning (Raimi-Abraham et al., 2015). The pressurized gyration system consists of a rotating perforated chamber, which is fed with a polymer solution, containing a series of orifices (24) with dimensions of 0.5 mm on its midline circumference. The rotating speed (12000-36000 rpm) of the chamber and the pressurized gas ($1x10^5$-$3x10^5$ Pa) affects the characteristics of fibers in terms of final morphology. Essentially, the polymer solution in the chamber is extruded out from the orifices following the

rotation of the chamber, and dry fibrous patches are obtained following solvent evaporation of the extruded polymer solution (Heseltine et al., 2018).

In our study, we aim to produce a patch that can be administered vaginally to prevent preterm birth with some possible advantages compared to other treatment strategies, such as reducing side effects, providing a higher bioavailability, and reducing the frequency of dosage. Moreover, the larger production capacity of pressurized gyration for the production of P4-loaded fibrous patches was evaluated and compared to electrospinning. Thus, P4-loaded fibrous patches were produced with two different techniques: Electrospinning and pressurized gyration. These fibrous patches are compared with respect to their ability to increase the dissolution of the poorly soluble drug P4 and also drug incorporation, characterization, release characteristics, tensile strength, short-term cell attachment, long-term viability, and cell proliferation have been tested. In addition, the effect of maintenance tocolysis with P4-loaded fibrous polymeric patches were examined in the uterus of pregnant rats using organ bath experiments, and also compared with the oral route (Figure 1).

Figure 1. Schematic illustration of the experiments. (A) Production processes of progesterone-loaded fibrous patches of two different techniques; electrospinning and pressurized gyration, (B) characterization of produced fibrous patches, (C) comparisons of the tocolytic effects of progesterone-loaded fibrous patch and oral progesterone using organ bath experiments.

2. Materials and methods

2.1. Materials

Poly(lactic acid) (PLA) was obtained from Nature Works LLC, Minnetonka, MN. Progesterone (P4, Mw ~ 314 g mol^{-1}, aqueous solubility: 8.81 mg/L (at 25°C), log P: 3.87), (-)-noradrenaline (Mw ~ 169.18 g mol^{-1}), chloroform (99.9%, v/v), phosphate buffer saline (PBS), Dulbecco's Modified Eagle Medium (DMEM/F12), penicillin/streptomycin, fetal bovine serum (FBS), 3-(4,5-dimethyl-2-thiazolyl)-2,5-diphenyl-2H-tetrazolium bromide (MTT), dimethylsulfoxide (DMSO), ethanol (99.9%, v/v), paraformaldehyde, Triton X-100, and L-glutamine were from Sigma-Aldrich (UK). Phosphate buffer saline (PBS) and bovine serum albumin (BSA) were obtained from Amresco (USA). Alexa Fluor 488 Phalloidin (AF488) and (4',6-diamidino-2-phenylindole, dihydrochloride) (DAPI) was purchased from Life Technologies (USA). Simulated vaginal fluid (pH = 4.7) was prepared according to the formula developed by Owen and Katz (Owen and Katz, 1999). All chemical and biological agents were cell culture grade and used as received without further sterilization.

2.2. Preparation and Characterization of Solutions

The polymer solutions were prepared with the mixtures of PLA, P4 and chloroform as a solvent, by continuous magnetic stirring. Firstly, PLA was dissolved in chloroform at four different concentrations of 8, 10, 12 and 15% (w/v) and then P4 (10%, w/w) was added to solution at the ambient temperature (25°C) and mixed for almost an hour. The physical parameters such as viscosity, surface tension, electrical conductivity and density for the solutions were measured by viscometer (Brookfield DV-111, Harlow,

UK), force tensiometer (Kruss K9, Hamburg, Germany), electrical conductivity probe (Cond 3110 SET 1, WTW, Germany), and density bottle (10 mL specific density bottle, Boru Cam Inc., Turkey). All the measurements were repeated three times at ambient temperature. These equipments were calibrated prior to measurements.

2.3. Fibrous Patch Preparation and Characterization

Pure and P4-loaded PLA fibrous patches were produced in four different polymer concentrations (8, 10, 12 and 15%, w/v) with a constant P4 ratio (10%, w/w) by pressurized gyration at ambient temperature (25°C) and humidity (56%) using the pressurized gyration method described previously (Mahalingam and Edirisinghe, 2013). According to the results obtained from scanning electron microscopy (SEM) of fibrous patches produced by pressurized gyration, optimal ratio was chosen and this ratio was used for electrospinning. In brief, 10 ml of drug-polymer mixture was prepared using chloroform and placed in an aluminum vessel and spun at a rotational speed of 12000-36000 rpm and a working pressure of 0.1 MPa to produce P4-loaded fibrous patches (Table 1A).

The morphology and size of the fibrous patches were investigated using SEM. Post-decision on the optimal polymer ratio of the fibrous patches produced by pressurized gyration, fibrous patches were produced using electrospinning at 12% (w/v) PLA and 10% (w/w) P4. For the electrospinning procedure, two working distances (130 and 150 mm), three flow rates (10, 20 and 30 µl/min) and four voltages (6, 8, 10, 12 kV) were used (Table 1B). The material compositions were investigated using thermal and spectroscopic techniques (see below).

2.4. Scanning Electron Microscopy

The morphologies of the composite fibrous patches were investigated with scanning electron microscopy (JCM-5700, JEOL, Japan). The surface of the samples was gold sputter coated for 60 seconds. The applied accelerating voltage was 20 kV and the working distance was 25 mm. The average fiber diameter and their distribution were determined by using the software ImageJ (Brocken Symmetry Software).

2.5. Attenuated Total Reflection-Fourier Transform Infrared Spectroscopy (ATR-FTIR)

ATR–FTIR measurements were performed using Bruker Vertex 90 spectrometer and spectrographs were examined using OPUS Viewer version 6.5 software for analyzing molecular contents of fibrous patches and to confirm the presence of P4 into the fibrous patches. The measurements were carried out at room temperature (23°C) in the transmission mode over the range 4000–500 cm^{-1} and averaged over 32 scans with 4 cm^{-1} resolution.

2.6. X-ray Powder Diffraction

D/Max-BR diffractometer (RigaKu, Tokyo, Japan) with Cu Kα radiation was used to analyze structure and crystalline forms of the fibrous patch contents. Analyses were performed at 40 mV and 30 mA over 2θ range of 5–60° at a rate of 2°/min. OriginPro 7.0 software (OriginLab Corporation, MA, USA) was used to convert the obtained data to diffractograms and for their evaluation.

2.7. Differential Scanning Calorimetry (DSC)

Differential scanning calorimetry (DSC) measurements were conducted using Perkin Elmer Jade DSC and Pyris software (PerkinElmer Inc., Mass., USA) at a heating rate of 10°C min^{-1} between 0 and 300°C under dynamic argon atmosphere (20 ml min^{-1}) to determine thermal properties of the fibrous patches. Temperature calibration of DSC was performed according to the indium melting point and melting enthalpy. Perkin Elmer aluminum sample pans and covers were used. Before measurement, samples of approximately 7.0 mg of mass, were placed in the pan and crimped. Peak temperature of endotherms was considered as melting temperature. Tg values were determined at half height of the displacement.

2.8. Drug Encapsulation Efficiency

A standard assay procedure was used to determine the P4 content in the fibrous patches. The fibrous patches dissolved completely in chloroform and were detected by UV at 270 nm (Wilson, 2009). P4-loaded fibrous patch samples were weighed (1 mg) and dissolved into 10 ml of absolute chloroform in a volumetric flask. The flask was stirred gently over a period of 1 h to provide complete dissolution of P4 into the chloroform. 3 ml of solution was taken and evaluated using a UV-visible spectrophotometer using a wavelength 270 nm (Jenway 6305, Bibby Scientific, Staffordshire, UK). The % encapsulation efficiency was calculated using:

Encapsulation efficiency (%) =

mass of actual drug loaded in fibrous scaffolds/

mass of drug used in fibrous scaffolds fabrication x 100% (1)

2.9. Release Studies

Franz diffusion cells with cellulose acetate membranes of pore size 0.2 µm were used for performing in vitro drug release studies. This approach was chosen for the release study because there would be a close similarity between drug permeation through 0.2 µm acetate membrane and the mucosal membrane (Khdair et al., 2013). 3 ml of PBS, pH 7.4 and a stir bar was placed in the receptor chamber to provide sufficient mixing of P4 transported through the membrane into the PBS in the receptor chamber of apparatus. The cellulose acetate membrane, which was priorly submerged into simulated vaginal fluid (SVF) for 30 min, was placed onto the receptor chamber. Finally, the donor chamber was mounted onto the receptor chamber and thus the membrane was compressed between two chambers. 1 ml of SVF was put in the donor chamber and fibrous patches containing 1 mg of P4 and, separately, pure P4 solution including 1 mg P4 was placed inside. The Franz diffusion cell was kept at a constant temperature of 37°C. The quantity of drug released through the membrane was measured taking 1 ml aliquots from the receptor chamber at certain times (0.5, 1, 2, 3, 4, 16, 24 h) and quantified using UV spectroscopy.

2.10. Tensile Tests of Fibrous Patches

The tensile strength of fibrous patches was determined and evaluated using an Instron 4411 tensile test machine at ambient conditions (23°C). The results were analyzed using Bluehill 2 software (Elancourt, France). Six fibrous patch (1x5 cm) specimens were tested for each set of samples and the thicknesses of the specimens were measured using a digital micrometer (Mitutoyo MTI Corp., USA). Both ends of each specimen were compressed by the top and bottom grip. They were subjected to a

245 tensile test under conditions of 5 mm min^{-1} test speed and 10 mm distance between
246 grips.

247 **2.11. *In Vitro* Cytotoxicity Studies**

248 In vitro cytotoxicity of the fibrous patches was investigated with a commercial Vero
249 epithelial cell line (ATCC CCL-81) for 7 days (Karuppannan et al., 2017). Samples for
250 the studies were prepared in circular shape with 10 mm diameter cut from the fibrous
251 patches. The samples for both pure and P4-loaded fibrous patches were sterilized with
252 UV (both sides) for 15 min in 24 well plates prior to the culture and seeded with initial
253 cell concentration of $5x10^4$ cells/ml under standard aseptic conditions. The well plates
254 used were coated with parafilm to prevent cells from attaching/proliferating to the well
255 bottom instead of the test samples. Blank commercial tissue culture polystyrene (TCPS)
256 Petri dishes were used as the control group and seeded with the initial cell
257 concentration as the patch samples. DMEM/F12 supplemented with 10% (v/v) FBS, 1%
258 (v/v) L-glutamine and 1% (v/v) penicillin/streptomycin (100 units/ml penicillin, 100 µg/ml
259 streptomycin) was used as culture medium and refreshed every 24 hours. The cultured
260 samples were incubated under 5% CO_2 at 37°C. The cytotoxicity of the fibrous patches
261 were investigated in terms of initial cell attachment, 7-day viability as well as yield and
262 visual morphology by using haemocytometric counting, MTT colorimetric assay and
263 fluorescence imaging. The control groups were utilized only for attachment, viability,
264 and yield studies.

265 **2.11.1. Cell Attachment**

266 The initial cell attachment capability of the fibrous patches was determined for the
267 first 3 h after the initial seeding at 30 min intervals by using haemocytometric cell

counting. Briefly, the cultured test samples corresponding to each interval were gently removed from the culture dishes without disturbing the cells attached. The cells in the medium remaining inside the dish wells were then counted. The difference between the initial number of cells seeded and the remaining cells counted in the dish was taken as the number of cells attached to the test sample at that specific time interval. For the control TCPS wells, the cells were counted directly from the medium inside, since there were no test samples to remove. The results were presented as the percent cells attached against time. Then, the ratio of the number of cells attached to the test sample/TCPS well to the number of cells seeded initially was given as a percentage value to represent the attachment concentration of the test samples/TCPS wells at specific intervals.

2.11.2. Viability and Yield

The viability of the cells seeded was monitored for the total course of the culture conducted for 7 days. MTT colorimetric assay was utilized every 48 h, starting at the end of the first 24 h of the culture. Briefly, the cultured test samples corresponding to each interval were transferred to a clean Petri dish and gently washed 3 times with PBS. Then the samples were incubated for 3 h with fresh medium containing 10% (v/v) MTT solution. After the incubation, the medium/MTT solution was replaced with DMSO (1 ml/sample) and the samples were incubated for an additional hour. Finally, aliquots of the incubated DMSO solution were transferred into 96 well plates and the cell viabilities of that specific interval for all the test samples were measured in terms of absorbance using a microplate reader at 540 nm. The same protocol was directly applied to the control TCPS wells without transferring the cells to another clean dish. The cell yields at

the end of the culture were also calculated from the absorbance values obtained at the 7^{th} day for the test samples as well as the control wells by plotting a calibration curve throughout the culture period. It defines the correlation between the number of viable cells and the corresponding absorbance value.

2.11.3. Visual Inspection

In addition to attachment, viability and yield assays, the cytotoxicity of the test samples obtained from pure and P4-loaded fibrous patches was also investigated visually in order to see if there was any negative effect on the morphology of the cells cultured. Fluorescence imaging was conducted on the cultured test samples on the 3^{rd} and 7^{th} day with AF-488/DAPI dual staining. Briefly, test samples were transferred to a clean Petri dish on the corresponding days, gently washed with PBS three times and fixed with 4% (v/v) paraformaldehyde for 45 min at ambient temperature (22°C). The fixative was then washed away with PBS again at least 3 times, and the test samples were permeabilized with 0.1% Triton X-100 for 5 min, blocked with BSA for 30 min and finally stained with AF-488 for 20 min and with DAPI for 10 min at the ambient temperature in the dark. Finally, the staining solutions were washed away with PBS twice and the imaging was conducted immediately after using a fluorescent microscope (AMG EVOS-FL, USA) at x10 and/or x40 magnifications. The excitation and the emission wavelengths of AF-488 and DAPI were λ_{ex}: 495 nm and λ_{em}: 518 nm, and λ_{ex}: 345 nm and λ_{em}: 455 nm, respectively.

2.12. In Vivo Testing

All *in vivo* experiments were carried out with the approval of the Marmara University, Animal Experiments Local Ethics Committee (MUHDEK) (permission

number: 92.2018.mar). Pregnant Sprague-Dawley rats were obtained from The Experimental Animal Implementation and Research Centre (DEHAMER). The rats were housed under controlled temperature (20-23°C), in humidity (40-60 %) and light (12 h light/dark regime)-regulated rooms. The animals were kept on a standard rodent pellet diet, with tap water available ad libitum.

2.12.1. Experimental Design of *In Vivo* Studies

Pregnant rats were randomly divided into 4 groups of 6 animals as follows: naive control group (NC), drug-free (pure PLA) fibrous patches implantation group (DFF), P4-loaded fibrous patch/electrospinning implantation group (PF) and oral P4 treatment group (OP). The NC group did not undergo any treatment or implantation during their pregnancy. DFF and PF were implanted with drug-free and P4-loaded fibrous patches respectively on the 15^{th} day of pregnancy. Oral P4 treatment began on the 15^{th} day of pregnancy and continued to the 21^{st} day. On the 22^{nd} day of pregnancy, all the rats were decapitated and the uterine tissues were removed.

2.12.2. Implantation of Fibrous Patches into Rats

Drug-free fibrous patches and P4-loaded fibrous patches were prepared by cutting an area 10 cm^2 (1 mg P4 in 10 cm^2). Following anesthetization with ether, the fibrous patch pieces were implanted intravaginally to the rats (Kim et al., 2013).

2.12.3. Oral Progesterone In Vivo Treatment

The treatment of the oral P4 group also started on the 15^{th} day of pregnancy. The given P4 was dissolved in olive oil (Hajagos-Tóth et al., 2016) and the administration

was given via oral gavage every day up to day 21 in a dose of 50 mg/kg (Khan and Ahmed, 1969).

2.12.4. In Vitro Organ Bath Experiments

2.12.4.1. Uterus Preparation

Uterus was removed from the all 22-day-pregnant rats (250-350 g) (n=6 in each group). 5 mm-long muscle rings were sliced from uterine horns; subsequently, the surrounding mesentery and fat tissues were carefully removed from the uterine rings and rings were mounted vertically in an organ bath containing 20 ml Krebs-Henseleit buffer (KHB; composition: 118 mM NaCl, 4.7 mM KCl, 2.5 mM $CaCl_2$, 1 mM $MgSO_4$, 1 mM KH_2PO_4, 25 mM $NaHCO_3$, and 11 mM glucose) at pH 7.40. The temperature of the organ bath was maintained at 37°C, and carbogen (95% O_2 and 5% CO_2 gas mixture) was perfused through the bath. After mounting, the rings were equilibrated for approximately 60 minutes before experiments began; with a buffer change every 15 minutes. The initial tension of the preparation was set to about 1 g. The tension of the myometrial rings was measured with a gauge transducer (TDA-94 Commat, Commat LTD., Ankara, Turkey) and recorded on-line on a computer via a four channel transducer data acquisition system using appropriate software (Polywin 95 ver 1.0. Commat, Commat LTD, Ankara, Turkey)

2.12.4.2. Contractility Studies

In the isolated uterine rings, rhythmic contractions were elicited with 124 mM KCl, and cumulative dose-response curves were constructed in each experiment in the presence of (-)-noradrenaline (NA) ($10^{-8.5}$ to $10^{-3.5}$) (Kim et al., 2004). Following the

addition of each concentration of (-)-noradrenaline, recordings were taken for 120 s. Concentration-response curves were fitted and areas under the curves (AUC) were evaluated and analyzed statistically with the Prism 6.5 (Graphpad Software Inc. San Diego, CA, USA) computer program. From the AUC values, the maximal inhibitory effect of NA (Emax) and the concentration of NA eliciting 50% of the maximal inhibition of uterine contraction (EC_{50}) values were calculated.

2.13. Statistical Analysis

Values in the animal test were presented as mean ± standard error of the mean, whereas in SEM micrographs, tests were presented as mean ± standard deviation. Differences in the contractile effect of KCl and cumulative NA were analyzed using analysis of variance (ANOVA) tests with the Tukey multiple comparison test. Concentration-response curves were fitted, areas under the curves (AUC) were determined, and Emax and EC_{50} calculated with the Prism 6.5 software. The assays conducted for attachment, viability as well as yield were repeated three times (n = 3) for each type of samples as well as blank controls. The statistical differences were determined with ANOVA followed by Tukey multiple comparison test using IBM SPSS v24.0 Statistics software. Probability of the data was considered statistically significant for p-values less than 0.05 and statistically highly significant for p-values less than 0.01. The results were marked with (*) for $p < 0.05$, (**) for $p < 0.01$.

3. Results

3.1. Physical properties of solutions

Several solutions were prepared for the production of fibrous patches using both pressurized gyration and electrospinning. Ambient conditions (i.e. temperature and humidity), process conditions (i.e. working pressure and rotational speed for pressurized gyration; working distance, polymer solution feed rate, applied voltage for electrospinning) solution properties (e.g. viscosity, surface tension for pressurized gyration; viscosity, density, surface tension and electrical conductivity for electrospinning) are main parameters that affect the formation and homogeneity of fibrous patches obtained by electrospinning and pressurized gyration. Solution properties were also measured.

When comparing pure PLA (12%, w/v) solutions with P4 (10%, w/w) mixed solution, the addition of P4 caused a small increase in surface tension from 69.9 m Nm^{-1} to 70.4 m Nm^{-1}, an increase in density from 1.56 g/ml to 1.60 g/ml and a decrease in viscosity from 4465 mPa s to 2092 mPa s. Both solutions were found to lack electrical conductivity. The surface tension values of the two solutions were both within a suitable range and thus fibrous patches produced with 12% PLA were not found to be beaded. The fiber diameter increased significantly with the increase of density. There was an increase in fiber diameter despite the decrease in viscosity with the addition of P4.

3. 2. Electrospinning and pressurized gyration process conditions

There are several significant points in the forming processes such as the working pressure and rotational speed for pressurized gyration (Table 1A); working distance, polymer solution feed rate and applied voltage for electrospinning (Table 1B). The gas pressure affects the yield of fibers produced by pressurized gyration. Higher pressure during the spin-up time of the motor causes polymer solution to displace without forming

a polymer jet, thereby some solvent is lost via the orifices. Any increases in the rotational speed causes increase in the centrifugal force acting on the polymer solution. If this force does not sufficiently exceed the surface tension of the polymer solution, a polymer jet is not formed and fibers will not accumulate. 12000 rpm was enough to obtain fibers at the lowest concentration (8% PLA) but the speed was inadequate to produce fibers at higher polymer concentrations. As a result, the rotation speed was increased to 24000 rpm for 10% and 12% PLA solutions; 36000 rpm for the 15% PLA solution. Working gas flow pressure was 0.1 MPa and kept constant for all concentrations.

In the production of fibers using electrospinning, lower solution feed rates allow for fibers with low diameters to be formed, and higher feed rates resulted in thicker fibers. It is known that increasing the applied voltage leads to unstable streams, changes in the Taylor cone, a higher degree of whipping instability and more beaded fibers. On the contrary, fibrous patches couldn't be formed at a low applied voltage. It was observed that by increasing the working distance the fibers would decrease in diameter due to the extra drying time afforded by the increase in distance between the needle and the collector. Additionally, while producing P4-loaded fibrous patches, the diameter of fibers increased as a consequence of increase in flow rates.

Table 1. Main parameters in the production of fibrous patches using (A) pressurized gyration and (B) electrospinning. The same parameters were applied for pure and P4-loaded fibrous patches produced by pressurized gyration.

A. Pressurized gyration

PLA conten	Rotation speed	Working pressur	Obtained patches per ml	Obtained patches per ml	Relative Humidity	Tempe rature

t (w/v)	(rpm)	e (Pa)	(mg) Pure	(mg) P4-loaded	(%)	(C^o)
8%	12000	$1x10^5$	17.0	30.0	56	25
10%	24000	$1x10^5$	32.4	34.2	56	25
12%	24000	$1x10^5$	102.4	114.7	56	25
15%	36000	$1x10^5$	57.8	64.8	56	25

B. Electrospinning

Solutions	Working Distance (mm)	Voltage (kV)	Flow rate (µl/min)
Pure	130/150	6	10
	130/150	8	20
	130/150	10	30
PLA+P4	130	10	10/20/30
	150	12	10/20/30

3.3. Morphological Characterization of Microfiber

The change in the fiber size and morphology of pure and P4-loaded fibrous patches using pressurized gyration and electrospinning in different polymer concentrations and processing conditions were analyzed using SEM, results are shown in Figure 2. Firstly, fibrous patches of four different PLA concentrations (8%, 10%, 12%, 15%) were produced with and without 10% P4 by pressurized gyration (Figure 2). According to the results obtained from pressurized gyration, we concluded that adding P4 to the 8% PLA solution created beaded and nonhomogeneous fibers. The diameter of the pure 8% PLA fibrous patches is 7.34 ± 1.11 µm and increased to 7.61 ± 1.13 µm by adding P4. With the pure 10% PLA fibrous patches, the diameter of the fibers was 7.92 ± 1.27 µm, it increased slightly to 7.96 ± 1.79 µm by the addition of P4. It was clearly seen that the addition of P4 to 10% PLA solution caused heavily beaded fibers and loss in

homogeneity. The highest production yield per ml solution also belonged to the 12% PLA solutions obtaining 102.4 mg/ml in pure fibrous patches and 114.7 mg/ml in P4-loaded fibrous patches compared to other concentrations. The production yields per ml solution with the same polymer ratio by electrospinning were 78.2 mg/ml in pure fibrous patches and 86.7 mg/ml in P4-loaded fibrous patches. The diameter of pure 12% PLA (6.76 ± 1.82 µm) fibrous patches increased by adding P4 (12.36 ± 3.60 µm). The diameters of pure 15% PLA fibrous patches (26.29 ± 4.69 µm) and also with P4 (24.25 ± 2.40 µm) were much greater and were not investigated further. In summary, 12% PLA was chosen for the further tests and forming of fibrous patches using both pressurized gyration and electrospinning, the latter was with different process conditions directly related to electrospinning (Table 1).

Figure 2. SEM images and fiber diameter distributions of pure and P4-loaded fibrous patches produced by pressurized gyration. (A) 8% (w/v) PLA, (B) P4-loaded 8% PLA, (C) 10% PLA, (D) P4-loaded 10% PLA, (E) 12% PLA, (F) P4-loaded 12% PLA, (G) 15% PLA, and (H) P4-loaded 15%. In all diameter distributions, n = 100.

In the production of pure fibrous patches using electrospinning, when the flow rate and applied voltage remained constant and working distance increased, the diameter of fibrous patches decreased (Figure 3A to 3F). In comparison, at 20 µl/min flow rate and 8 kV applied voltage, working distance was changed from 150 mm to 130 mm and the diameter of fibrous patches increased from 6.86 ± 1.30 µm to 7.11 ± 1.29 µm. In another sample, at 30 µl/min and 10 kV, the diameter of fibrous patches increased from 6.41 ± 1.40 µm to 7.02 ± 1.39 µm when the working distance was changed from 150

mm to 130 mm. Optimized fibrous patches were produced at 130 mm, 10 µl/min, 6 kV process conditions due to smaller diameters (6.09 ± 0.96 µm) and higher uniformity.

In the forming of P4-loaded fibrous patches using electrospinning, when the working distance and applied voltage remained constant and flow rate increased, the diameter of fibrous patches increased (Figure 3G to 3L). Thus at 150 mm and 12 kV, increasing the flow from 10 to 30 µl/min caused the diameter of fibrous patches to increase from 7.22 ± 1.09 to 7.89 ± 1.38 µm. The same effect was observed in other samples. Thus, fibrous patch forming by electrospinning was optimized at in 150 mm, 10 µl/min, and 12 kV process conditions due to thinner diameter (7.22 ± 1.09 µm) and higher homogeneity. We used the optimized samples in our further studies.

Figure 3. SEM images and fiber diameter distributions of pure (A-F) and P4-loaded (G-L) fibrous patches produced by electrospinning. (A) 150 mm, 10 µl/min, 6 kV (B) 150 mm, 20 µl/min, 8 kV (C) 150 mm, 30 µl/min, 10 kV (D) 130 mm, 10 µl/min, 6 kV (E) 130 mm, 20 µl/min, 8 kV (F) 130 mm, 30 µl/min, 10 kV (G) 150 mm, 10 µl/min, 12 kV (H) 150 mm, 20 µl/min, 12 kV (I) 150 mm, 30 µl/min, 12 kV (J) 130 mm, 10 µl/min, 10 kV (K) 130 mm, 20 µl/min, 10 kV (L) 130 mm, 30 µl/min, 10 kV. The values represent working distance, flow rate and applied voltage, respectively. In all diameter distributions, n = 100.

3.4. Attenuated Total Reflection-Fourier Transform Infrared Spectroscopy (ATR-FTIR)

The molecular structures of P4 and PLA only and P4-loaded PLA fibrous patches produced by pressurized gyration and electrospinning are indicated in Figure 4. For pure PLA, the characteristic absorption bands observed were: CH_3 and C-H stretching vibrations at 2994 and 2947 cm^{-1}, C=O stretching bands at 1750 cm^{-1}, CH_3 asymmetric scissoring at 1458 cm^{-1}, CH_3 and C-H bending vibrations at 1386 and 1358 cm^{-1}, C-O-C stretching vibration at 1265 cm^{-1}, ester C-O asymmetric stretching at 1182 cm^{-1}, ester C-O symmetric stretching at 1133 cm^{-1}, alcohol C-O stretching vibration at 1084 cm^{-1}, C-CH_3 stretching at 1042 cm^{-1}, O-H bending at 950 cm^{-1} and C-COO stretching at 873 cm^{-1} (Yu et al., 2014).

For pure P4, the characteristic peaks were: C=O stretching bands at C_3 and C_{20} (two ketone groups at C_3 and C_{20}) at 1661 cm^{-1} and 1698 cm^{-1}, these typically separate P4 from other steroids. Other peaks present were C-H asymmetrical stretching at 2923 cm^{-1}, C-H symmetric stretching at 2851 cm^{-1} and C=C-H bending at 870 cm^{-1} (Leimann et al., 2015). Thus, weaker peaks for C=O stretching were observed between 1600 and 1700 cm^{-1} in both P4-loaded PLA fibrous patches, these prove the presence of P4. Zhang et al. (2018) investigated P4 in detail and calibration curve and FTIR spectra were drawn up. According to the results, the carbonyl (C=O) stretching band at 1675 cm^{-1} is the strongest absorbance band in the spectrum, which was used to quantify its adsorption.

Figure 4. FTIR spectra of pure PLA, P4, and P4-loaded PLA fibrous patches produced by pressurized gyration and electrospinning. ES: Electrospinning, PG: Pressurized gyration, P4: Progesterone.

3.5. X-ray Powder Diffraction

XRD studies were applied to P4 powders, pure PLA (12%) and P4-loaded PLA fibrous patches to confirm the encapsulated P4 in the PLA fibrous patches. In the XRD patterns of PLA and P4, several diffraction peaks were observed. The crystallinity of P4 was determined at 12.7 and 16.9 2Θ degrees, while the crystallinity for PLA was detected at 21.2 and 22.1 2Θ degrees (Oliveira et al., 2013). In P4-loaded PLA fibrous patches, it is confirmed that P4 was encapsulated in the PLA fibrous patches in its crystalline form (Figure 5). As a result, PLA rich domains were observed in both ATR-FTIR and XRD spectra and characteristic peaks of PLA and P4 were also seen (indicated with arrows).

Figure 5. XRD patterns of (a) P4, (b) pure PLA, (c) P4-loaded PLA fibrous patches produced by electrospinning and (d) pressurized gyration. ES: Electrospinning, PG: Pressurized gyration, P4: Progesterone.

3.6. Differential Scanning Calorimetry (DSC)

DSC analyses of the samples were performed to determine the effect of P4 and the production technique on the morphological structure of PLA based fibrous patches. DSC curves of fibrous patches, produced by pressurized gyration and electrospinning techniques, are given in Figure 6 together with and without P4 in the temperature range of 0-240^{o}C. DSC thermal data of the samples, including glass transition (Tg), cold crystallization (Tc) and melting temperatures (Tm), melting (ΔHm) and cold

crystallization (ΔH_{cc}) enthalpies and crystallinity (Xc), are collected in Table 2. The Xc of the samples was calculated using the following equation; (Jia et al., 2017).

$$Xc = (\Delta H_m - \Delta H_{cc}) / f_\omega \Delta H^o$$

Where ΔH^o= 93.7 J/g is the melting enthalpy for 100% crystalline PLA (Jia et al., 2017). f_ω is the weight fraction of PLA in the corresponding formulation. ΔH_m and ΔH_{cc} are the melting and cold crystallization enthalpies, respectively. The curves a and c in Figure 6 represent PLA fibrous patches, produced by electrospinning and pressurized gyration, respectively. Although Tg and Tm of native PLA are 63^{o}C and 165^{o}C, respectively, these temperatures did not change significantly with the sample produced by pressurized gyration. However, the electrospinning sample had lower Tg and Tm temperatures, compared to native PLA (Tg=59^{o}C and Tm=164^{o}C). This could be due to the slightly lower crystallinity and increased free volume of the PLA chains, caused by electrospinning (Table 2). Furthermore, to determine the molecular interactions between P4 and PLA at a molecular scale, DSC curves of P4 and the loaded PLA patch samples, prepared by electrospinning and pressurized gyration were recorded. P4 caused lower Tm and Xc values compared to those of pure PLA fibrous patch of electrospinning and pressurized gyration (Table 2). This might be due to the suppression of PLA crystallinity with P4 through intermolecular interactions (Demirkaya et al., 2015). While P4 had a melting endotherm at 132^{o}C (curve e, Figure 6), absence of an endotherm at around this temperature (curves b and d) was considered as a proof that P4 was homogeneously distributed in pressurized gyration and electrospinning samples in the amorphous form. This could be additional evidence for the intermolecular interaction between PLA and P4.

548 **Figure 6.** DSC curves of pure and P4-loaded PLA fibrous patches produced by
549 electrospinning and pressurized gyration. ES: Electrospinning, PG: Pressurized
550 gyration, P4: Progesterone.

551

552 **Table 2.** DSC data of the samples
553

Sample	T_g (^oC)	T_m (^oC)	ΔH_{cc} (J/g)	ΔH_m (J/g)	Crystallinity (%)
Pure PLA fibrous patch/ES	59.0	164.1	-17.3	31.0	14.6
Pure PLA fibrous patch/PG	62.7	165.2	-7.5	23.8	17.4
P4-loaded fibrous patch/ES	56.6	160.7	-13.8	21.8	9.4
P4-loaded fibrous patch/PG	53.5	161.5	-10.1	19.0	10.4

554 ES: Electrospinning, PG: Pressurized gyration, P4: Progesterone.

555

556 **3.7. Tensile Testing of Fibrous Patches**

557 Tensile strength and strain at break were investigated for each of the samples
558 (Figure 7). The loading of P4 into PLA increased the mechanical properties of the
559 patches. As the P4 concentration increased in the pressurized gyration technique,
560 tensile strength of fibrous patches was enhanced, from 0.884 MPa to 1.658 MPa. This
561 increase is also observed in electrospinning with the addition P4 as seen by the
562 increase in tensile strength from 0.353 MPa to 0.554 MPa. It is clearly seen that fibrous
563 patches obtained by pressurized gyration are more durable than with electrospinning.

564 According to the literature data, the tensile strength increase may due to the increase in
565 diameter of fibers or the amorphous form of P4 (Kong et al., 2014). However, it must be
566 noted that strain at break slightly decreased by loading P4 into the fibers with
567 electrospinning.

568

569 **Figure 7.** Tensile properties of fibrous patches: (a) tensile strength and (b) strain at
570 break. ES: Electrospinning, PG: Pressurized gyration, P4: Progesterone.

571 **3.8. In Vitro Drug Release Studies**

572 Initially, UV spectra was used to acquire the concentration range of P4 from 0.625
573 to 10 µg/mL and a linear standard calibration curve was created from P4 absorption
574 values (R^2=0.9880). This spectrum was used for quantitative determination of the drug
575 release. Although the fibrous patches were submerged in the simulated vaginal fluid, P4
576 passed through the membrane to PBS. The P4 releasing profiles of P4-loaded fibrous
577 patches and P4 solution were measured in PBS of pH 7.4 and a controlled temperature
578 of 37^{o}C to mimic the normal physiological *in vivo* conditions. As shown in Figure 8, the
579 membrane had no impact on drug diffusion from the liquid formulation, indicating that an
580 adequate membrane was chosen (Klein, 2013). P4 can be successfully released from
581 fibrous patches over a period of 24 hours according to the first-order kinetic model; both
582 production techniques exhibited sustained release in 24 hours (pressurized gyration:
583 24.72% and electrospinning: 24.89%). However, burst release was seen within first 4h
584 in both fibrous patches (pressurized gyration: 17.7% and electrospinning: 18.1%). The
585 drug encapsulation efficiency was calculated to be ~ 97% for both forming scenarios,
586 pressurized gyration and electrospinning. As a result, P4 was released from both fibrous

patches successfully and in a controlled manner. There is no significant difference between the forming techniques in terms of drug release.

Figure 8. Progesterone release profiles of P4-loaded fibrous patches, produced by pressurized gyration and electrospinning, and pure P4 solution according to first-order model. All the values were obtained from the averages of three experiments, and the errors were less than 5%. ES: Electrospinning, PG: Pressurized gyration, P4: Progesterone.

3.9. In Vitro Cytotoxicity Studies

3.9.1. Cell Attachment

The initial cell attachment performance of the samples extracted from the developed fibrous patches as well as blank TCPS control is given as a percentage of the cell concentration initially seeded, in Figure 9A. Over the course of 3 h, the Vero cells were found to be attached to the surfaces of the samples as well as the blank TCPS controls with a steadily increasing tendency. Within the first hour of the initial seeding, the attachment on all fibrous patch samples reached almost 50% of the initial cell concentration where blank control managed to support only 25% of the cells initially seeded. At the end of the 3rd hour, the samples reached attachment concentration around ~75-80% and ~80-85% of the cells initially seeded for pure and P4-loaded patches, respectively. However, considering the statistical deviation of the results, the small amount of the initial cell concentration and the short duration of the assay, the difference between pure and P4-loaded patches could be considered relatively small,

and the difference between the patches produced with pressurized gyration and electrospinning was almost insignificant (~2-3%) to consider.

3.9.2. Viability and Yield

MTT assay is a colorimetric assay in which the determined values represent the cell viability and/or proliferation. The assay is based on the reduction of yellow colored tetrazolium dye to purple colored formazan crystals. The assay represents the cell viability and proliferation since this reduction is carried out by mitochondria of viable cells and the amount of reduction, which is measured in terms of absorption intensity, depends on the metabolic activity of the cells (Chen et al., 2014). Therefore, in this study, MTT assay was used as a measure of cell viability and/or proliferation. The absorbance intensity of the fibrous patches was initially found to be similar to the blank control dishes (Figure 9B). However, according to the measurements done over a total course of 7 days, as the culture progressed, the fibrous patches began to show higher absorbance than TCPS controls as a result of increased metabolic activity due to their high surface area provided by their fibrous structures, similar in observation during the initial attachment performances. As a result, the metabolic activity continued to increase steadily at 48 h intervals without showing any cytotoxicity for the Vero cells. The blank controls were also performed sufficiently in the culture without any cytotoxicity as expected from commercial TCPS dishes (Maghdouri-White et al., 2014). The cell yields obtained at the end of the culture showed consistent results with 7-day MTT assay as it showed that the fibrous structure of the patches provided additional anchorage points for cells to attach and proliferate, not only on the surface but also within the patch since the number of cells counted on the patches exceeded the number of cells that can

possibly proliferate as a monolayer on a 1 cm^2 surface (Figure 9C). Since, the increased cell yield as well as the constant increase in the metabolic activity according to the MTT assay can be interpreted as the increase in the cell number, the cell functionality as well as the cell viability (Pagliacci et al., 1993), it can be concluded that the fibrous patches provided a more suitable environment for cells to stay healthy and viable throughout the course of 7 days.

Figure 9. Cell culture results for fibrous patches. (A) 3 h attachment, (B) 7 day viability, and (C) cell yield (at 7^{th} day) performances of the pure and progesterone-loaded fibrous patches produced by pressurized gyration and electrospinning as well as blank TCPS control Petri dishes. The symbols "*" and "**" indicate the significant differences (* for $p < 0.05$ and ** for $p < 0.01$). The statistical analyses were carried out with ANOVA tests with the Tukey multiple comparison test. ES: Electrospinning, PG: Pressurized gyration, P4: Progesterone.

3.9.3. Visual Inspection

In addition to quantitative assays, the culture was also monitored visually to inspect any changes in morphology of the cells seeded on the produced fibrous patches. For sufficient coverage of the culture progress, the mid-period and end-period were inspected. Therefore, images of the cultured samples were obtained at the end of the 3^{rd} and the 7^{th} day of the culture from AF-488/DAPI dual stained samples by using fluorescence microscopy. AF-488 and DAPI are both widely used fluorescence stains to label actin filaments of cytoskeleton and nucleus of the cells, respectively. The dual utilization of these stains can provide good visualization of the cell morphology. The

fluorescence images obtained from the cultured samples were consistent with the previous quantitative assay results (Figure 10). Even on the 3rd day of the culture, the cell population density on all samples was significantly high and the well-defined Vero cell morphology was intact. At the end of the culture, it can be seen that not only the surface of the samples was highly covered with almost a monolayer of cells, but also cells have grown on top of each other in a 3 dimensional pattern (out of focus and less bright cells).

Figure 10. Fluorescence images obtained at the end of the 3rd day of culture: (A) pure PLA/pressurized gyration, (B) pure PLA/electrospinning, (C) P4-loaded PLA/pressurized gyration, (D) P4-loaded PLA/electrospinning fibrous patches, and at the end of the 7th day of culture from (E) pure PLA/pressurized gyration, (F) pure PLA/electrospinning, (G) P4-loaded PLA/pressurized gyration, (H) P4-loaded PLA/electrospinning fibrous patches. Magnifications: x40. Green: AF-488 stained actin filaments, Blue: DAPI stained nucleus.

3.10. In Vitro Organ Bath Experiments

The results obtained from the in vitro organ bath are given below as responses to KCl and cumulative (-)-noradrenaline. In vivo tests were completed with only P4-loaded fibrous patches/electrospinning because the fibrous patches obtained by electrospinning had several advantages compared to pressurized gyration technique such as better morphology, smaller fiber diameter and also electrospinning is a commonly used technique.

3.10.1. Contracting Effect of KCl

Results of isolated organ bath experiment studied on the 22-day-pregnant rats demonstrated that P4-loaded fibrous patches/electrospinning decreased myometrial contracting effect at 124 mM KCl ($p<0.05$), which may be acted via voltage-gated calcium channels (Figure 11A). These changes in the KCl response may be due to changes in calcium influx (Grazzini et al., 1998).

Figure 11. In vitro organ bath experiment's results. (A) In vitro organ bath contraction of rat uterine smooth muscle induced by 124 mM KCl in the 22-day-pregnant rat myometrium with progesterone treatments. *$p<0.05$ versus naive control group. (B) Effects of progesterone treatments on the (-)-noradrenaline-evoked contractions in the 22-day-pregnant rat myometrium. *$p<0.05$ versus naive control group and drug-free fibrous patch implantation group. Changes in contraction intensity were calculated using the areas under the curve and expressed as mean ± SEM (n=6). (C and D) Changes in the uterus contracting effect of (-)-noradrenaline (EC_{50} and Emax values, respectively) in the 22-day-pregnant rat myometrium with progesterone treatment. *$p<0.05$ versus naive control group and drug-free fibrous patch implantation group. The statistical analyses were carried out with ANOVA tests with the Tukey multiple comparison test. NC: Naive control group, DFF: Drug-free fibrous patch implantation group, PF: Progesterone-loaded fibrous patch/electrospinning implantation group, OP: Oral progesterone group, EC_{50}: The contractions of (-)-noradrenaline, which elicits half of the maximum contracting effect of (-)-noradrenaline, Emax: The maximum contracting effect of (-)-noradrenaline.

3.10.2. Contracting Effect of Cumulative (-)-Noradrenaline

Myometrial contracting effect of (-)-noradrenaline in the concentration range of $10^{-8.5}$-$10^{-3.5}$ M in the 22-day-pregnant myometrium is shown in Figure 11B. In previous studies, P4 showed a relaxing effect on the contractions (Kubli-Garfias et al., 1983). Similar results have been reported on muscle rings from pregnant and non-pregnant human uterus in vitro (Beck et al., 1982).

P4-loaded fibrous patch/electrospinning and oral P4 treatments decreased the myometrial contracting effect of (-)-noradrenaline in the concentration range of $10^{-7.5}$-$10^{-3.5}$ M when compared with the naive control group and the drug-free fibrous patch implantation group ($p<0.05$). But these treatments did not decrease the myometrial contracting effect of (-)-noradrenaline in the concentration range of $10^{-8.5}$-10^{-8} compared with the naive control group and the drug-free fibrous patches implantation groups. In addition, oral P4 treatment caused lower myometrial contractions (Emax=30.6 ± 2.5) compared with the P4-loaded fibrous patch/electrospinning implantation group (Emax=32.1 ± 4.4), but there is no significant difference between these groups at any concentrations. According to these results, the relaxing effect of P4 was moderated at low concentrations ($10^{-8.5}$-10^{-8}) of (-)-noradrenaline, while the relaxing effect is greater in concentrations over $10^{-7.5}$ in both the oral and fibrous patch treatment groups.

The curves of EC50 and Emax values are shown in Figure 11C and 11D, respectively. P4 treatments reduced the maximum myometrial contracting effect and the EC_{50} values of (-)-noradrenaline.

4. Discussion

P4-loaded fibrous patches were created for intra-vaginal application to prevent preterm birth using two different techniques, electrospinning and pressurized gyration. The characterization of solutions and patches, in vitro and in vivo analyses of patches were performed, and also production techniques were compared.

Fiber diameter and morphology are affected by solution viscosity in both methods (Ahmed et al., 2018). Bead and droplet defects are observed in SEM when the polymer concentration is low. In this case, electrospraying occurs instead of electrospinning where beads are formed instead of fibers. There is a direct correlation between viscosity and fiber morphology, at higher viscosities the fibers have larger diameters. The surface tension of the polymer solutions has a crucial role in influencing electrospinning and pressurized gyration fiber formation. As the surface tension needs to be overcome in order to form fibers with both techniques, a high surface tension can cause fibers to not form or be heavily beaded (Brako et al., 2018). In electrospinning, the augmentation in electrical conductivity leads to the formation of smaller, bead-free fibers.

After production of patches by both techniques, morphological characterizations were done and the increase of polymer concentration caused the rise in the diameter of the fibers, and also adding P4 to the solutions made the fibers thicker. The addition of P4 to lower than 12% PLA solution caused heavily beaded fibers and loss in homogeneity. Fibers with 12% PLA + P4 solution were homogeneously dispersed and distributed within the polymer matrices, and the highest production yield per ml solution also belonged to the 12% PLA. Pressurized gyration has an advantage compared to electrospinning in generating a higher production yield.

ATR-FTIR and XRD were used to confirm that the drug was successfully encapsulated. The halo diffraction pattern sighted between 10 and 40 2Θ is the characteristic of material showing amorphous characteristics in the drug-loaded fibrous patches. It is most probably related to the polymeric carrier (Jain et al., 2008).

It is well known that, human body temperature varies between 36.1°C and 37.8°C in healthy individuals and fluctuates by about 0.5°C during the day. Internal vaginal temperature is ~ 37^{o}C (Boyd et al., 2015). A body temperature over 40°C is considered very high, and temperatures over 41.5^{o}C cause hyperthermia. According to the DSC results, P4-loaded PLA fibrous patches can safely be applied by the intra-vaginal route without risk of melting and also P4 and PLA exhibited intermolecular interactions and, thus, distributed the PLA crystallinity (Demirkaya et al., 2015).

Drug release studies of P4-loaded fibrous patches were performed according to the first-order kinetic model. Here a Franz diffusion cell with a cellulose acetate membrane and simulated vaginal fluid was used to investigate P4 release from fibrous patches across an artificial membrane mimicking the mucosal environment of the vagina, especially to investigate whether P4-loaded fibrous patches demonstrated release over a period of time appropriate with that required clinically. In our previous study, fibers were compared under the same experimental conditions with Cyclogest, which is a commercial pessary including P4. The commercial pessary released ~12% and P4-loaded fibers released ~20% of all ingredients in 210 min (Brako et al., 2018). In the present study, it is considered that fibrous patches are too large to pass through the vaginal mucosa; hence they would be expected to remain on the vaginal mucosa gradually releasing their contents over time (Jelvehgari et al., 2006). P4-loaded fibrous

patches released ~16% of all ingredients at the same time interval and the release of P4 was more rapid from fibrous patches compared the to commercial pessary. Our results indicate that fibrous patches were able to increase the permeation rate of poorly water-soluble drugs. These tests indicated whether the required amount of drug was released from fibrous patches in the clinically feasible period. These results were also used in the planning of in vivo tests. As a result, P4 was released from both fibrous patches successfully and in a controlled manner. Therefore, the same effect on maintenance tocolysis can be obtained with reduced frequency of dosage and the amount of drug.

The cytotoxicity of the pure and P4-loaded fibrous patches produced by pressurized gyration and electrospinning was studied with Vero epithelial cells, and TCPS Petri dishes, which are commercially used for routine cell culture and used as the blank to compare the performance. The result obtained from cell culture tests was a clear outcome comparing the fibrous/porous 3 dimensional structures of the samples, which provided a distinctive advantage in terms of attachment compared to the 2 dimensional surfaces of the blank TCPS. Since the Vero cells, as with all animal cells, are anchorage-dependent, these fibrous/porous 3 dimensional structures became a better host for them because of the higher amount of focal points for cells to adhere due to their surface area (Ozkan and Turkoglu Sasmazel, 2016). Besides, the most important outcome of the assay conducted was that the patches prepared with either method, whether they were drug loaded or not, did not affect the cell attachment mechanism negatively, which indicated no short term cytotoxicity and considerably more attachment compared to blank controls because of the fibrous structure. The fibrous patches showed better cell proliferation because of the advantage gained during the initial cell

attachment, resulting in early initiation of the metabolic activity and better overall proliferation of the cells at the end of 7 days (Maghdouri-White et al., 2014). Both the pure and P4-loaded fibrous patches, whether produced with pressurized gyration or electrospinning, performed similarly compared to each other without showing any significant difference in performance; therefore, it should be noted that neither PLA nor P4-loading or the production methods caused any kind of cytotoxicity or negative effect on viability and proliferation of the Vero cells. Because of the non-woven fibrous structure, the cells attached faster and in larger quantities which resulted in this better 7-day performance of the patches (Ozkan and Turkoglu Sasmazel, 2017). It can also be noted that there is no significant observable differences between pressurized gyration or electrospinning produced patches or pure or P4-loaded patches. As a result, it can be concluded that because of the ability to grow in larger quantities without any observable morphology changes, fibrous patches developed with both methods, whether loaded with P4 or not, do not have any cytotoxicity on the morphology or growth of the Vero cells. There is no significant difference according to the results of drug release tests, DSC tests and cell culture tests between production techniques. Therefore, pressurized gyration can be used for scale-up of production with many advantages such as better production yield and tensile strength.

P4 plays a major role in the myometrial function during gestation, the main focus of our study was to elucidate the effects of P4-loaded PLA fibrous patches in late-pregnant uterine functions and compare these with oral P4 treatments in vivo using organ bath experiments. The mechanism of the effect of maintenance tocolysis with P4 has been demonstrated in previous studies. P4 increases the synthesis of B_2-adrenoceptors

during pregnancy and participates in the regulation of G-proteins in the myometrium (Riemer et al., 1988; Rossier et al., 1999). P4-loaded fibrous patches were inserted into the vagina of pregnant rats on the 15th day of the pregnancy. Oral P4 treatment began on the 15th day of the pregnancy and continued to the 21st day, this treatment period was equivalent to the third trimester of human pregnancy. On the 22nd day of pregnancy, all the rats were decapitated and the uterine tissues were removed. The frequency of the dosage was reduced and the side effects of P4 may have been decreased with patches compared to daily oral P4 treatment. The results obtained from the in vitro organ bath experiments showed that both P4-loaded fibrous patch and oral P4 treatment decrease myometrial contraction of both KCl and cumulative (-)-noradrenaline on pregnant rat uterus. The P4-loaded fibrous patch/ES implantation group inhibited uterine contractions as well as the oral P4 group and there is no significant difference between them. Consequently, P4 can be loaded into PLA fibers, thereby may be offering high bioavailability, fewer side effects, and reduced frequency of dosage by controlled release.

5. Conclusions

We have engineered intra-vaginal P4-loaded PLA fibrous patches using two different techniques, electrospinning and pressurized gyration, for the treatment of preterm birth with some advantages. Pressurized gyration had two advantages compared to electrospinning; better production rate and higher tensile strength. Our results indicated that both techniques showed sustained P4 release with a similar profile. DSC results of fibrous patches were similar, and they can be safely applied via

the intra-vaginal route without degradation. The patches did not affect the cell attachment, viability, and proliferation on Vero cells negatively. Pressurized gyration patches were produced at a much faster rate making them suitable for more high demand applications as seen for this type of medication. The effect of maintenance tocolysis with the P4-loaded fibrous patch was investigated and it significantly decreased uterine contractions as much as the standard oral route. Consequently, both techniques (pressurized gyration and electrospinning) are successful in the production of P4-loaded fibrous polymeric patches, which are a novel and beneficial treatment strategy with possible high bioavailability, reduced frequency of dosage, and the amount of drug.

Acknowledgments

The authors are grateful to the UK Engineering & Physical Sciences Research Council (EPSRC) for funding pressurized gyration forming research at University College London (Grants EP/S016872/1 and EP/N034228/1). Dr. M.E. Cam was supported by a TUBITAK 2219 Research Programme Grant (Scientific and Technological Research Council of Turkey-TUBITAK) and thanks UCL Mechanical Engineering for hosting his post-doctoral research in the UK.

Declaration of interests

The authors declare no conflict of interest.

References

Ahmed, J., Matharu, R.K., Shams, T., Illangakoon, U.E., Edirisinghe, M., 2018. A Comparison of Electric-Field-Driven and Pressure-Driven Fiber Generation Methods for Drug Delivery. Macromol. Mater. Eng. 303, 1700577.

Alenezi, H., Cam, M.E., Edirisinghe, M., 2019. Experimental and theoretical investigation of the fluid behavior during polymeric fiber formation with and without pressure. Appl. Phys. Rev. 6, 041401.

Balamurugan, R., Sundarrajan, S., Ramakrishna, S., 2011. Recent Trends in Nanofibrous Membranes and Their Suitability for Air and Water Filtrations. Membranes 1, 232-248.

Beck, P., Adler, P., Szlachter, N., Goldsmith, L.T., Steinetz, B.G., Weiss, G., 1982. Synergistic effect of human relaxin and progesterone on human myometrial contractions. Int. J. Gynaecol. Obstet. 20, 141-144.

Boyd, P., Desjardins, D., Kumar, S., Fetherston, S.M., Le-Grand, R., Dereuddre-Bosquet, N., Helgadóttir, B., Bjarnason, Á., Narasimhan, M., Malcolm, R.K., 2015. A temperature-monitoring vaginal ring for measuring adherence. PloS one 10, e0125682-e0125682.

Brako, F., Raimi-Abraham, B.T., Mahalingam, S., Craig, D.Q.M., Edirisinghe, M., 2018. The development of progesterone-loaded nanofibers using pressurized gyration: A novel approach to vaginal delivery for the prevention of pre-term birth. Int. J. Pharm. 540, 31-39.

879 Cam, M.E., Cesur, S., Taskin, T., Erdemir, G., Kuruca, D.S., Sahin, Y.M., Kabasakal, L.,
880 Gunduz, O., 2019a. Fabrication, characterization and fibroblast proliferative activity of
881 electrospun Achillea lycaonica-loaded nanofibrous mats. Eur. Poly. J. 120, 109239.
882 Cam, M.E., Crabbe-Mann, M., Alenezi, H., Hazar-Yavuz, A.N., Ertas, B., Ekentok, C.,
883 Ozcan, G.S., Topal, F., Guler, E., Yazir, Y., Parhizkar, M., Edirisinghe, M., 2020a. The
884 comparision of glybenclamide and metformin-loaded bacterial cellulose/gelatin
885 nanofibres produced by a portable electrohydrodynamic gun for diabetic wound healing.
886 Eur. Poly. J. 134, 109844.
887 Cam, M.E., Yildiz, S., Alenezi, H., Cesur, S., Ozcan, G.S., Erdemir, G., Edirisinghe, U.,
888 Akakin, D., Kuruca, D.S., Kabasakal, L., Gunduz, O., Edirisinghe, M., 2020. Evaluation
889 of burst release and sustained release of pioglitazone-loaded fibrous mats on diabetic
890 wound healing: an in vitro and in vivo comparison study. J. R. Soc. Interface 17,
891 20190712.
892 Cam, M.E., Zhang, Y., Edirisinghe, M., 2019b. Electrosprayed microparticles: a novel
893 drug delivery method. Expert Opin. Drug Del. 16, 895-901.
894 Chen, S.-H., Chang, Y., Lee, K.-R., Lai, J.-Y., 2014. A three-dimensional dual-layer
895 nano/microfibrous structure of electrospun chitosan/poly(d,l-lactide) membrane for the
896 improvement of cytocompatibility. J. Membrane Sci. 450, 224-234.
897 Demirkaya, Z.D., Sengul, B., Eroglu, M.S., Dilsiz, N., 2015. Comprehensive
898 characterization of polylactide-layered double hydroxides nanocomposites as packaging
899 materials. J. Polym. Res. 22, 1-13.
900 Goldenberg, R.L., Culhane, J.F., Iams, J.D., Romero, R., 2008. Epidemiology and
901 causes of preterm birth. Lancet 371, 75-84.

902 Goletiani, N.V., Keith, D.R., Gorsky, S.J., 2007. Progesterone: Review of safety for
903 clinical studies. Exp. Clin. Psychopharm. 15, 427-444.
904 Graham, J.D., Clarke, C.L., 1997. Physiological action of progesterone in target tissues.
905 Endocr. Rev. 18, 502-519.
906 Grazzini, E., Guillon, G., Mouillac, B., Zingg, H.H., 1998. Inhibition of oxytocin receptor
907 function by direct binding of progesterone. Nature 392, 509.
908 Hajagos-Tóth, J., Bóta, J., Ducza, E., Samavati, R., Borsodi, A., Benyhe, S., Gáspár,
909 R., 2016. The effects of progesterone on the alpha2-adrenergic receptor subtypes in
910 late-pregnant uterine contractions in vitro. Repod. Biol. Endocrinol. 14, 33-33.
911 Heseltine, P.L., Ahmed, J., Edirisinghe, M., 2018. Developments in Pressurized
912 Gyration for the Mass Production of Polymeric Fibers. Macromol. Mater. Eng. 303,
913 1800218.
914 Huang, C.-K., Zhang, K., Gong, Q., Yu, D.-G., Wang, J., Tan, X., Quan, H., 2020.
915 Ethylcellulose-based drug nano depots fabricated using a modified triaxial
916 electrospinning. Int. J. Biol. Macromol. 152, 68-76.
917 Jain, S.K., Jain, A., Gupta, Y., Kharya, A., 2008. Design and development of a
918 mucoadhesive buccal film bearing progesterone. Pharmazie 63, 129-135.
919 Jelvehgari, M., Siahi-Shadbad, M.R., Azarmi, S., Martin, G.P., Nokhodchi, A., 2006. The
920 microsponge delivery system of benzoyl peroxide: preparation, characterization and
921 release studies. Int. J. Pharm. 308, 124-132.
922 Jia, S., Yu, D., Zhu, Y., Wang, Z., Chen, L., Fu, L., 2017. Morphology, Crystallization
923 and Thermal Behaviors of PLA-Based Composites: Wonderful Effects of Hybrid
924 GO/PEG via Dynamic Impregnating. Polymers 9, 528.

925 Karuppannan, C., Sivaraj, M., Kumar, J.G., Seerangan, R., Balasubramanian, S.,
926 Gopal, D.R., 2017. Fabrication of Progesterone-Loaded Nanofibers for the Drug
927 Delivery Applications in Bovine. Nanoscale Res. Lett. 12, 116-116.
928 Khan, I., Ahmed, N., 1969. Effects of progesterone therapy on the stilboestrol-induced
929 sensitivity of isolated rat uterus preparations. Br. J. Pharmacol. 35, 332-338.
930 Khdair, A., Hamad, I., Al-Hussaini, M., Albayati, D., Alkhatib, H., Alkhalidi, B., 2013. In
931 vitro artificial membrane-natural mucosa correlation of carvedilol buccal delivery. J.
932 Drug Del. Sci. Tech. 23, 602-609.
933 Kim, I.D., Ahn, K.H., Lee, S., Hong, S.C., Kim, S.H., Kim, T., 2013. Effect of
934 ovariectomy, 17-beta estradiol, and progesterone on histology and estrogen receptors
935 of bladder in female partial bladder outlet obstruction rat model. J. Obstet. Gynaecol.
936 Res. 39, 1259-1267.
937 Kim, N.N., Min, K., Pessina, M.A., Munarriz, R., Goldstein, I., Traish, A.M., 2004. Effects
938 of ovariectomy and steroid hormones on vaginal smooth muscle contractility. Int. J.
939 Impot. Res. 16, 43-50.
940 Kindinger, L.M., Bennett, P.R., Lee, Y.S., Marchesi, J.R., Smith, A., Cacciatore, S.,
941 Holmes, E., Nicholson, J.K., Teoh, T.G., MacIntyre, D.A., 2017. The interaction between
942 vaginal microbiota, cervical length, and vaginal progesterone treatment for preterm birth
943 risk. Microbiome 5, 6.
944 Klein, S., 2013. Influence of different test parameters on in vitro drug release from
945 topical diclofenac formulations in a vertical diffusion cell setup. Pharmazie 68, 565-571.

Kong, H., Teng, C., Liu, X., Zhou, J., Zhong, H., Zhang, Y., Han, K., Yu, M., 2014. Simultaneously improving the tensile strength and modulus of aramid fiber by enhancing amorphous phase in supercritical carbon dioxide. RSC Adv. 4, 20599-20604.

Kubli-Garfias, C., Hoyo-Vadillo, C., Lopez-Nieto, E., Ponce-Monter, H., 1983. Inhibition of spontaneous contractions of the rat pregnant uterus by progesterone metabolites. Proc. West Pharmacol. Soc. 26, 115-118.

Leimann, F.V., Heloisa Biz, M., Kaufmann, K.C., Maia, W.J., Hess Honçalves, O., Cardozo Filho, L., Sayer, C., Hermes de Araújoli, P.H., 2015. Characterization of progesterone loaded biodegradable blend polymeric nanoparticles. Ciência Rural 45, 2082-2088.

Maghdouri-White, Y., Bowlin, G.L., Lemmon, C.A., Dréau, D., 2014. Mammary epithelial cell adhesion, viability, and infiltration on blended or coated silk fibroin-collagen type I electrospun scaffolds. Mat. Sci. Eng C-Mater. 43, 37-44.

Mahalingam, S., Edirisinghe, M., 2013. Forming of polymer nanofibers by a pressurised gyration process. Macromol. Rapid Commun. 34, 1134-1139.

McCormick, M.C., Litt, J.S., Smith, V.C., Zupancic, J.A., 2011. Prematurity: an overview and public health implications. Annu. Rev. Public Health 32, 367-379.

Mofidfar, M., Prausnitz, M.R., 2019. Electrospun Transdermal Patch for Contraceptive Hormone Delivery. Curr. Drug Deliv. 16, 577-83.

Nold, C., Maubert, M., Anton, L., Yellon, S., Elovitz, M.A., 2013. Prevention of preterm birth by progestational agents: what are the molecular mechanisms? Am. J. Obstet. Gynecol. 208, 223.e221-227.

968 Oliveira, J.E., Medeiros, E.S., Cardozo, L., Voll, F., Madureira, E.H., Mattoso, L.H.C.,
969 Assis, O.B.G., 2013. Development of poly(lactic acid) nanostructured membranes for
970 the controlled delivery of progesterone to livestock animals. Mater. Sci. Eng. C 33, 844-
971 849.
972 Owen, D.H., Katz, D.F., 1999. A vaginal fluid simulant. Contraception 59, 91-95.
973 Ozkan, O., Turkoglu Sasmazel, H., 2016. Effects of nozzle type atmospheric dry air
974 plasma on L929 fibroblast cells hybrid poly (ε-caprolactone)/chitosan/poly (ε-
975 caprolactone) scaffolds interactions. J. Biosci. Bioeng. 122, 232-239.
976 Ozkan, O., Turkoglu Sasmazel, H., 2017. Hybrid polymeric scaffolds prepared by micro
977 and macro approaches. Int. J. Polym. Mater. Po. 66, 853-860.
978 Pagliacci, M.C., Spinozzi, F., Migliorati, G., Fumi, G., Smacchia, M., Grignani, F.,
979 Riccardi, C., Nicoletti, I., 1993. Genistein inhibits tumour cell growth in vitro but
980 enhances mitochondrial reduction of tetrazolium salts: a further pitfall in the use of the
981 MTT assay for evaluating cell growth and survival. Eur. J. Cancer 29a, 1573-1577.
982 Qin, Z.-Y., Jia, X.-W., Liu, Q., Kong, B.-h., Wang, H., 2019. Fast dissolving oral films for
983 drug delivery prepared from chitosan/pullulan electrospinning nanofibers. Int. J. Biol.
984 Macromol. 137, 224-231.
985 Raimi-Abraham, B.T., Mahalingam, S., Davies, P.J., Edirisinghe, M., Craig, D.Q., 2015.
986 Development and Characterization of Amorphous Nanofiber Drug Dispersions Prepared
987 Using Pressurized Gyration. Mol. Pharm. 12, 3851-3861.
988 Riemer, R.K., Wu, Y.Y., Bottari, S.P., Jacobs, M.M., Goldfien, A., Roberts, J.M., 1988.
989 Estrogen reduces beta-adrenoceptor-mediated cAMP production and the concentration

of the guanyl nucleotide-regulatory protein, Gs, in rabbit myometrium. Mol. Pharmacol. 33, 389-395.

Rossier, O., Abuin, L., Fanelli, F., Leonardi, A., Cotecchia, S., 1999. Inverse agonism and neutral antagonism at alpha(1a)- and alpha(1b)-adrenergic receptor subtypes. Mol. Pharmacol. 56, 858-866.

Wilson, P., 2009. Development and validation of a liquid chromatographic method for the simultaneous determination of estradiol, estriol, estrone, and progesterone in pharmaceutical preparations. J AOAC Int. 92, 846-854.

Yu, T., Jiang, N., Li, Y., 2014. Study on short ramie fiber/poly(lactic acid) composites compatibilized by maleic anhydride. Compos. Part A-Appl. S. 64, 139-146.

***Conflict of Interest**

Declaration of interests

X The authors declare that they have no known competing financial interests or personal relationships that could have appeared to influence the work reported in this paper.

☐The authors declare the following financial interests/personal relationships which may be considered as potential competing interests:

Author Statement

Muhammet Emin Cam: Conceptualization, Methodology, Validation, Writing - Original Draft. **Ayse Nur Hazar-Yavuz:** Methodology, Resources, Investigation. **Sumeyye Cesur:** Methodology, Resources, Investigation. **Ozan Ozkan:** Investigation, Writing - Original Draft. **Hussain Alenezi:** Writing - Original Draft, Validation, Formal analysis. **Hilal Turkoglu Sasmazel:** Supervision, Writing - Original Draft. **Mehmet Sayip Eroglu:** Investigation, Writing - Original Draft. **Francis Brako:** Resources. **Jubair Ahmed:** Resources. **Levent Kabasakal:** Visualization, Formal analysis. **Guogang Ren:** Visualization, Writing - Review & Editing. **Oguzhan Gunduz:** Supervision. **Mohan Edirisinghe:** Visualization, Supervision, Project administration, Funding acquisition.

Figure 1

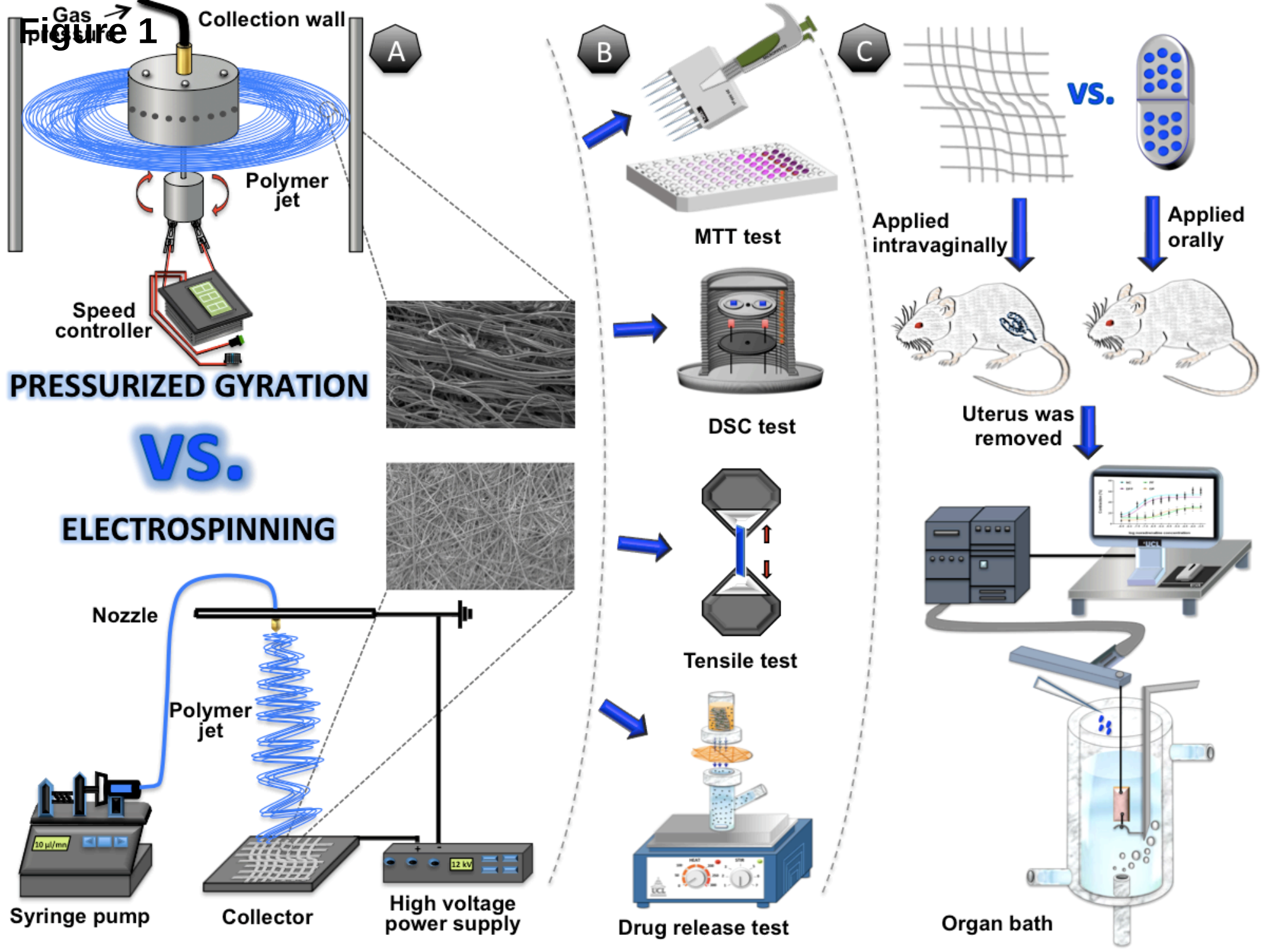
Gas
Collection wall
A
Polymer jet
Speed controller
PRESSURIZED GYRATION
VS.
ELECTROSPINNING
Nozzle
Polymer jet
10 µl/mn
12 kV
Syringe pump
Collector
High voltage power supply
B
MTT test
DSC test
Tensile test
Drug release test
C
VS.
Applied intravaginally
Applied orally
Uterus was removed
Organ bath

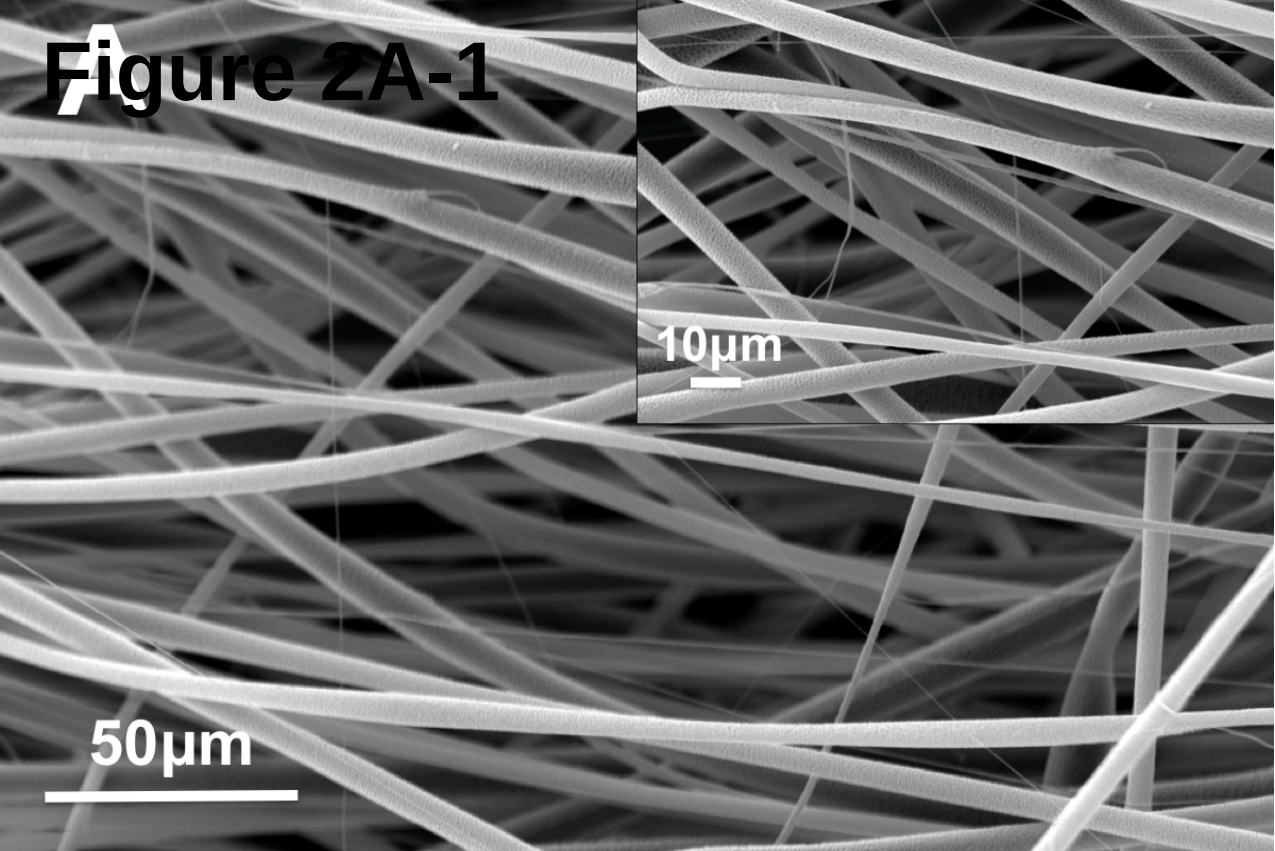
A
Figure 2A-1
10µm
50µm

Figure 2A-2

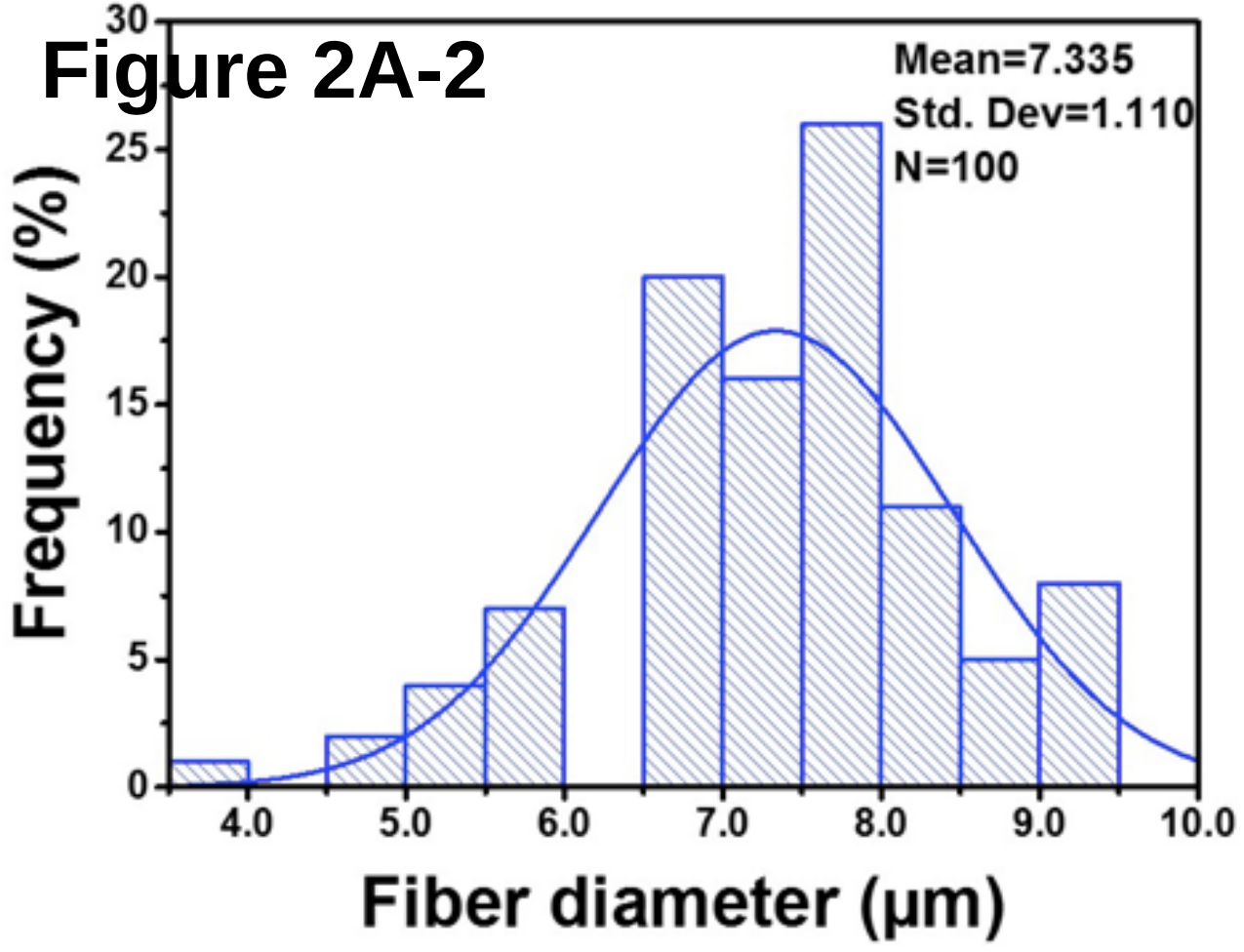
Mean=7.335
Std. Dev=1.110
N=100
Frequency (%)
0
5
10
15
20
25
30
4.0
5.0
6.0
7.0
8.0
9.0
10.0
Fiber diameter (μm)

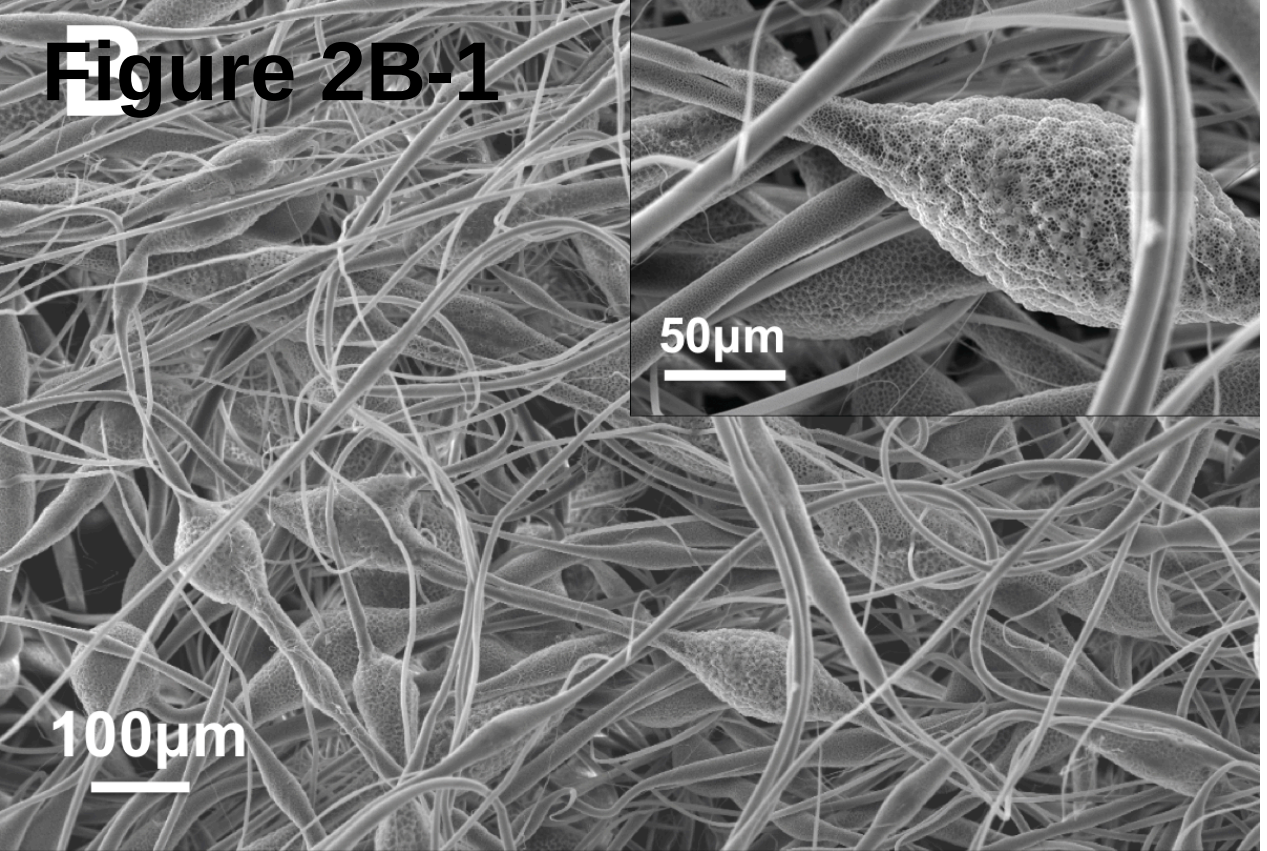
Figure 2B-1
50µm
100µm

Figure 2B-2

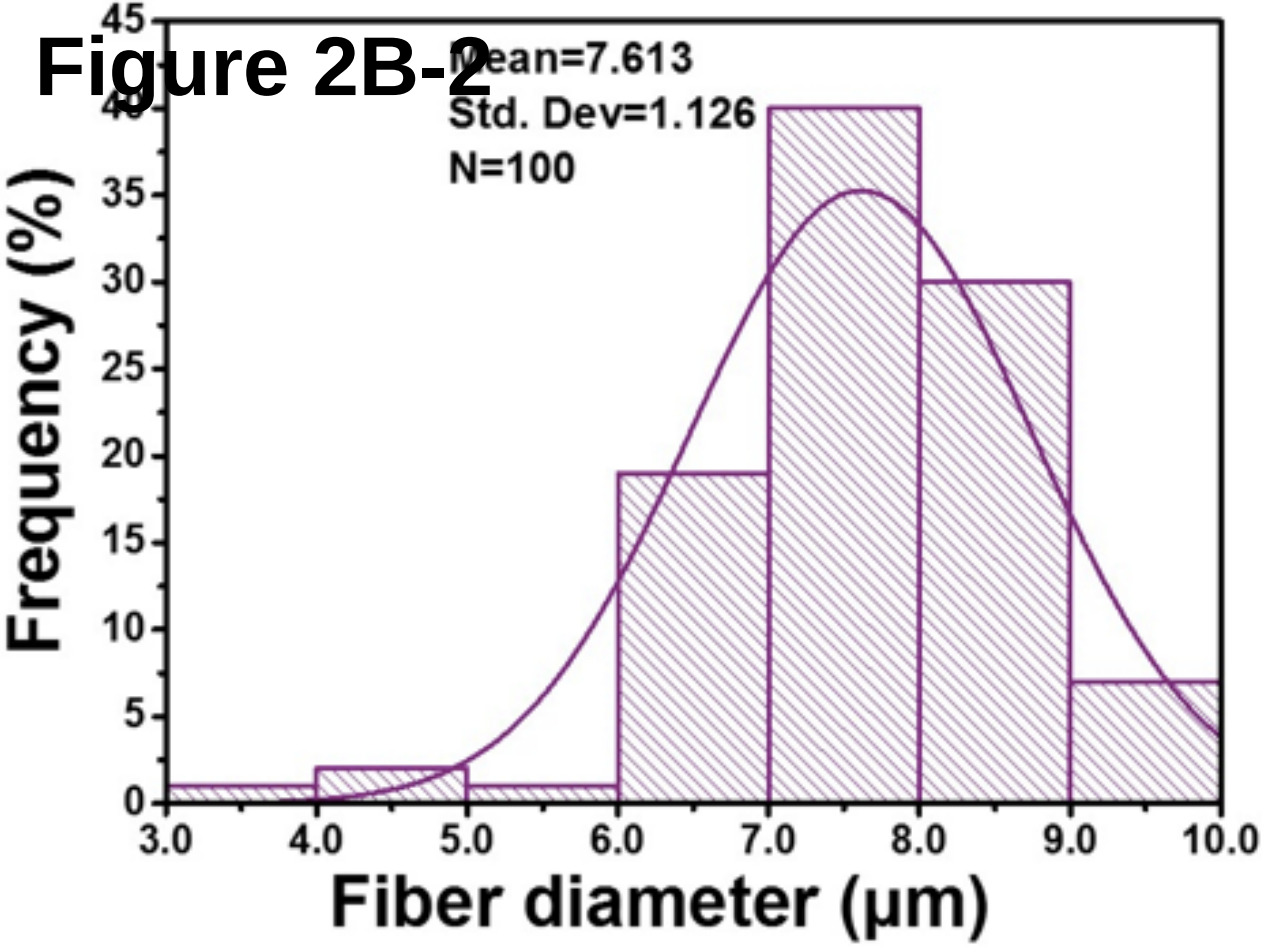
Mean=7.613
Std. Dev=1.126
N=100
Frequency (%)
0
5
10
15
20
25
30
35
40
45
3.0
4.0
5.0
6.0
7.0
8.0
9.0
10.0
Fiber diameter (μm)

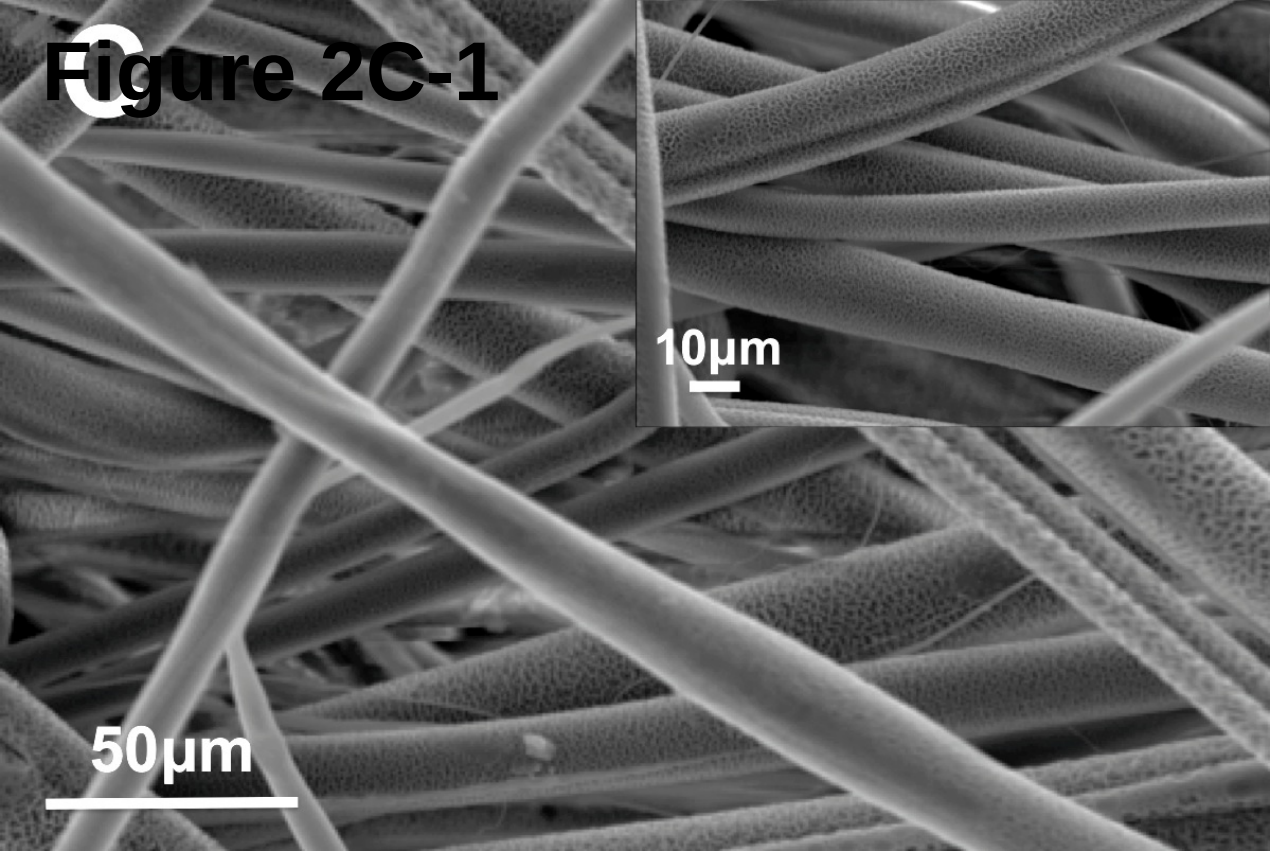
Figure 2C-1
10μm
50μm

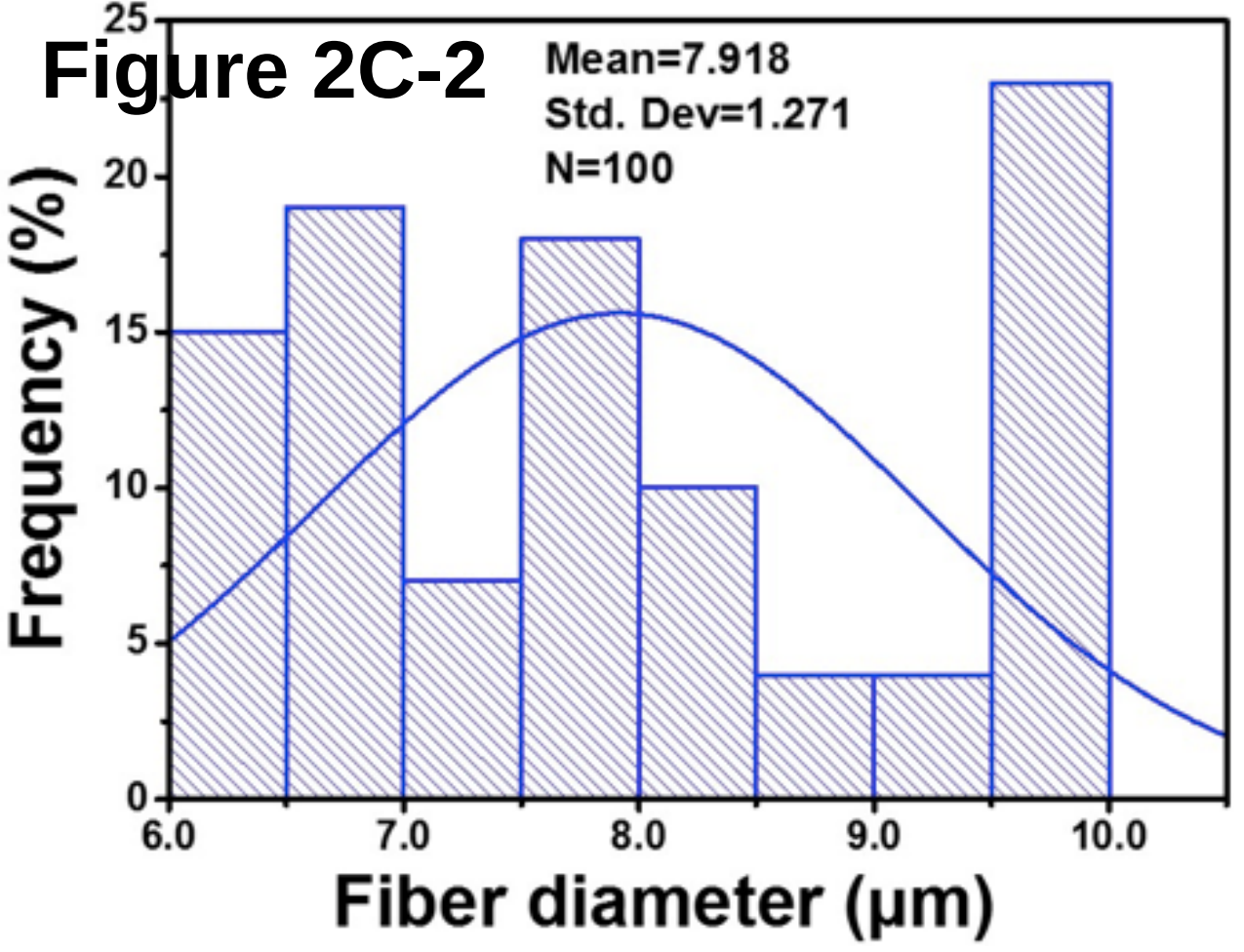
Figure 2C-2
Mean=7.918
Std. Dev=1.271
N=100
Frequency (%)
25
20
15
10
5
0
6.0
7.0
8.0
9.0
10.0
Fiber diameter (μm)

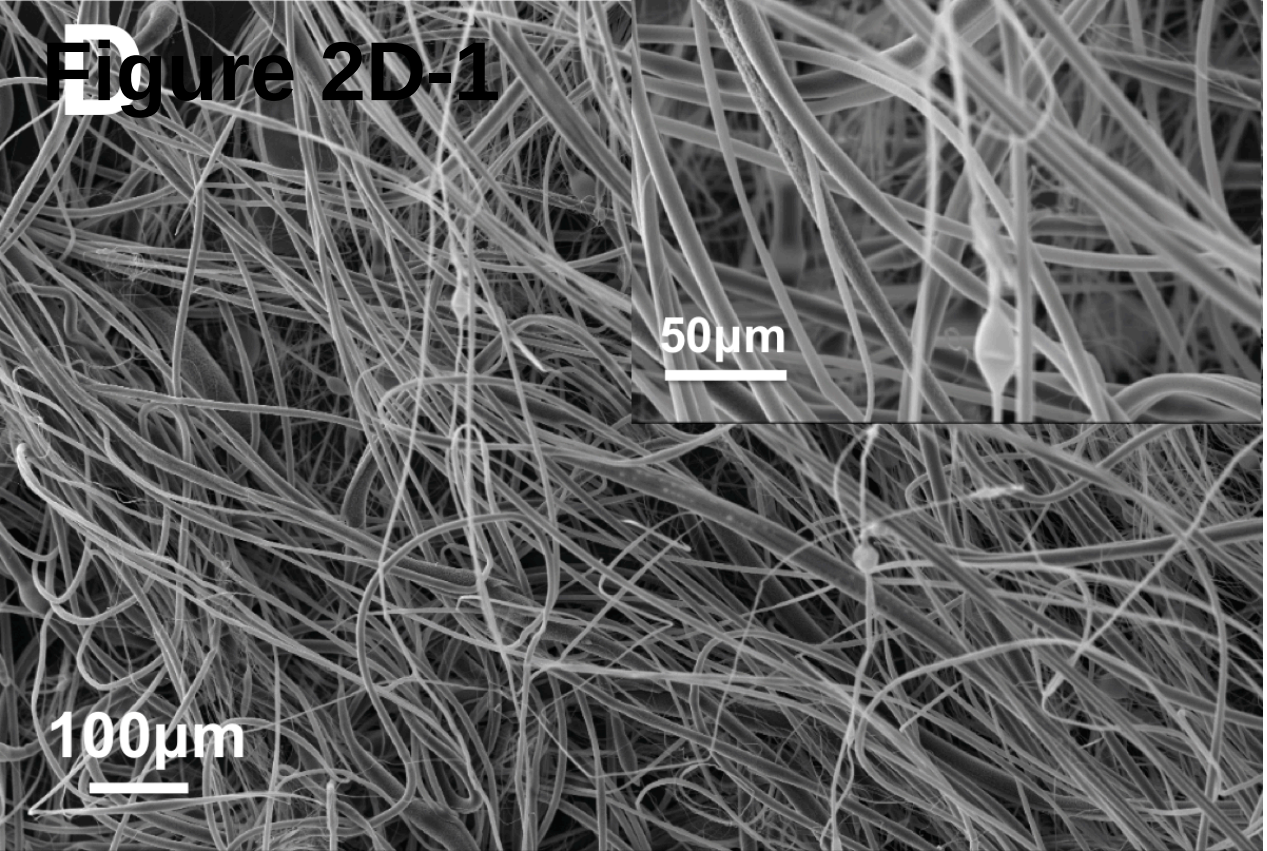
Figure 2D-1
50μm
100μm

Figure 2D-2

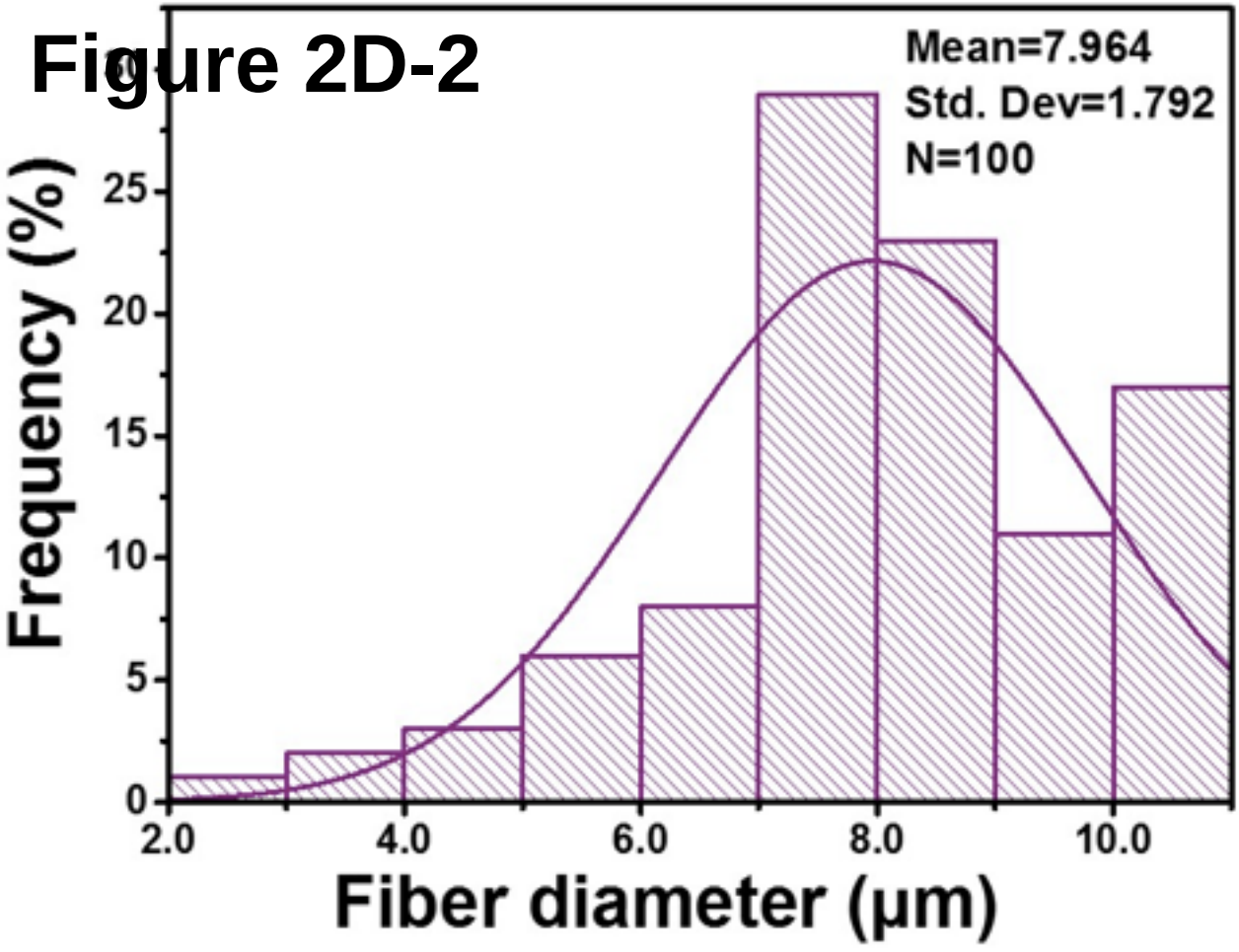
Mean=7.964
Std. Dev=1.792
N=100
Frequency (%)
0
5
10
15
20
25
2.0
4.0
6.0
8.0
10.0
Fiber diameter (μm)

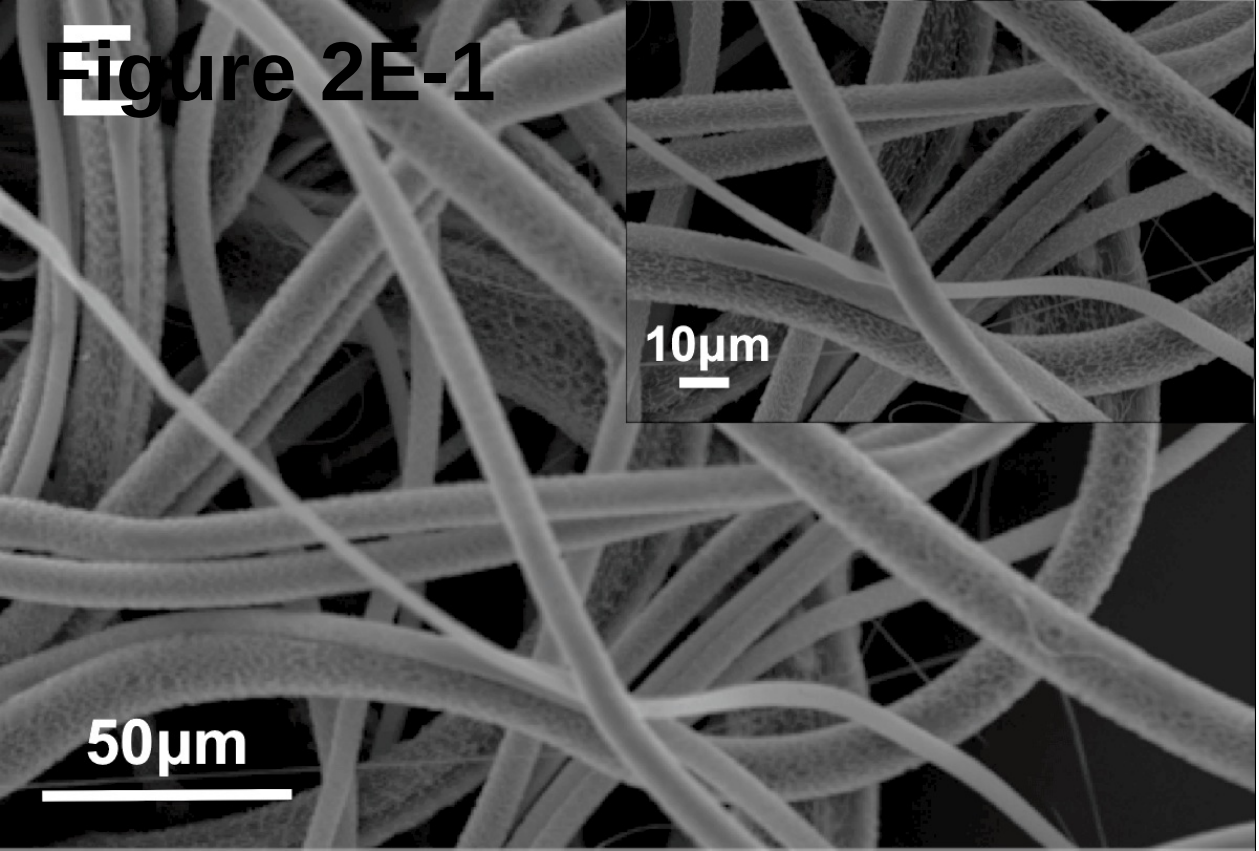
Figure 2E-1
10μm
50μm

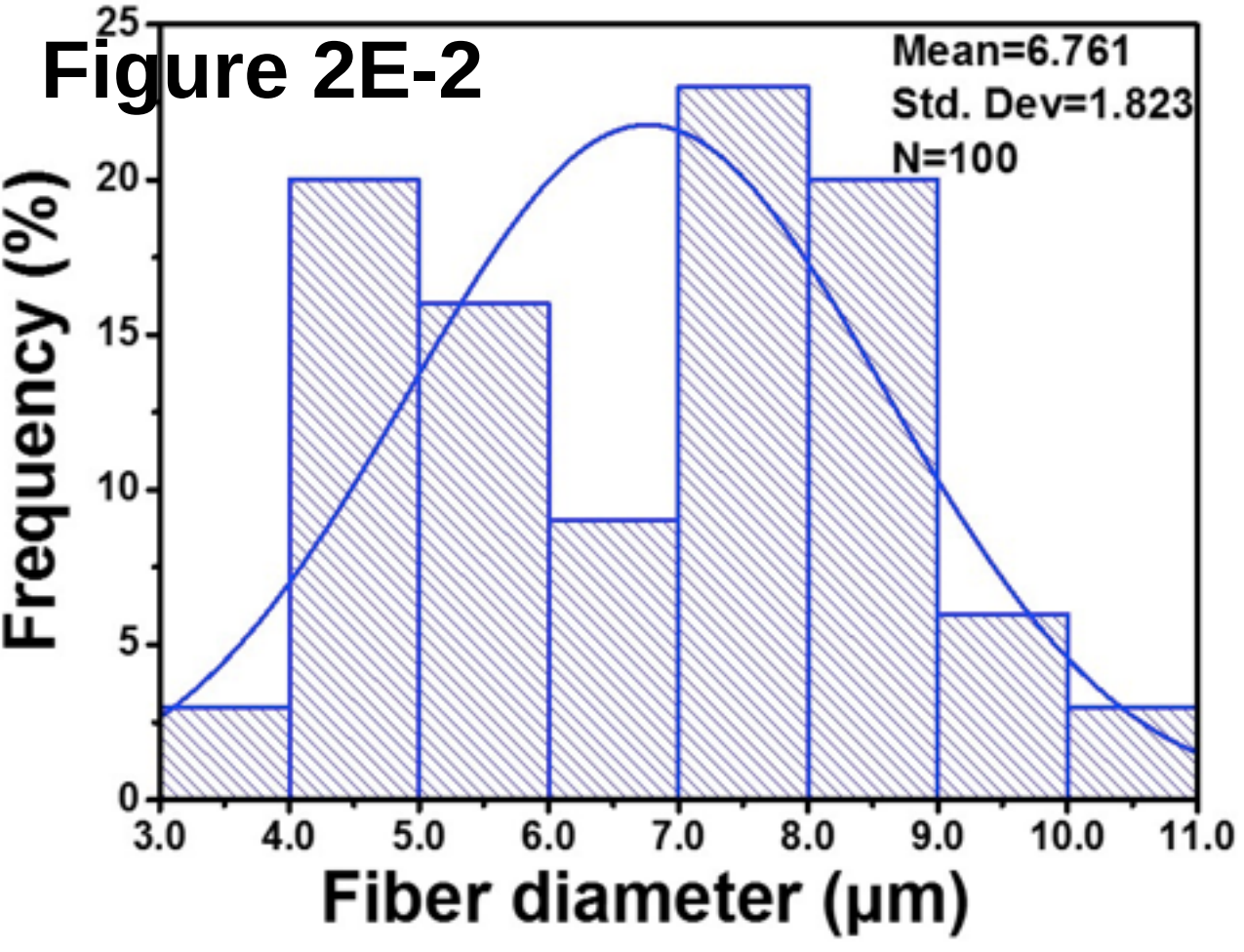
Figure 2E-2
Mean=6.761
Std. Dev=1.823
N=100
Frequency (%)
0
5
10
15
20
25
3.0
4.0
5.0
6.0
7.0
8.0
9.0
10.0
11.0
Fiber diameter (μm)

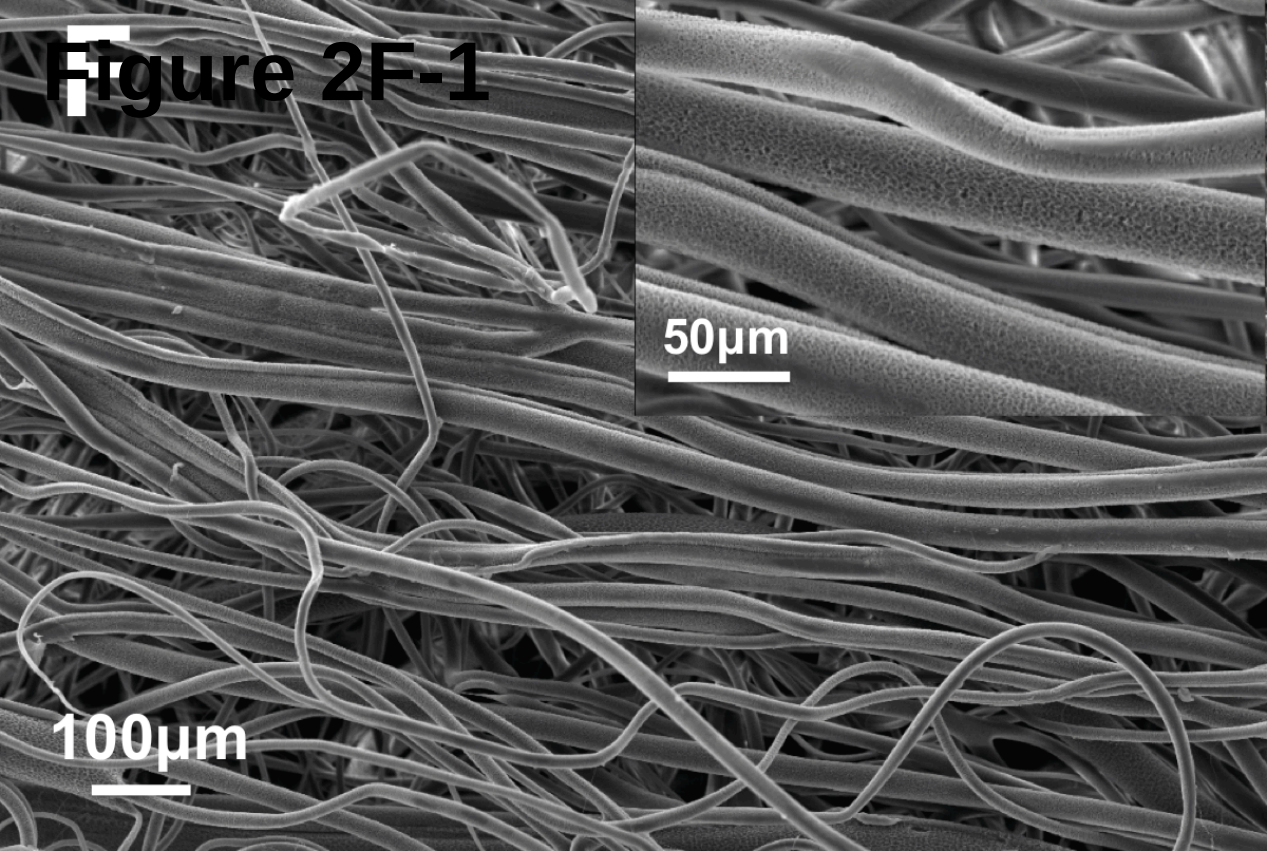
Figure 2F-1
50μm
100μm

Figure 2F-2

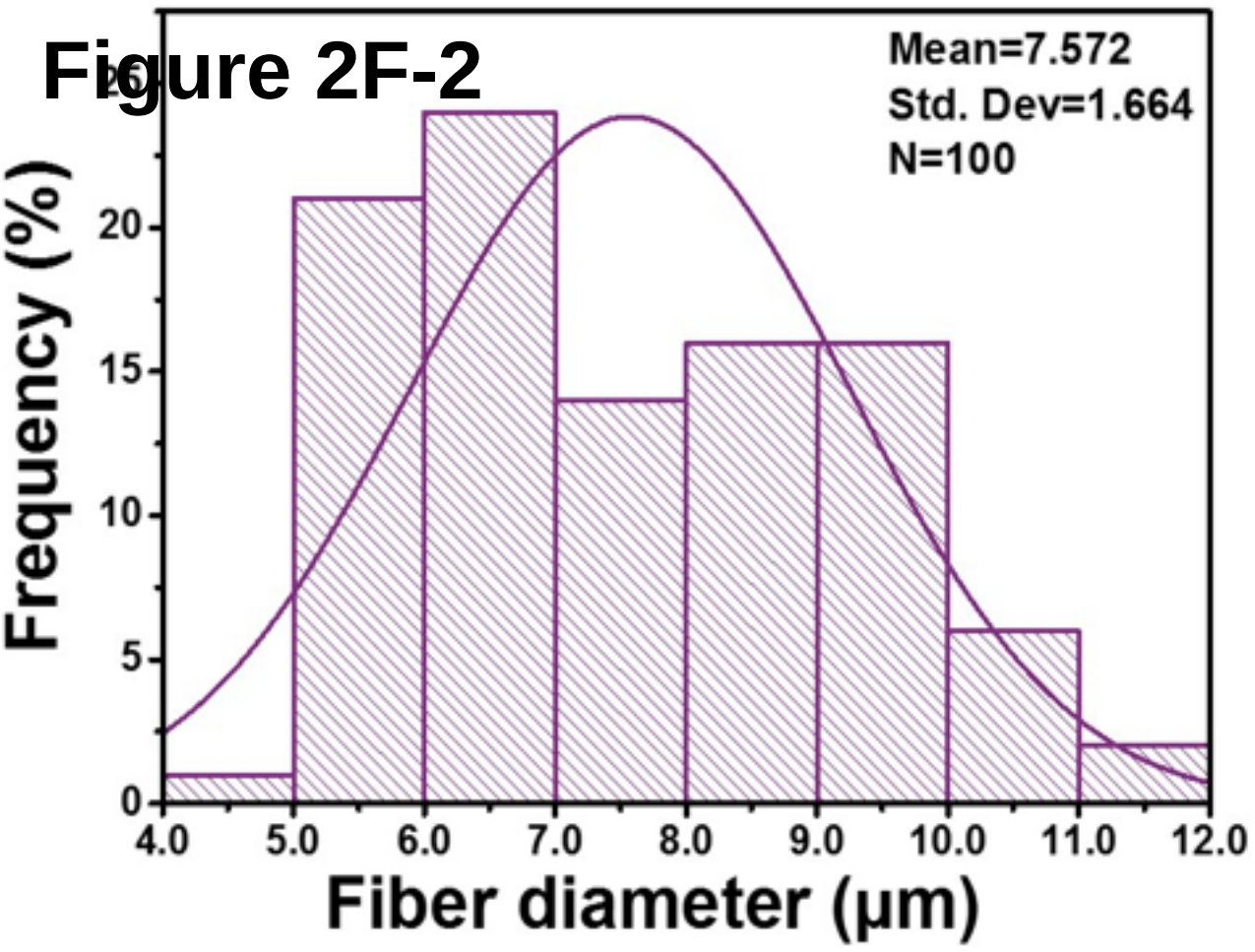
Mean=7.572
Std. Dev=1.664
N=100
Frequency (%)
0
5
10
15
20
4.0
5.0
6.0
7.0
8.0
9.0
10.0
11.0
12.0
Fiber diameter (μm)

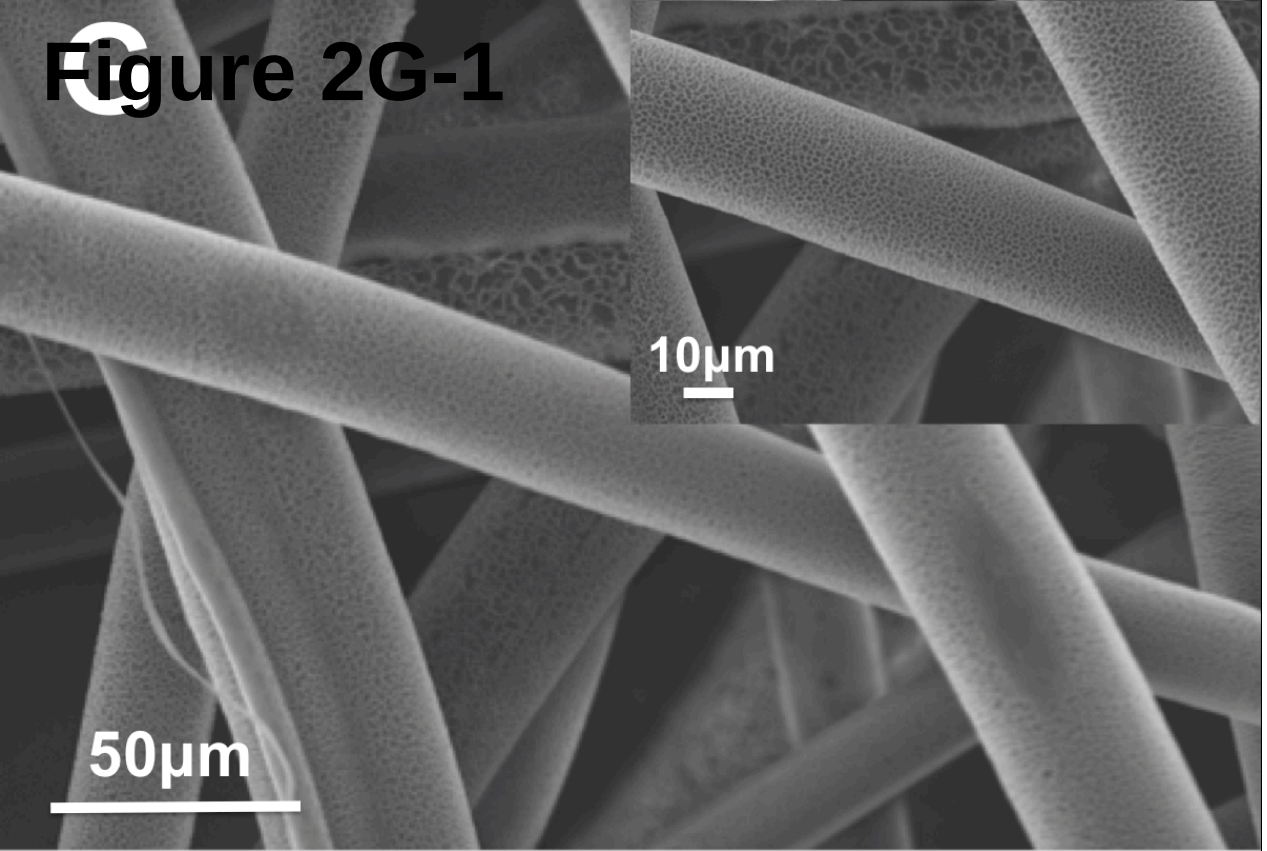
Figure 2G-1
10μm
50μm

Figure 2G-2

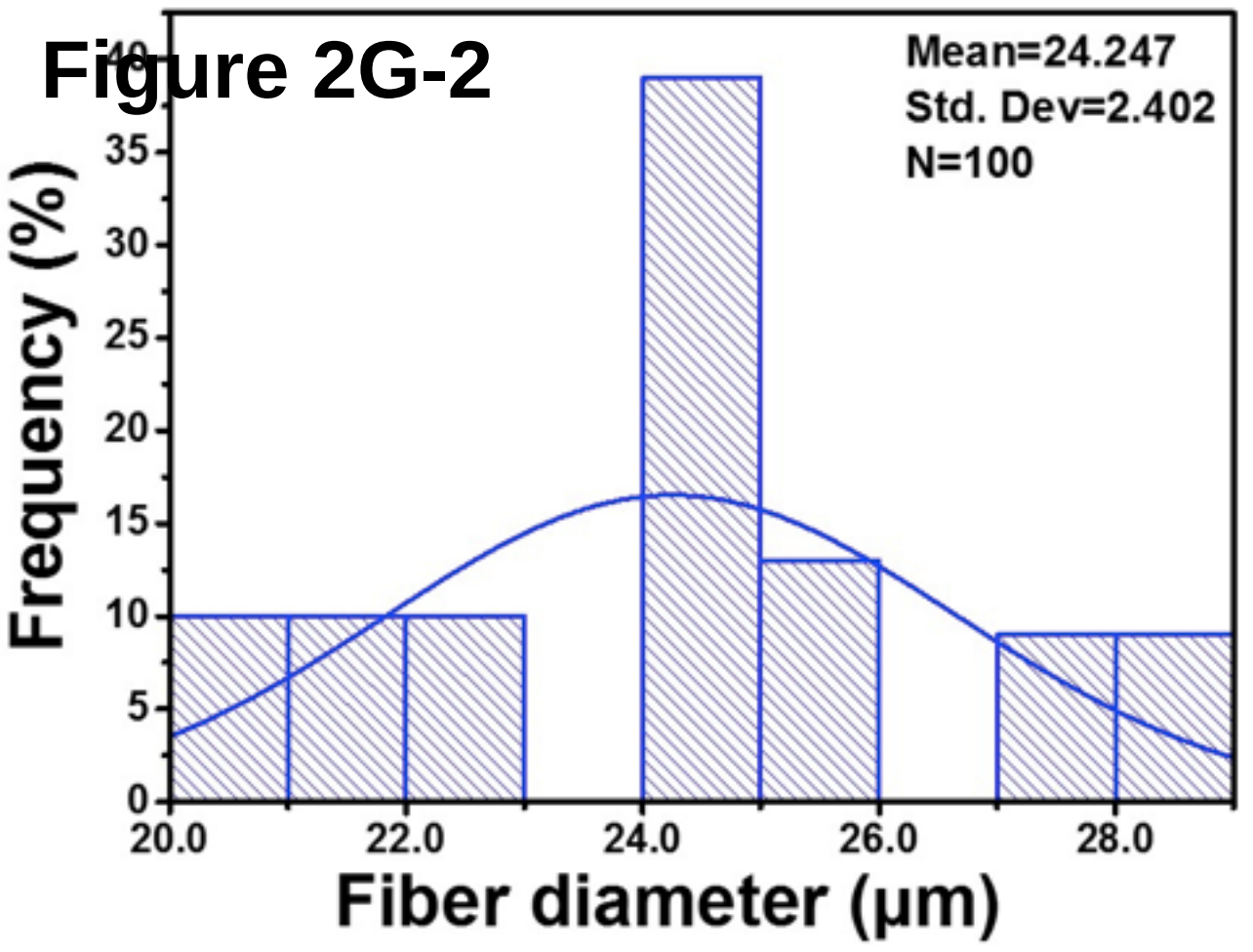
Mean=24.247
Std. Dev=2.402
N=100
Frequency (%)
0
5
10
15
20
25
30
35
40
20.0
22.0
24.0
26.0
28.0
Fiber diameter (μm)

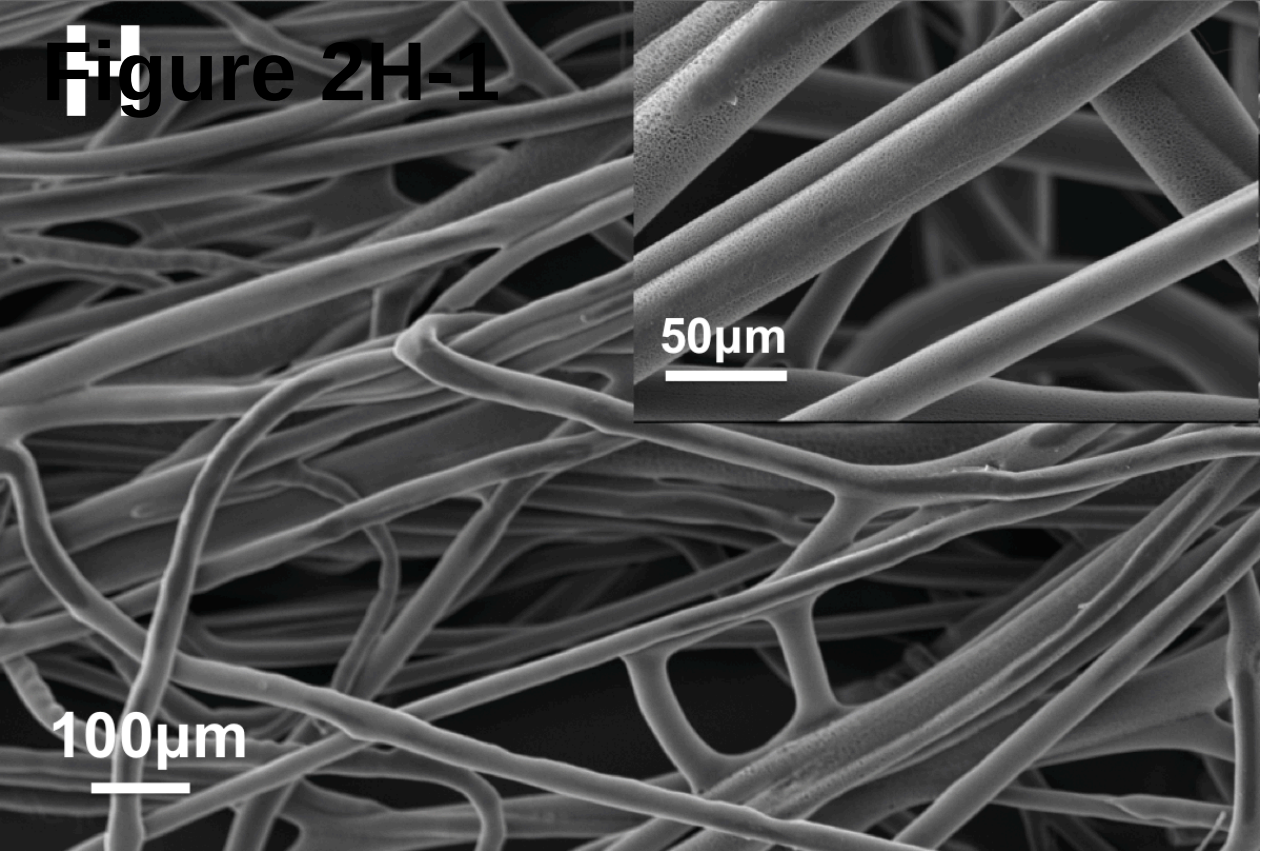
Figure 2H-1
50μm
100μm

Figure 2H-2

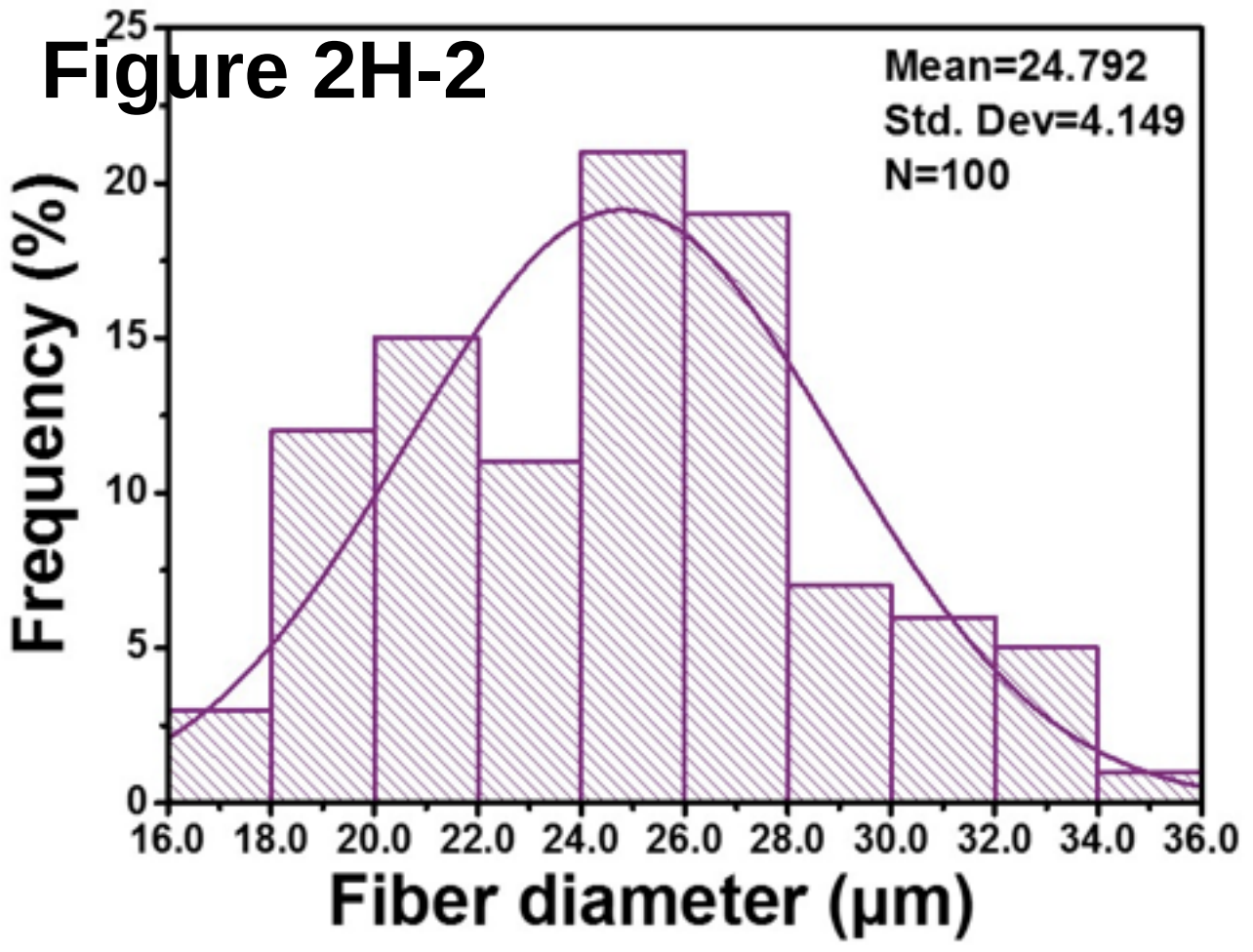
Mean=24.792
Std. Dev=4.149
N=100
Frequency (%)
0
5
10
15
20
25
16.0
18.0
20.0
22.0
24.0
26.0
28.0
30.0
32.0
34.0
36.0
Fiber diameter (μm)

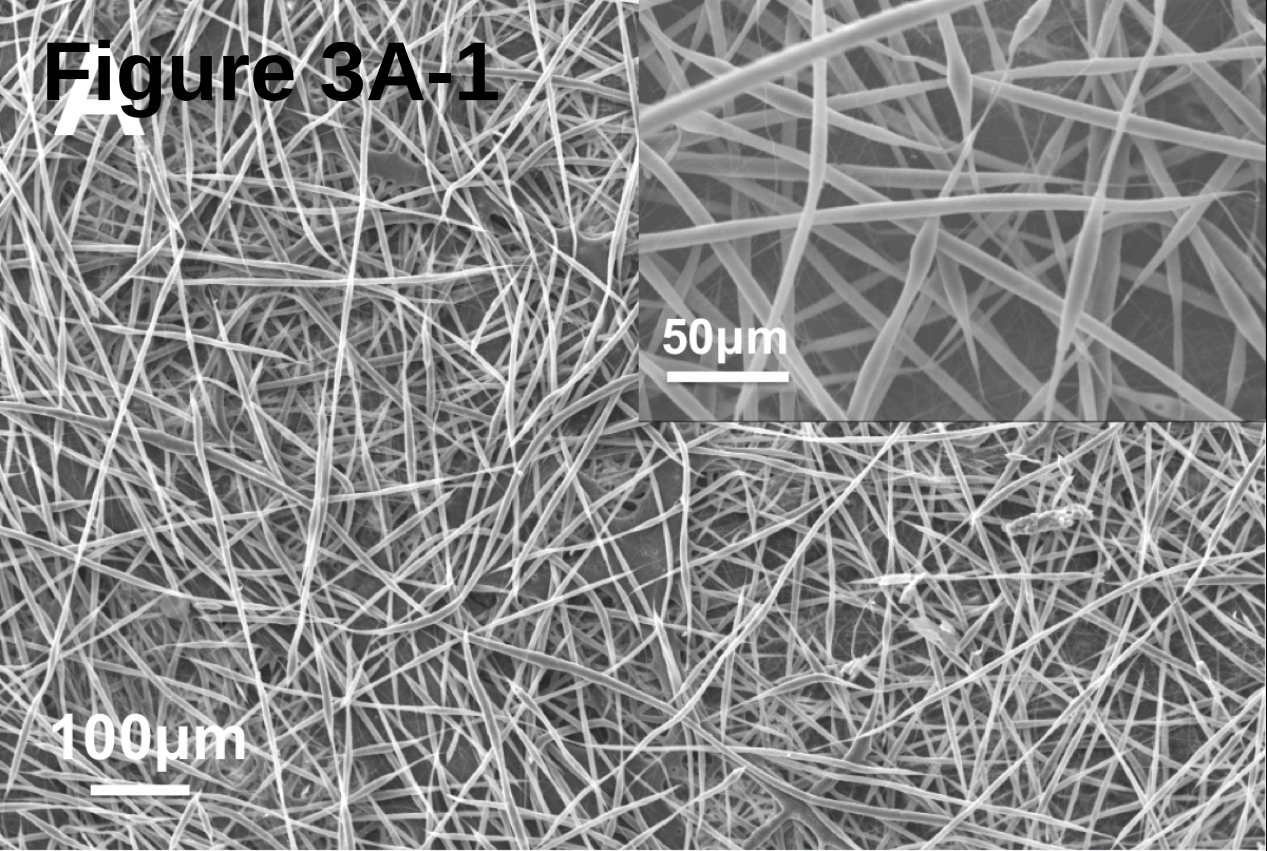
Figure 3A-1
50μm
100μm

Figure 3A-2

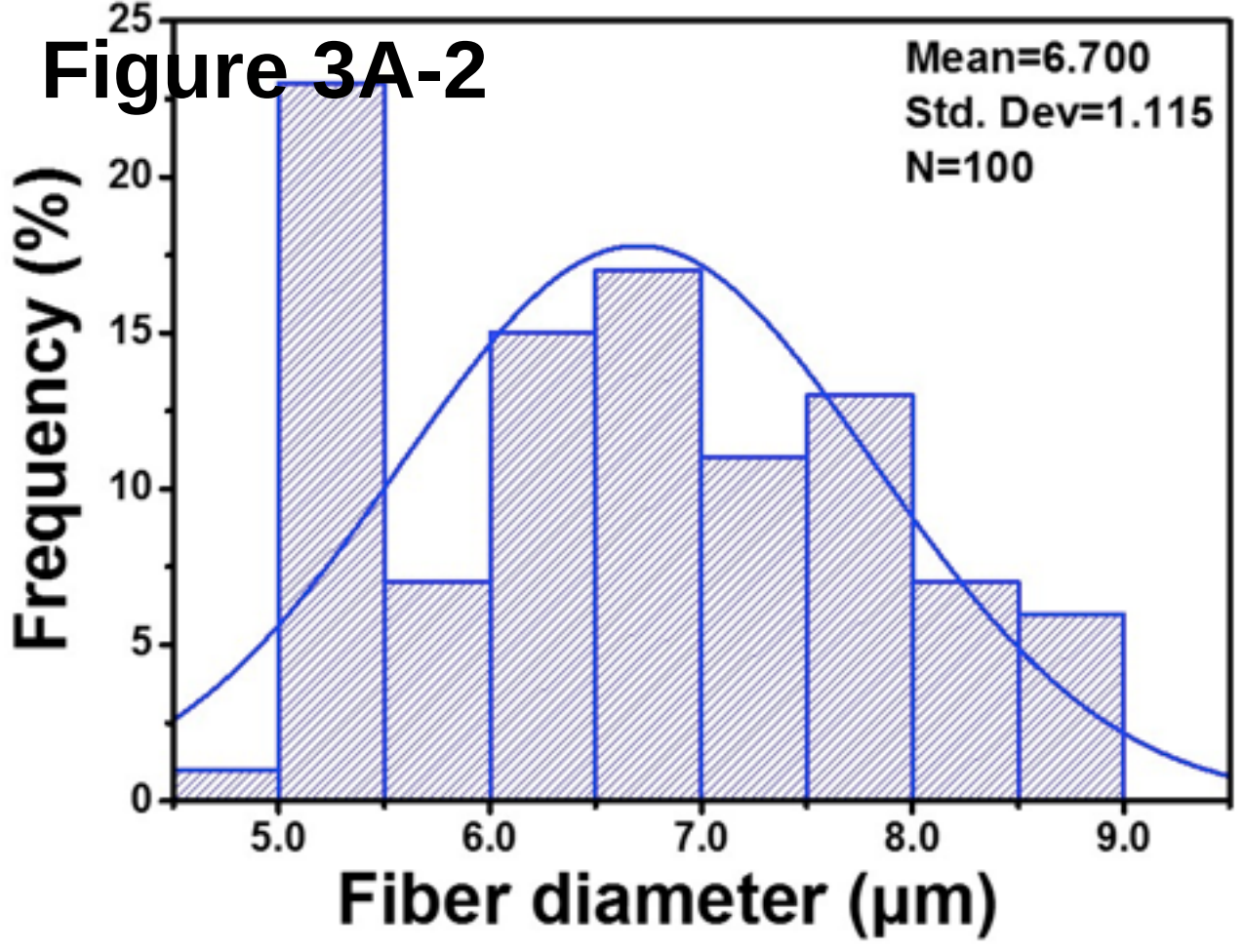
Mean=6.700
Std. Dev=1.115
N=100
Frequency (%)
0
5
10
15
20
25
5.0
6.0
7.0
8.0
9.0
Fiber diameter (μm)

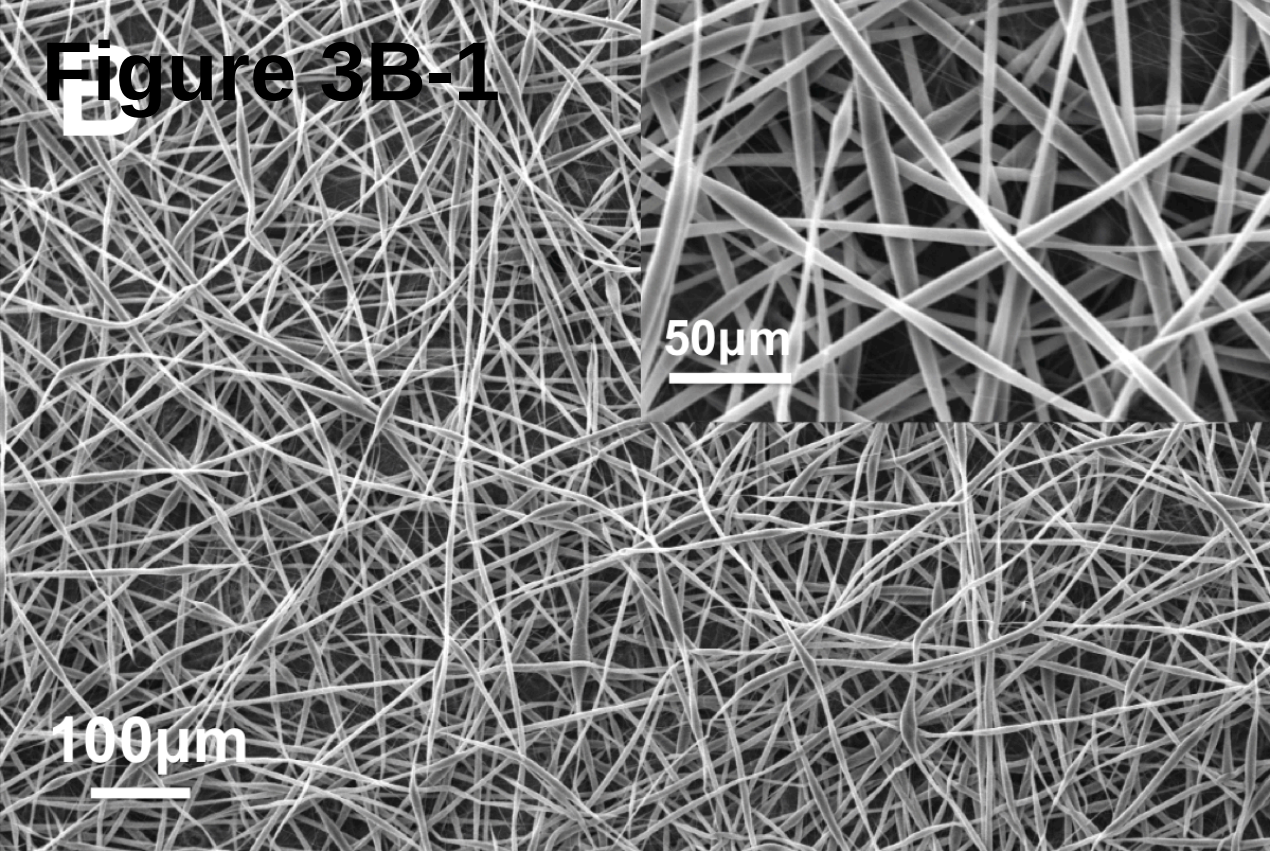
Figure 3B-1
50μm
100μm

Figure 3B-2

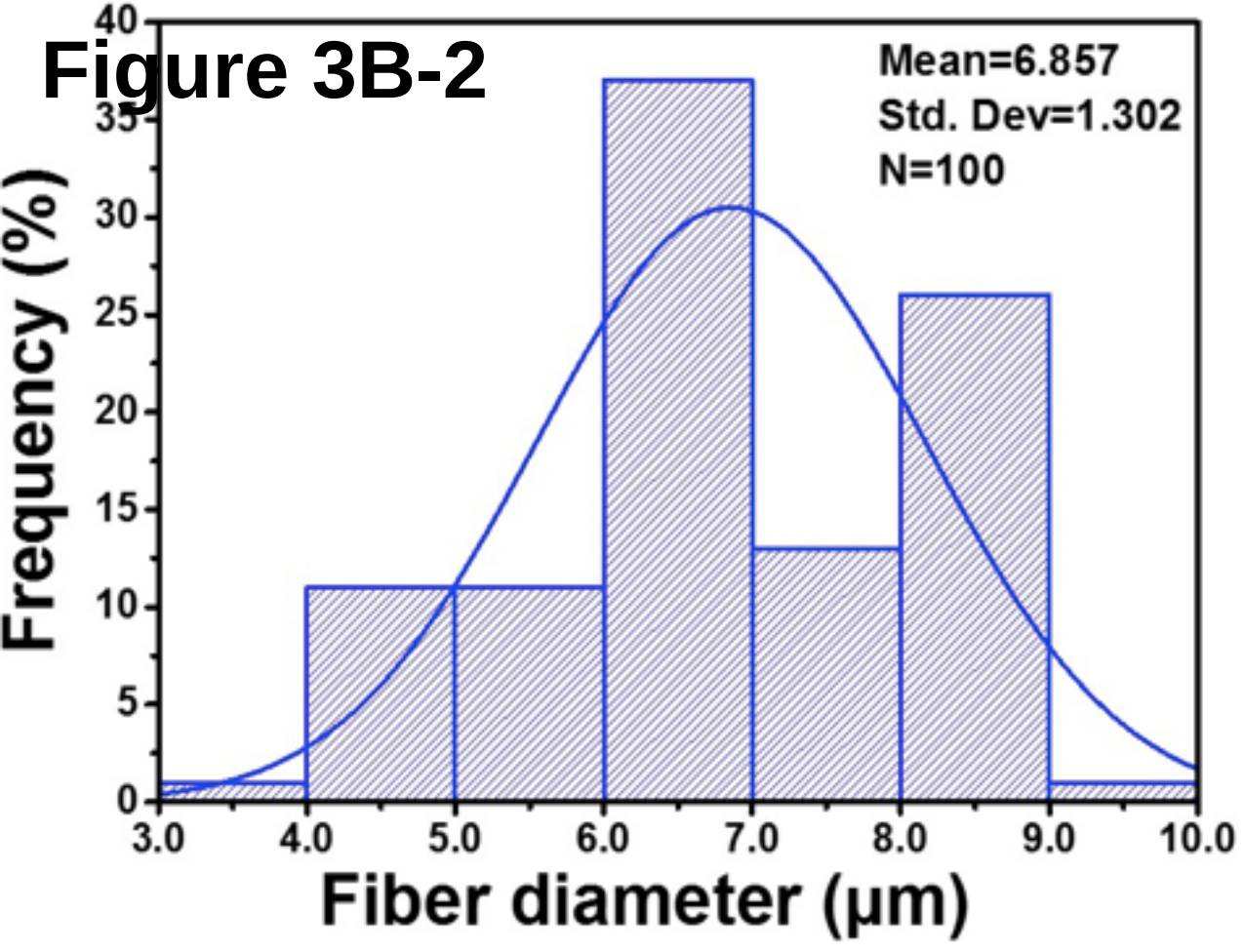
Mean=6.857
Std. Dev=1.302
N=100
Frequency (%)
0
5
10
15
20
25
30
35
40
3.0
4.0
5.0
6.0
7.0
8.0
9.0
10.0
Fiber diameter (μm)

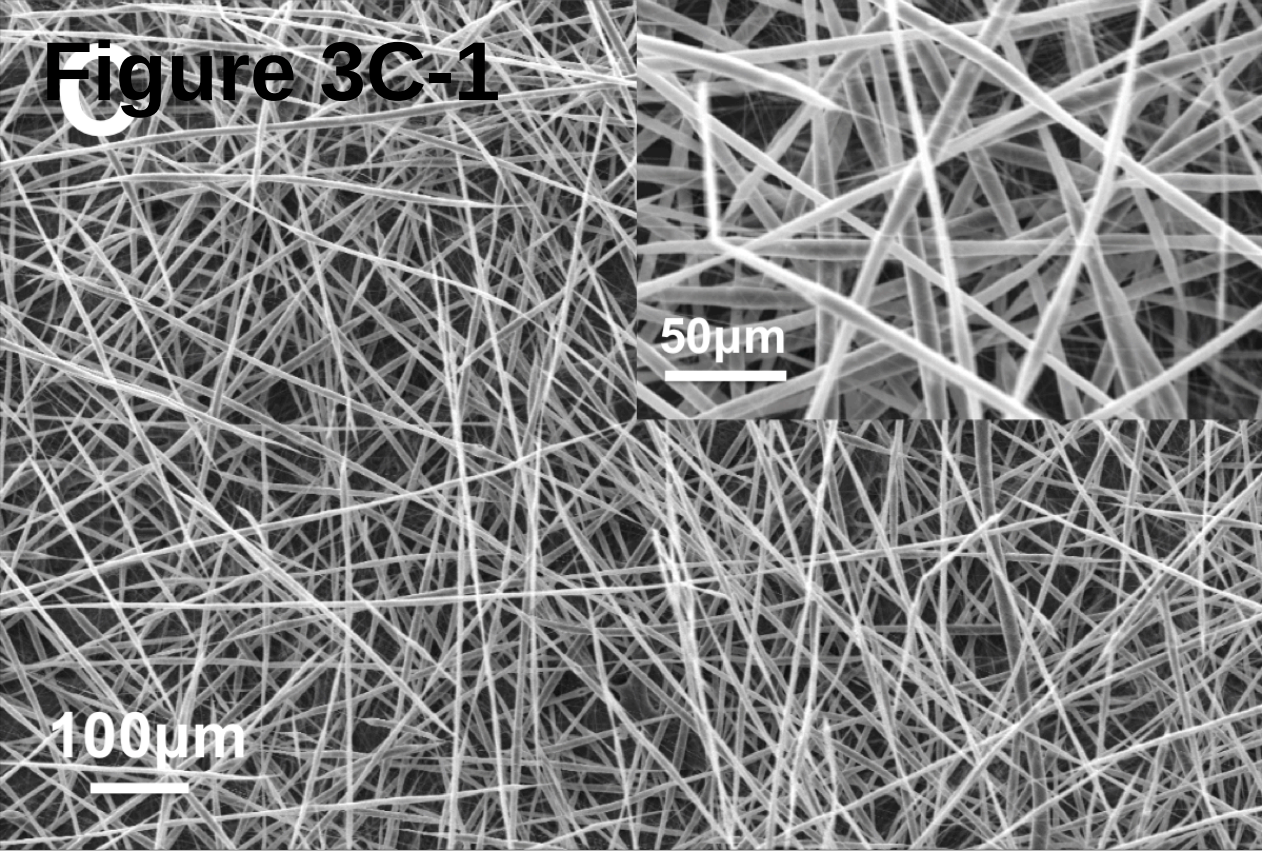
Figure 3C-1
50μm
100μm

Figure 3C-2

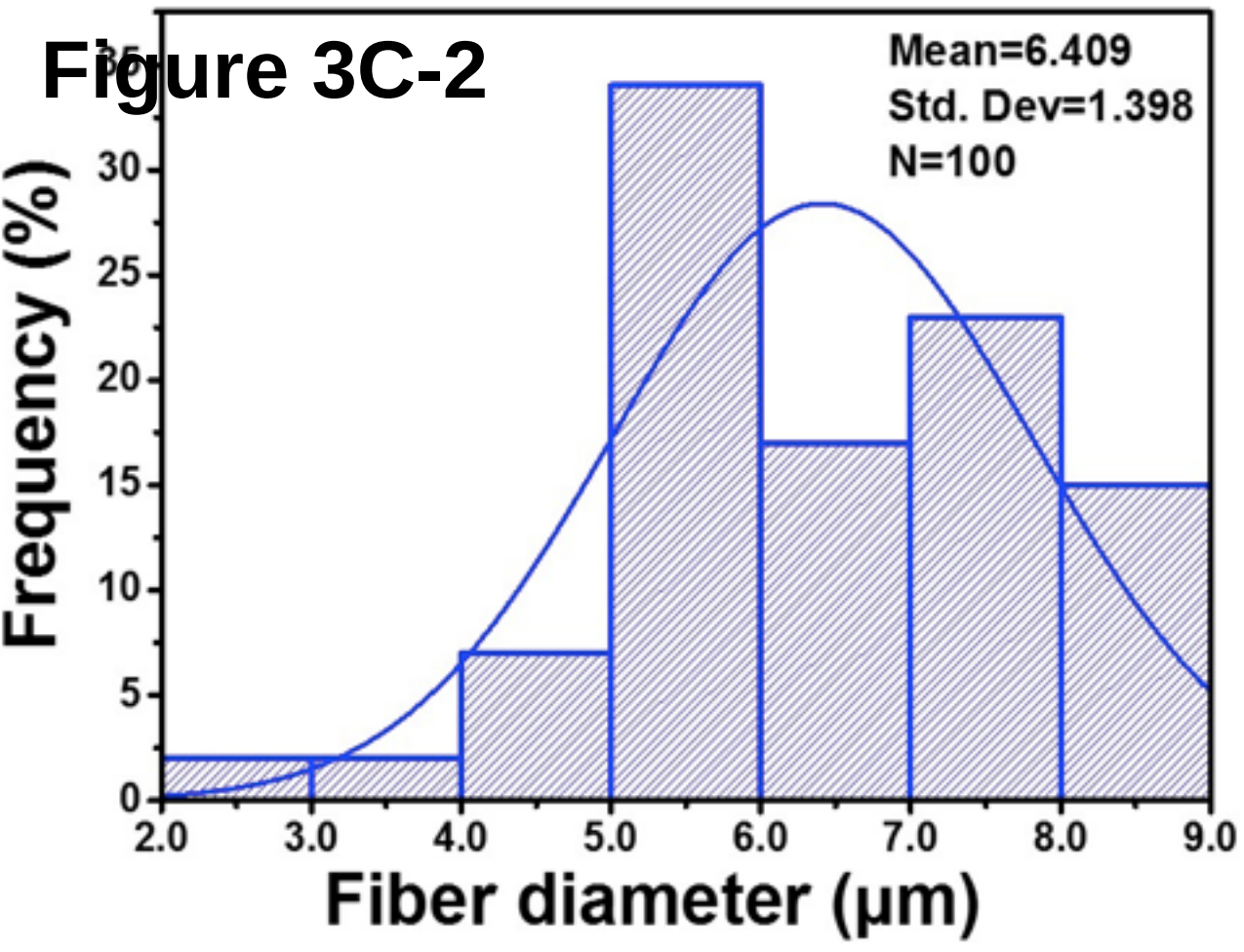
Mean=6.409
Std. Dev=1.398
N=100
Frequency (%)
0
5
10
15
20
25
30
2.0
3.0
4.0
5.0
6.0
7.0
8.0
9.0
Fiber diameter (μm)

Figure 3D-1

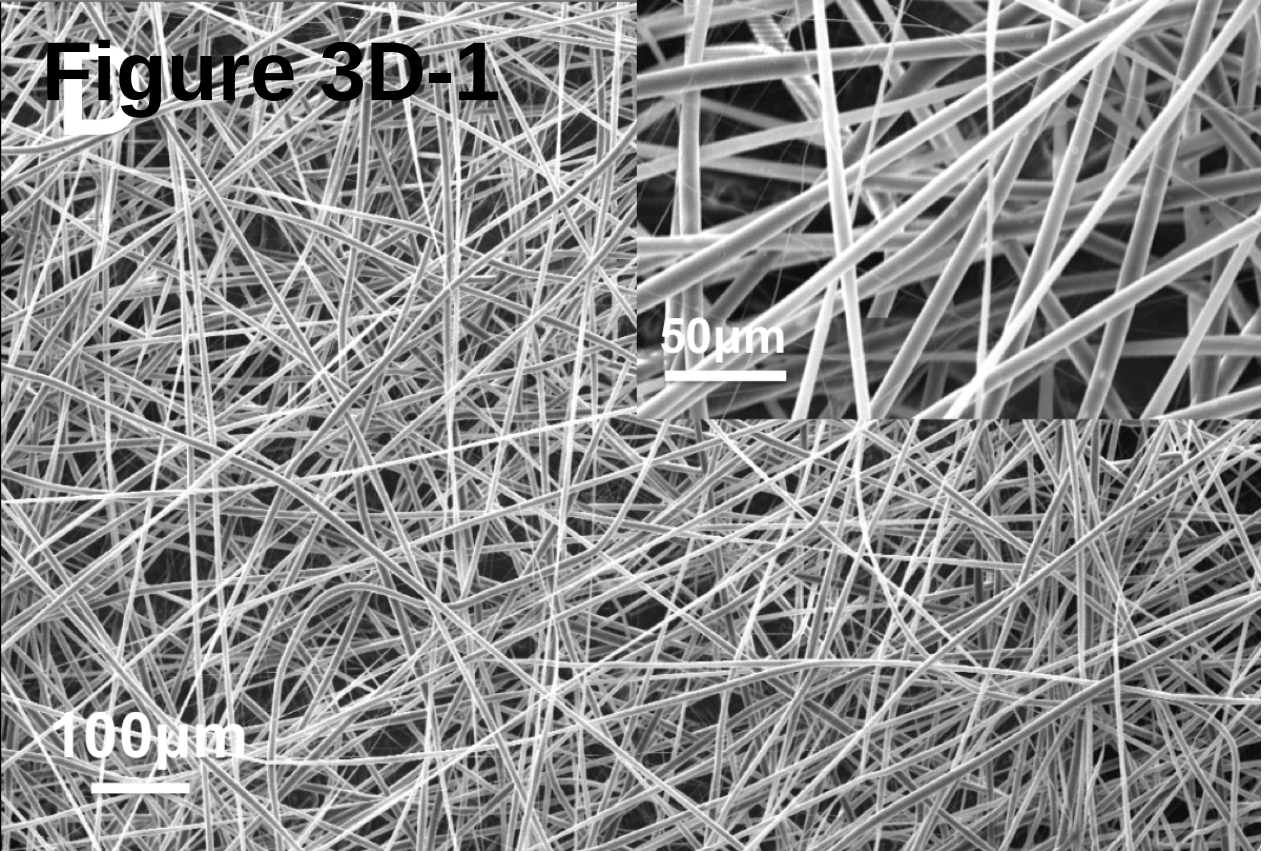

Figure 3D-2

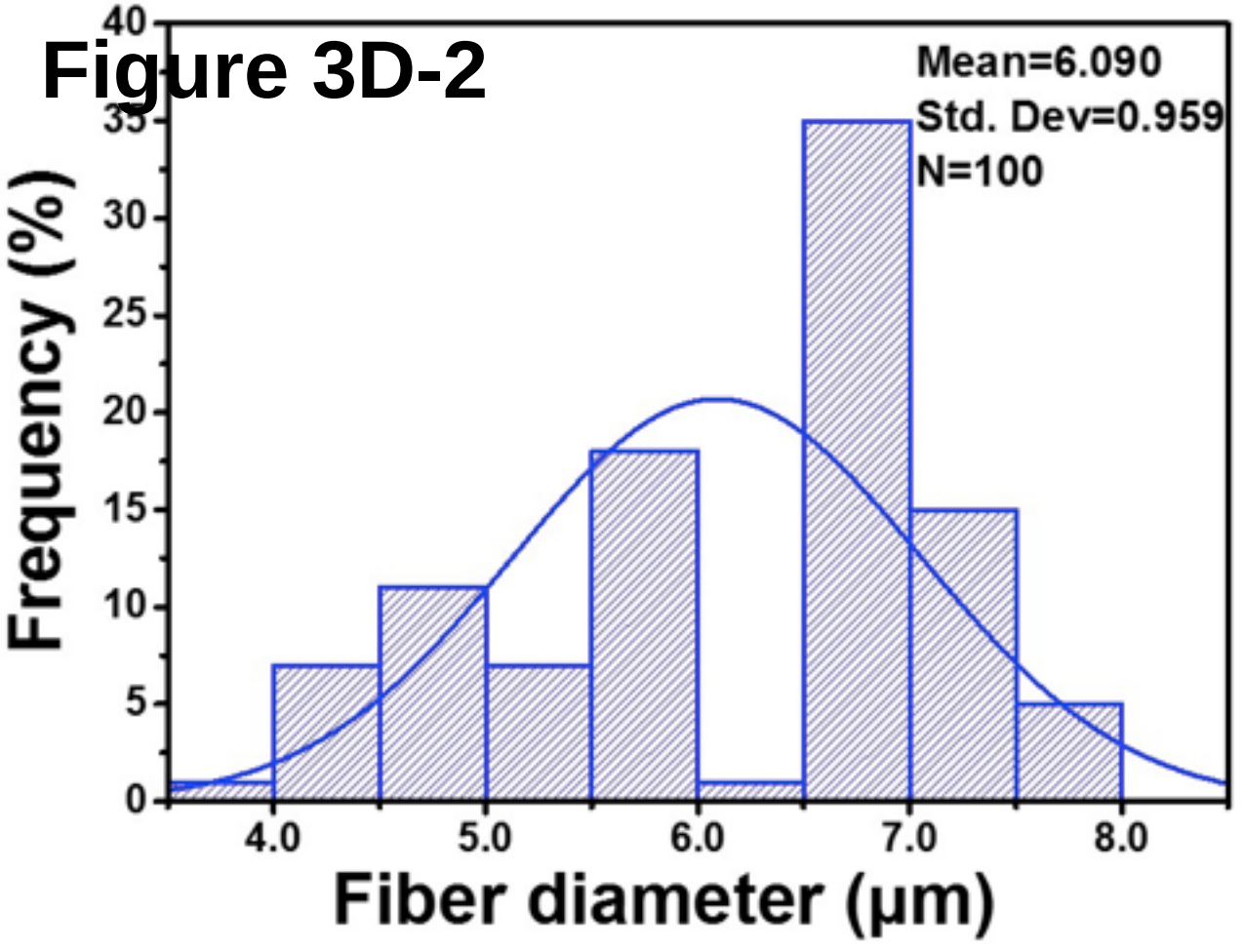
Mean=6.090
Std. Dev=0.959
N=100
Frequency (%)
0
5
10
15
20
25
30
35
40
4.0
5.0
6.0
7.0
8.0
Fiber diameter (μm)

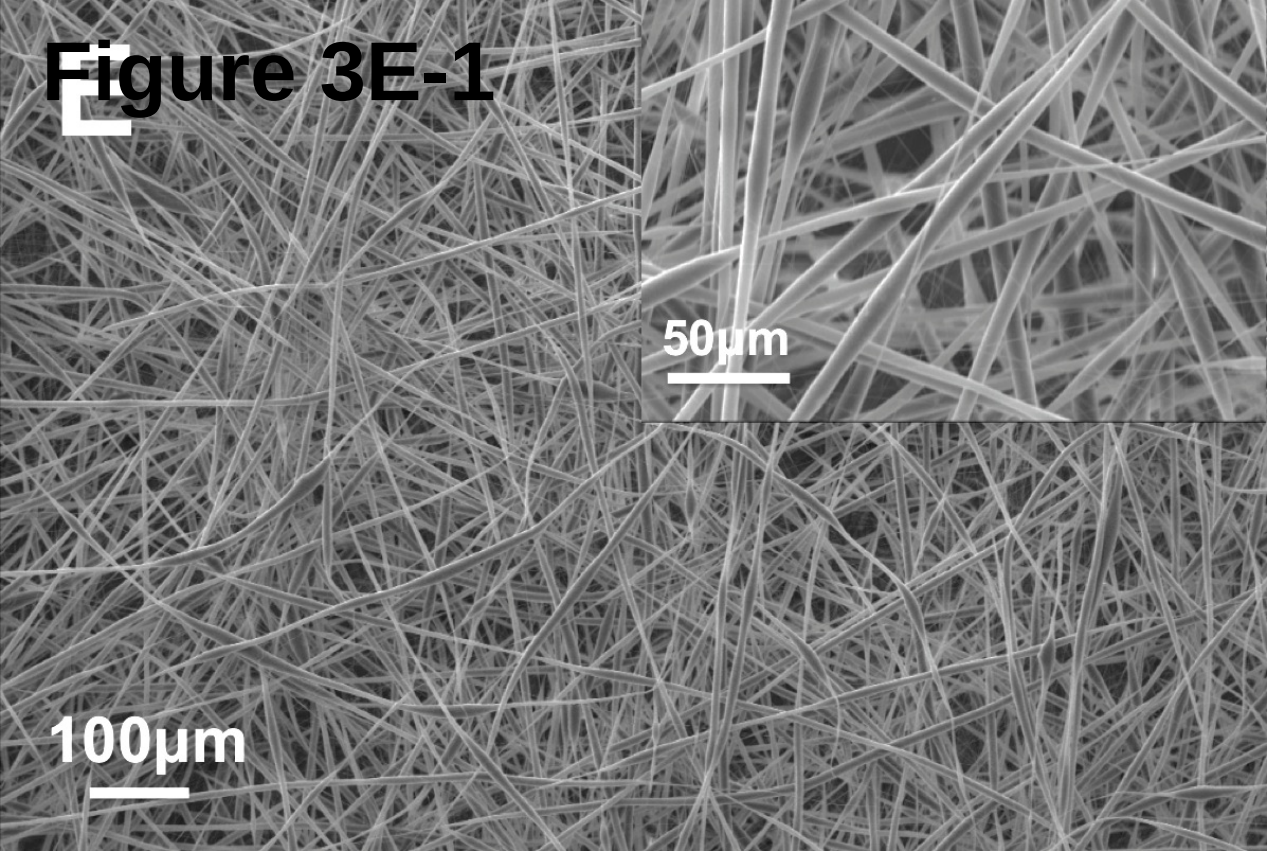
Figure 3E-1
50μm
100μm

Figure 3E-2

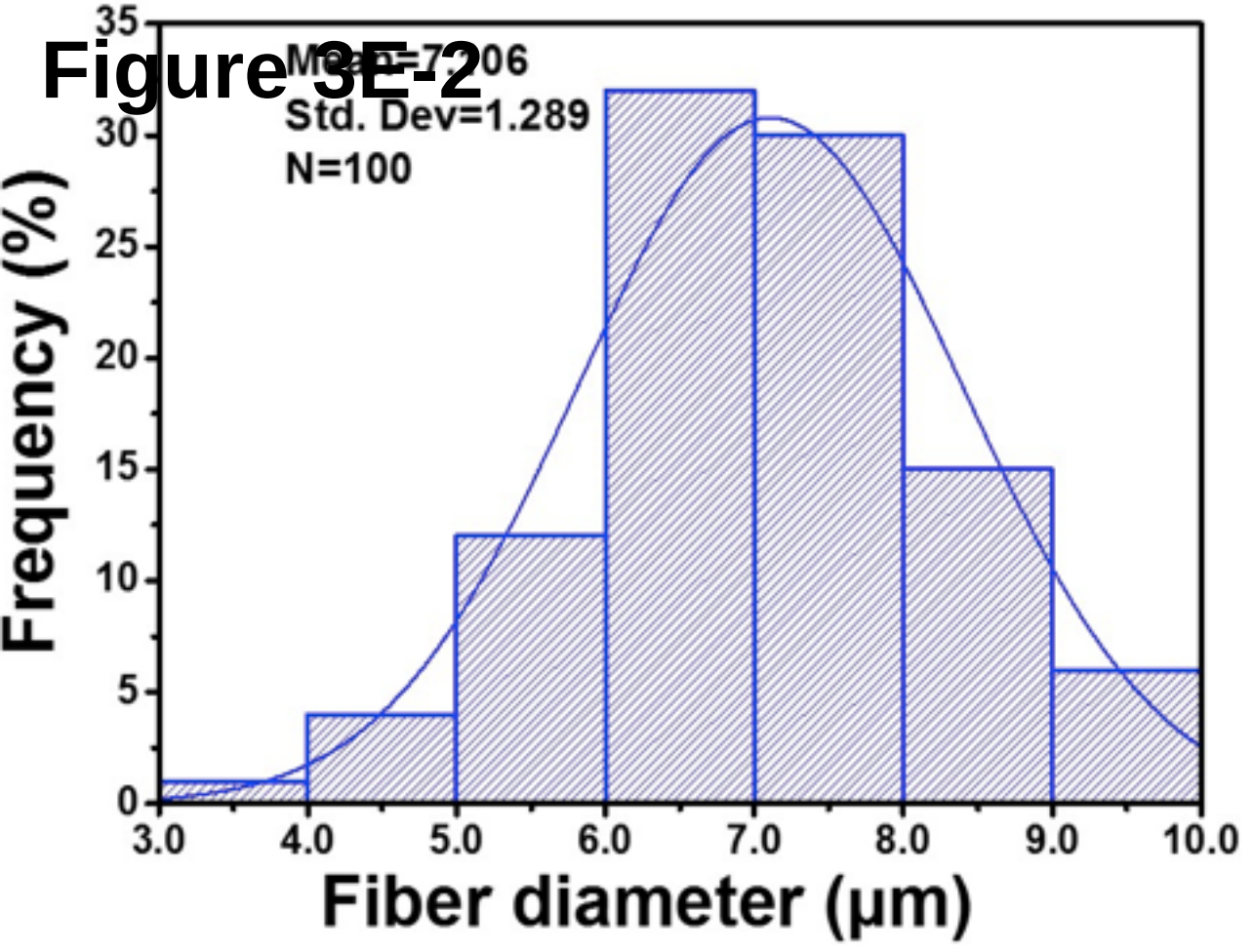
Std. Dev=1.289
N=100
Frequency (%)
0
5
10
15
20
25
30
35
3.0
4.0
5.0
6.0
7.0
8.0
9.0
10.0
Fiber diameter (μm)

Figure 3F-1

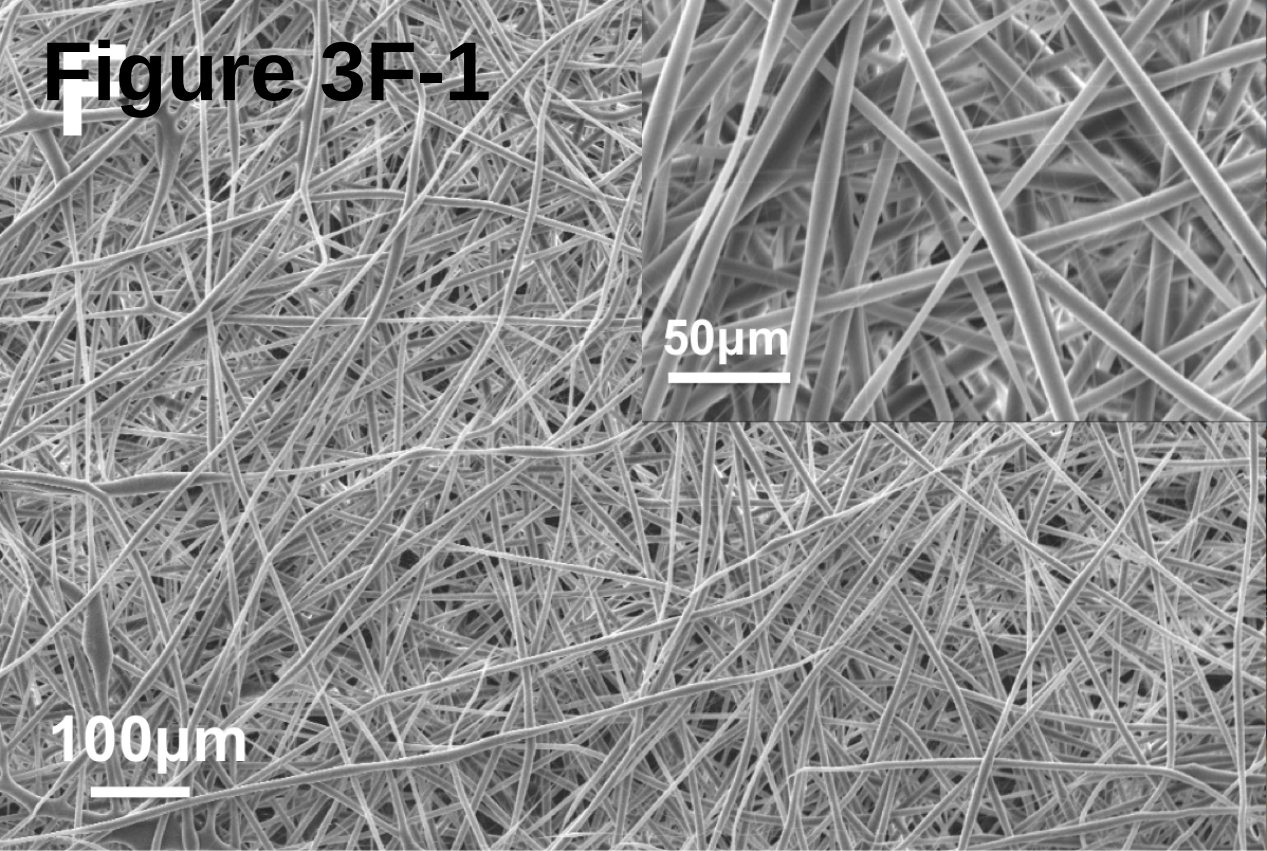

Figure 3F-2

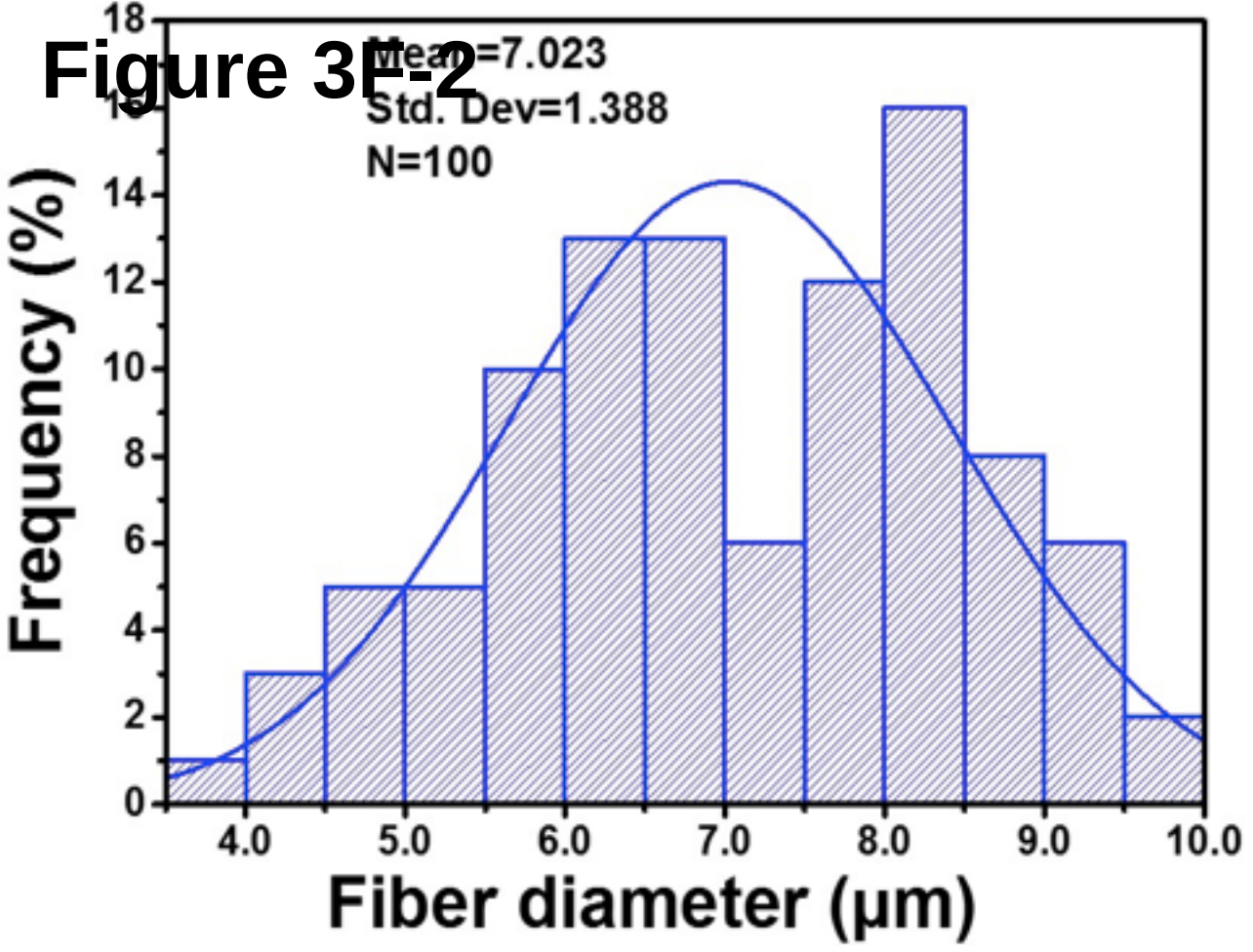
Mean=7.023
Std. Dev=1.388
N=100
Frequency (%)
0
2
4
6
8
10
12
14
18
4.0
5.0
6.0
7.0
8.0
9.0
10.0
Fiber diameter (μm)

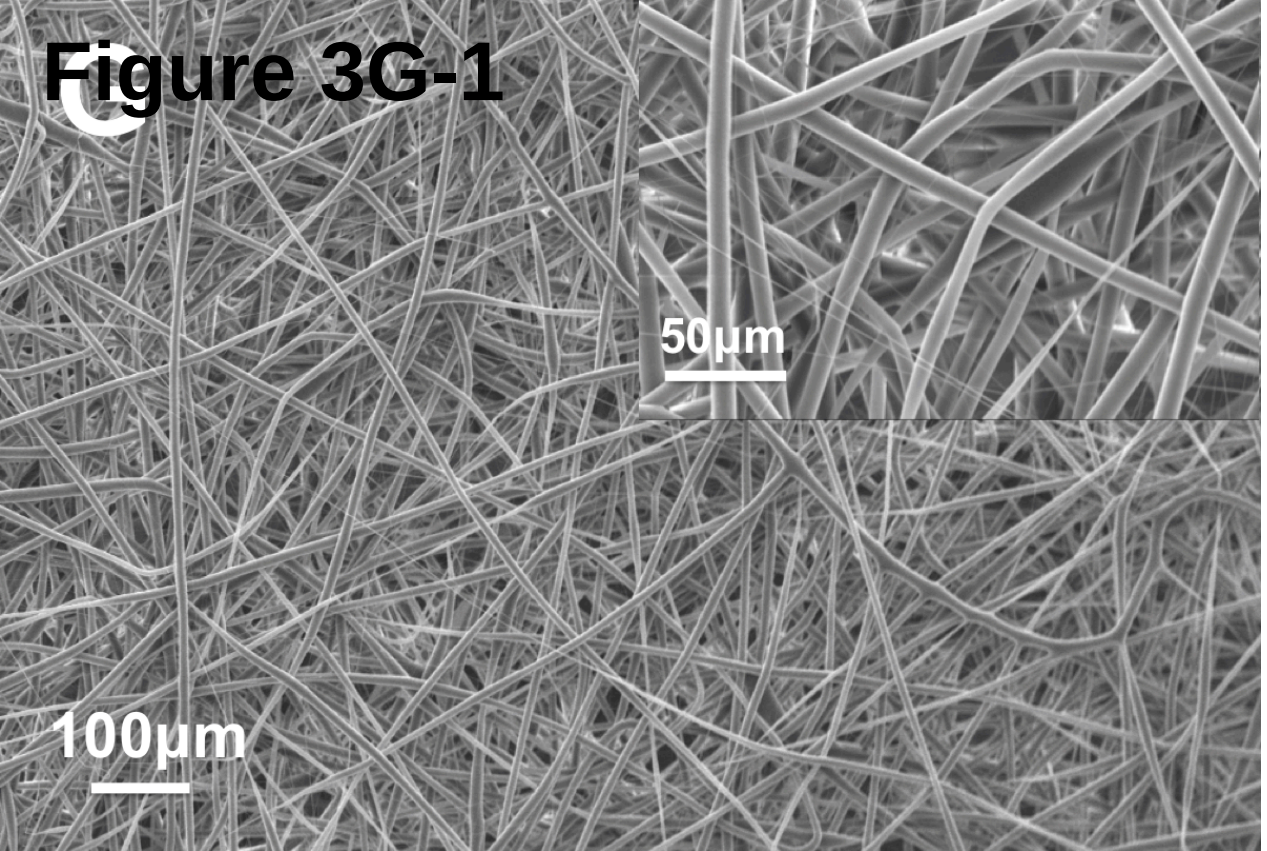
Figure 3G-1
50μm
100μm

Figure 3G-2

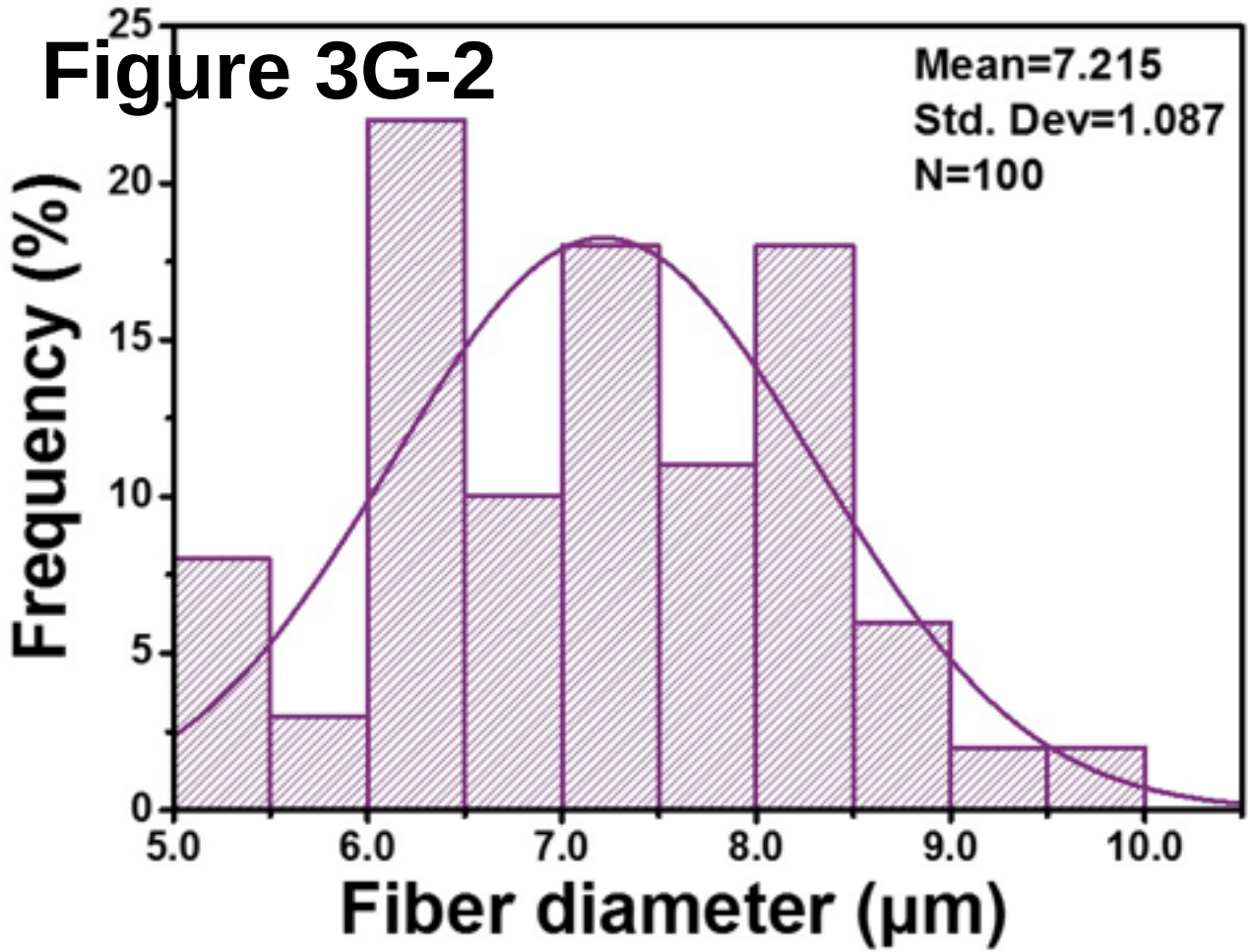
Mean=7.215
Std. Dev=1.087
N=100
Frequency (%)
0
5
10
15
20
25
5.0
6.0
7.0
8.0
9.0
10.0
Fiber diameter (μm)

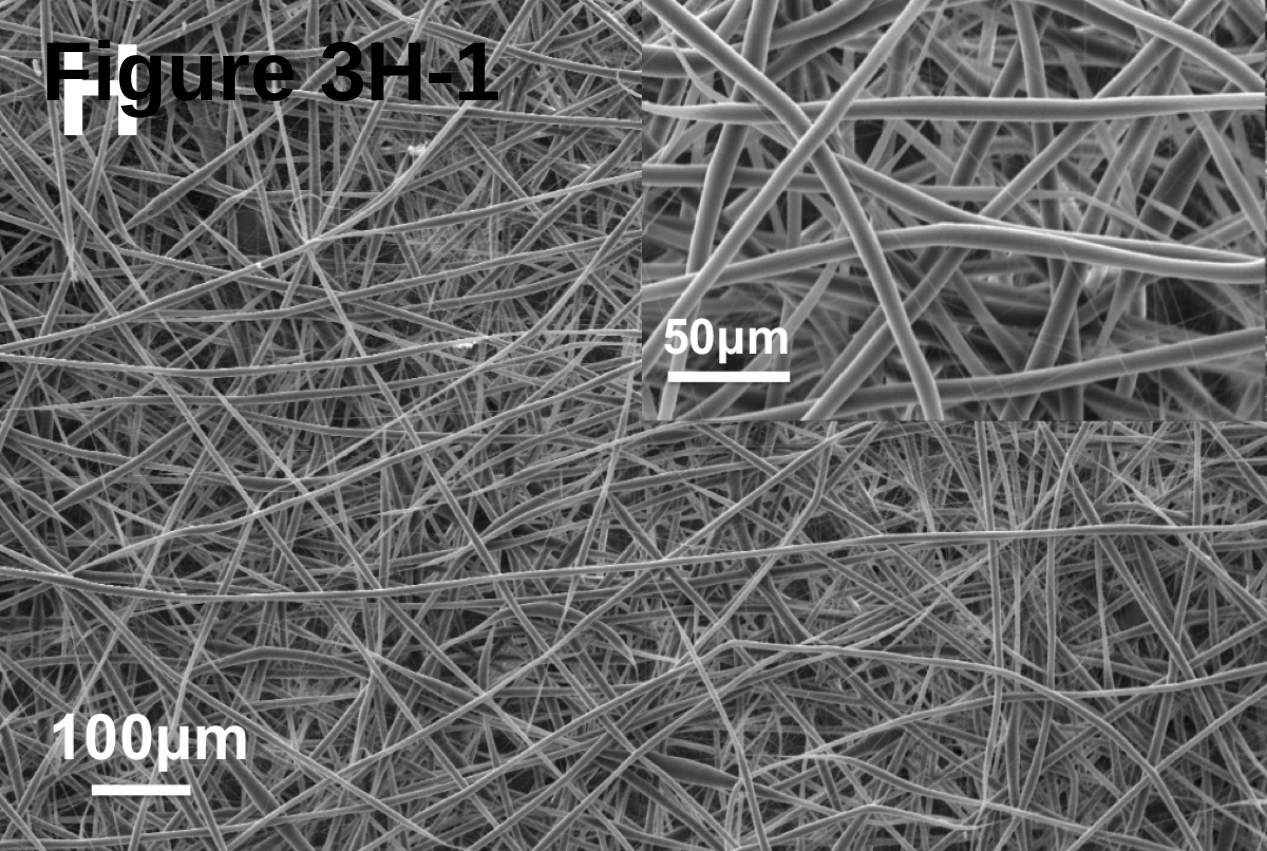
Figure 3H-1
50μm
100μm

Figure 3H-2

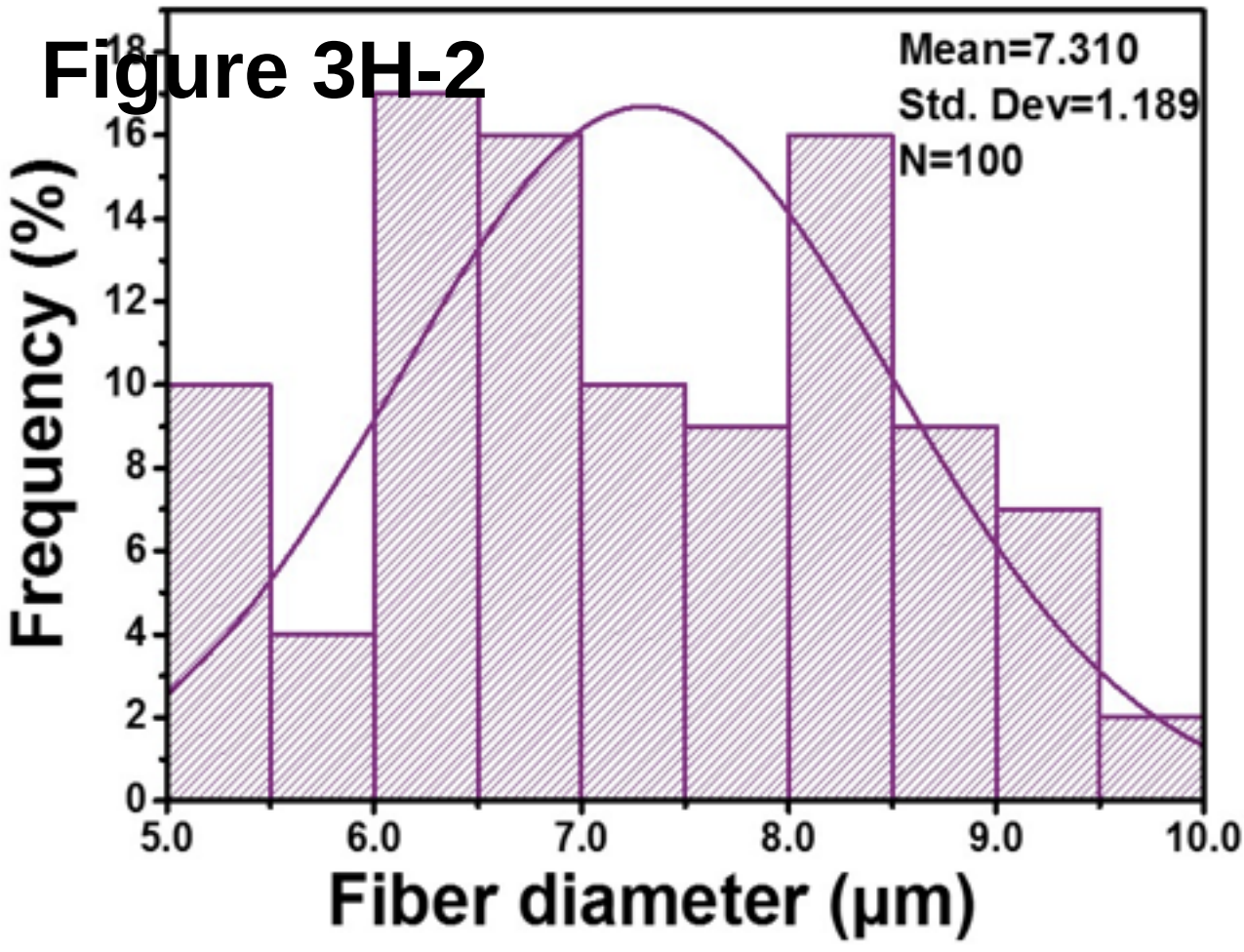
Mean=7.310
Std. Dev=1.189
N=100
Frequency (%)
0
2
4
6
8
10
12
14
16
18
5.0
6.0
7.0
8.0
9.0
10.0
Fiber diameter (μm)

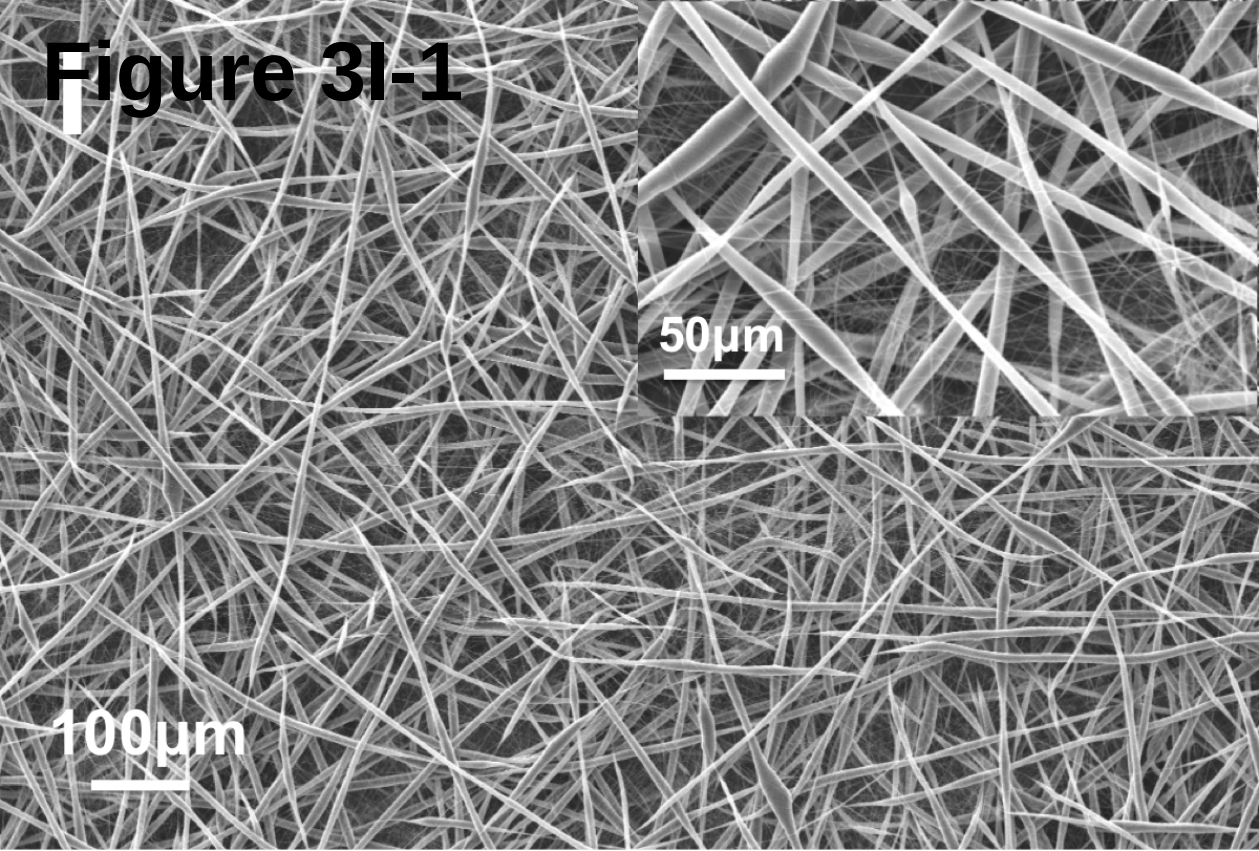
Figure 3I-1
50μm
100μm

Figure 3I-2

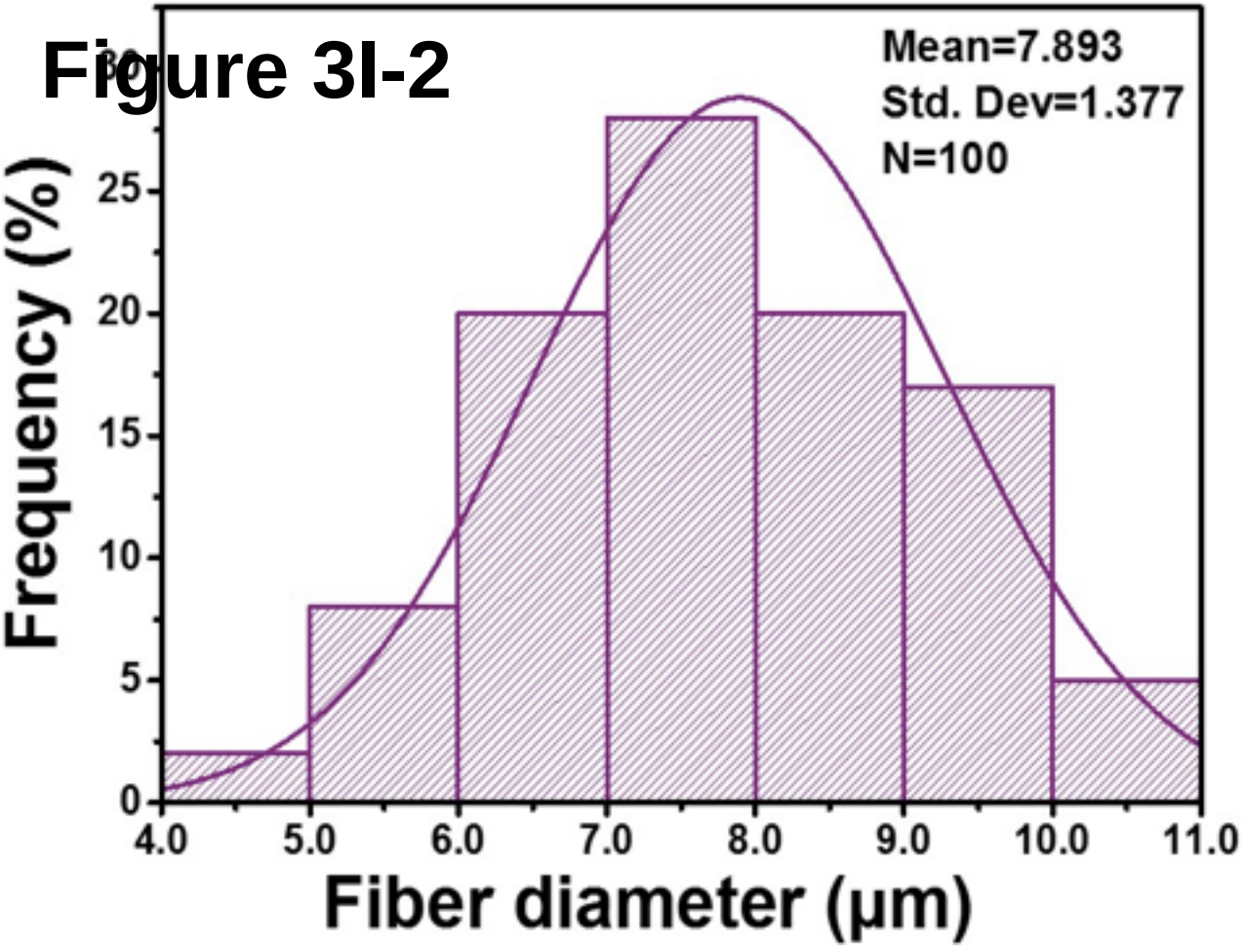
Mean=7.893
Std. Dev=1.377
N=100
Frequency (%)
0
5
10
15
20
25
4.0
5.0
6.0
7.0
8.0
9.0
10.0
11.0
Fiber diameter (μm)

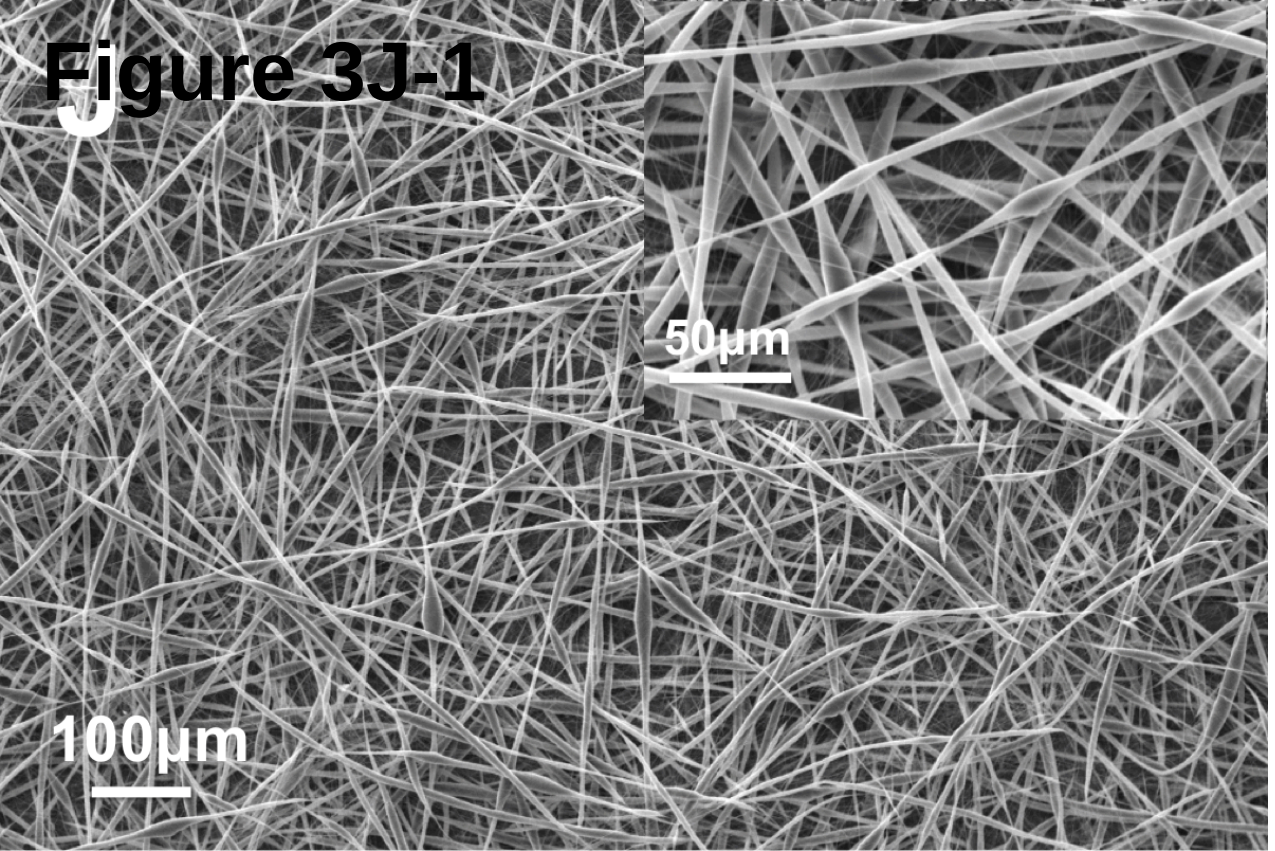
Figure 3J-1
50μm
100μm

Figure 3J-2

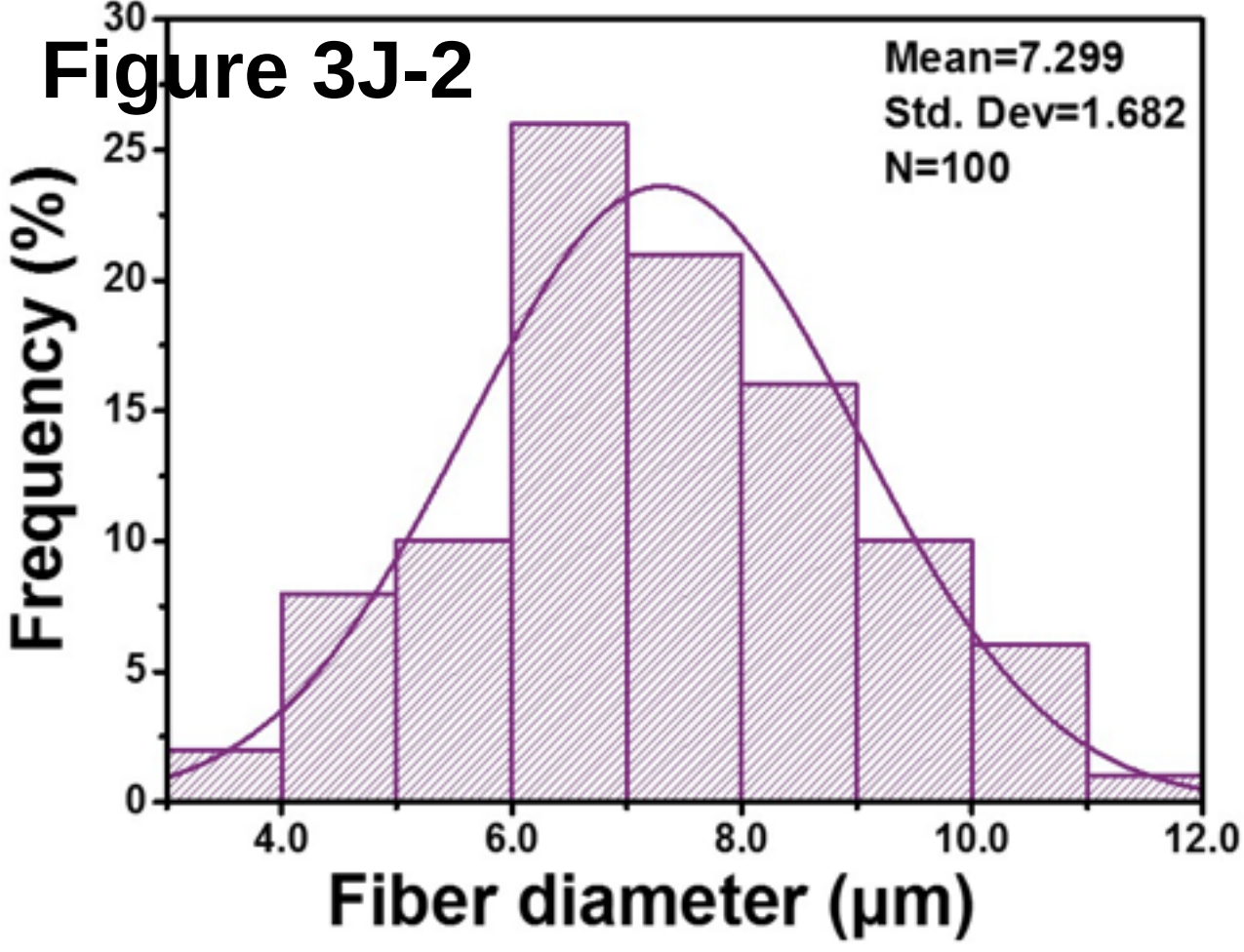
Mean=7.299
Std. Dev=1.682
N=100
Frequency (%)
0
5
10
15
20
25
30
4.0
6.0
8.0
10.0
12.0
Fiber diameter (μm)

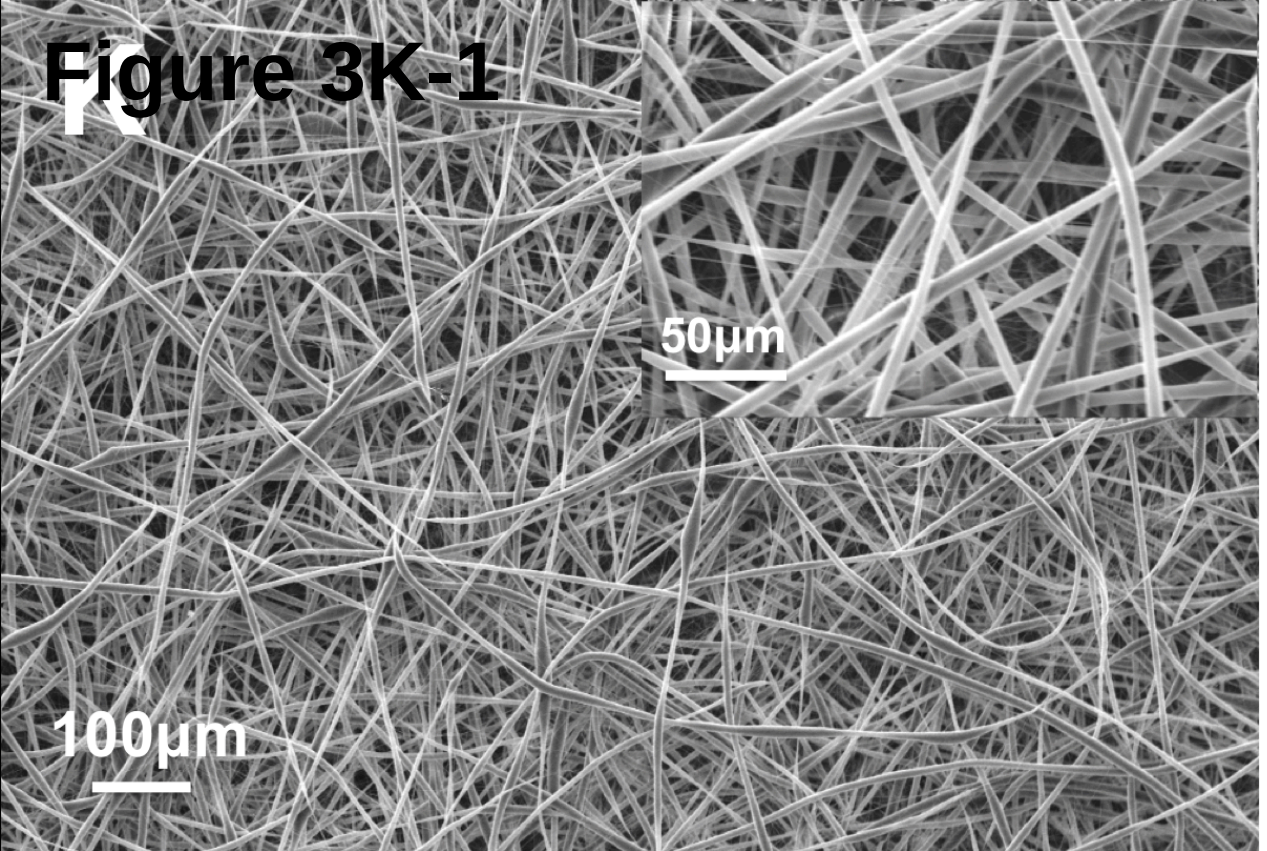
Figure 3K-1
50μm
100μm

Figure 3K-2

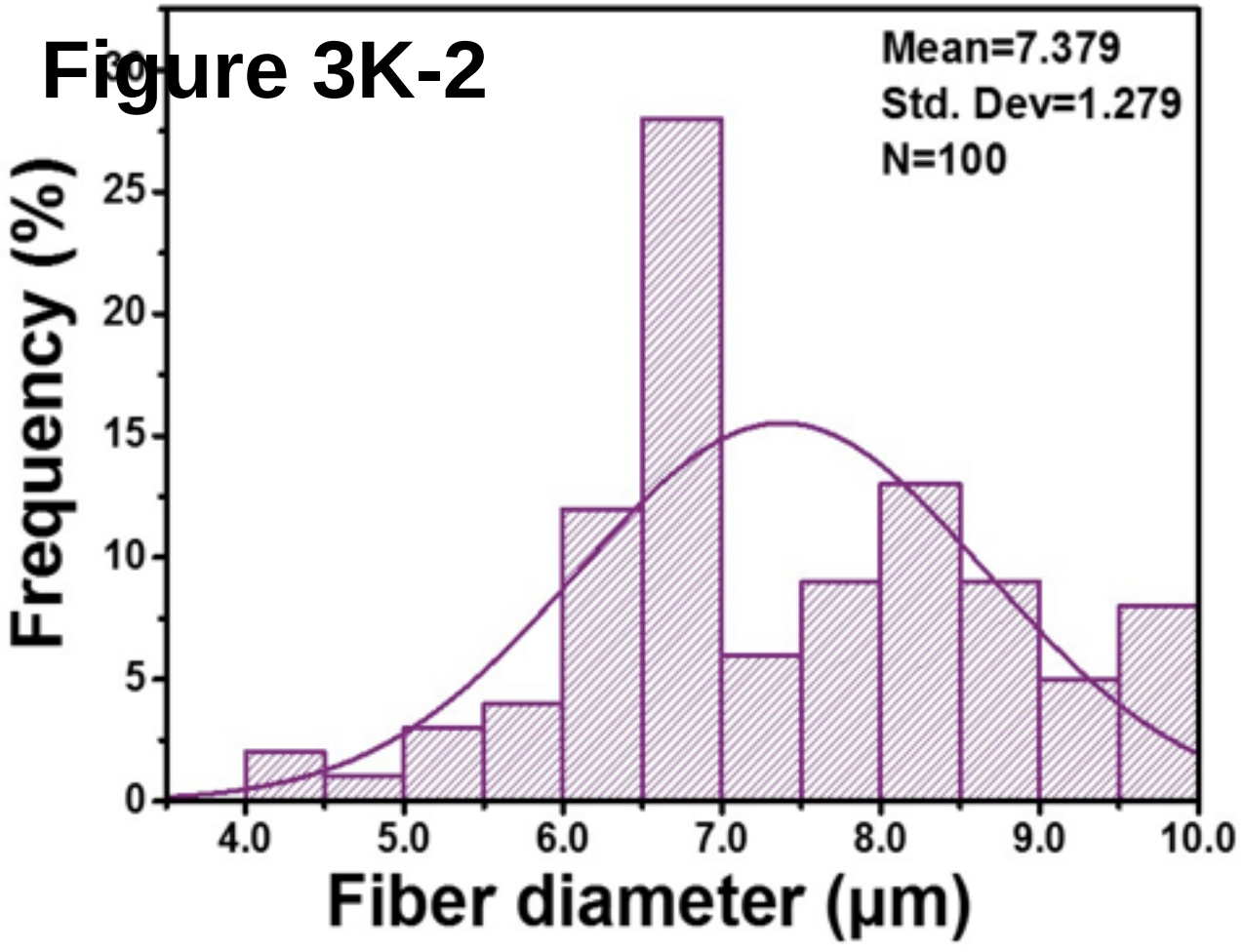
Mean=7.379
Std. Dev=1.279
N=100
Frequency (%)
0
5
10
15
20
25
30
4.0
5.0
6.0
7.0
8.0
9.0
10.0
Fiber diameter (μm)

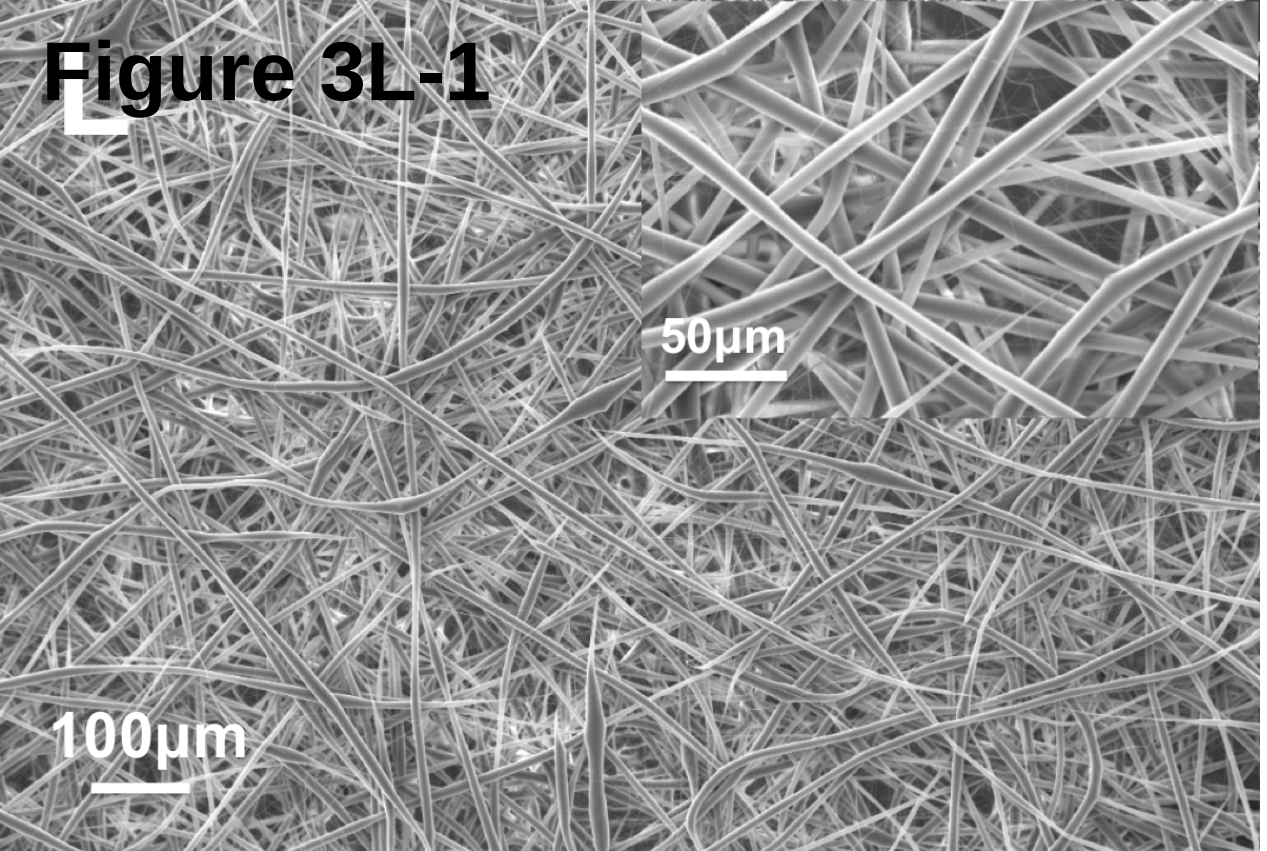
Figure 3L-1
50μm
100μm

Figure 3L-2

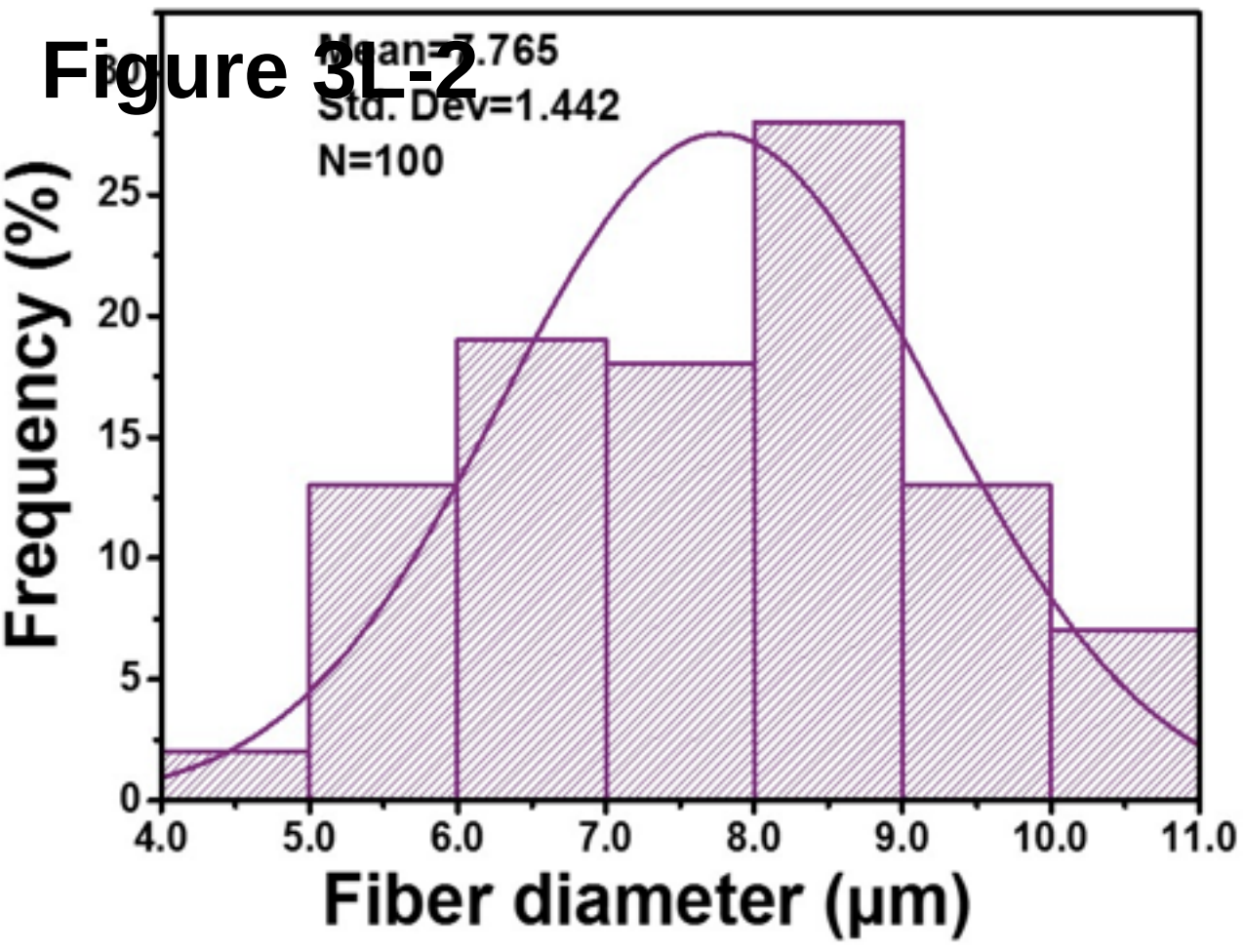
Mean=7.765
Std. Dev=1.442
N=100
Frequency (%)
0
5
10
15
20
25
4.0
5.0
6.0
7.0
8.0
9.0
10.0
11.0
Fiber diameter (μm)

Figure 4

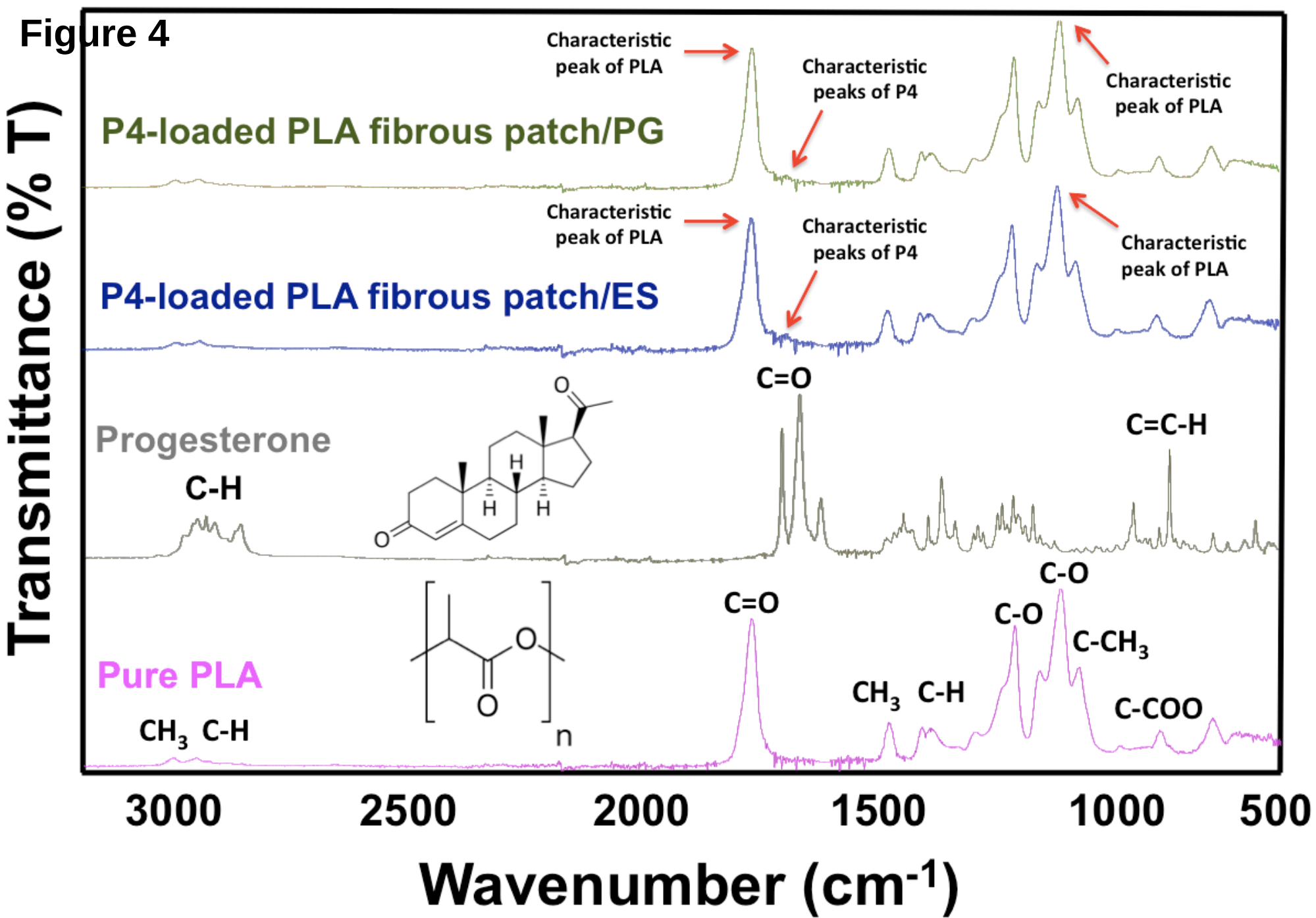
Characteristic peak of PLA
Characteristic peaks of P4
Characteristic peak of PLA
P4-loaded PLA fibrous patch/PG
Characteristic peak of PLA
Characteristic peaks of P4
Characteristic peak of PLA
P4-loaded PLA fibrous patch/ES
Progesterone
C-H
C=O
C=C-H
Pure PLA
CH3 C-H
C=O
C-O
C-O
C-CH3
CH3 C-H
C-COO
n
Transmittance (% T)
3000
2500
2000
1500
1000
500
Wavenumber (cm-1)

Figure 5

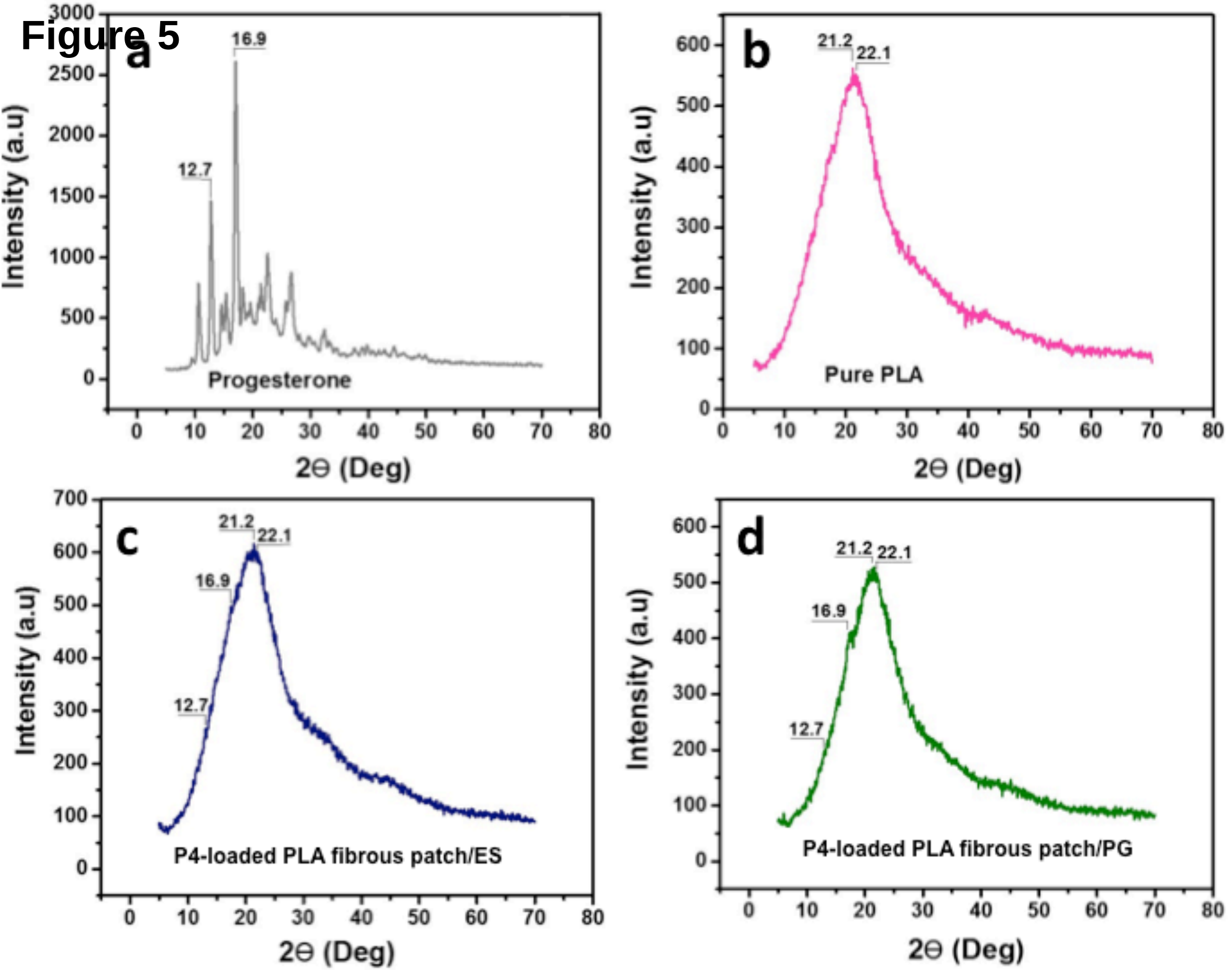
a
16.9
12.7
Progesterone
Intensity (a.u)
2Θ (Deg)
b
21.2
22.1
Pure PLA
Intensity (a.u)
2Θ (Deg)
c
21.2
22.1
16.9
12.7
P4-loaded PLA fibrous patch/ES
Intensity (a.u)
2Θ (Deg)
d
21.2
22.1
16.9
12.7
P4-loaded PLA fibrous patch/PG
Intensity (a.u)
2Θ (Deg)

Figure 6

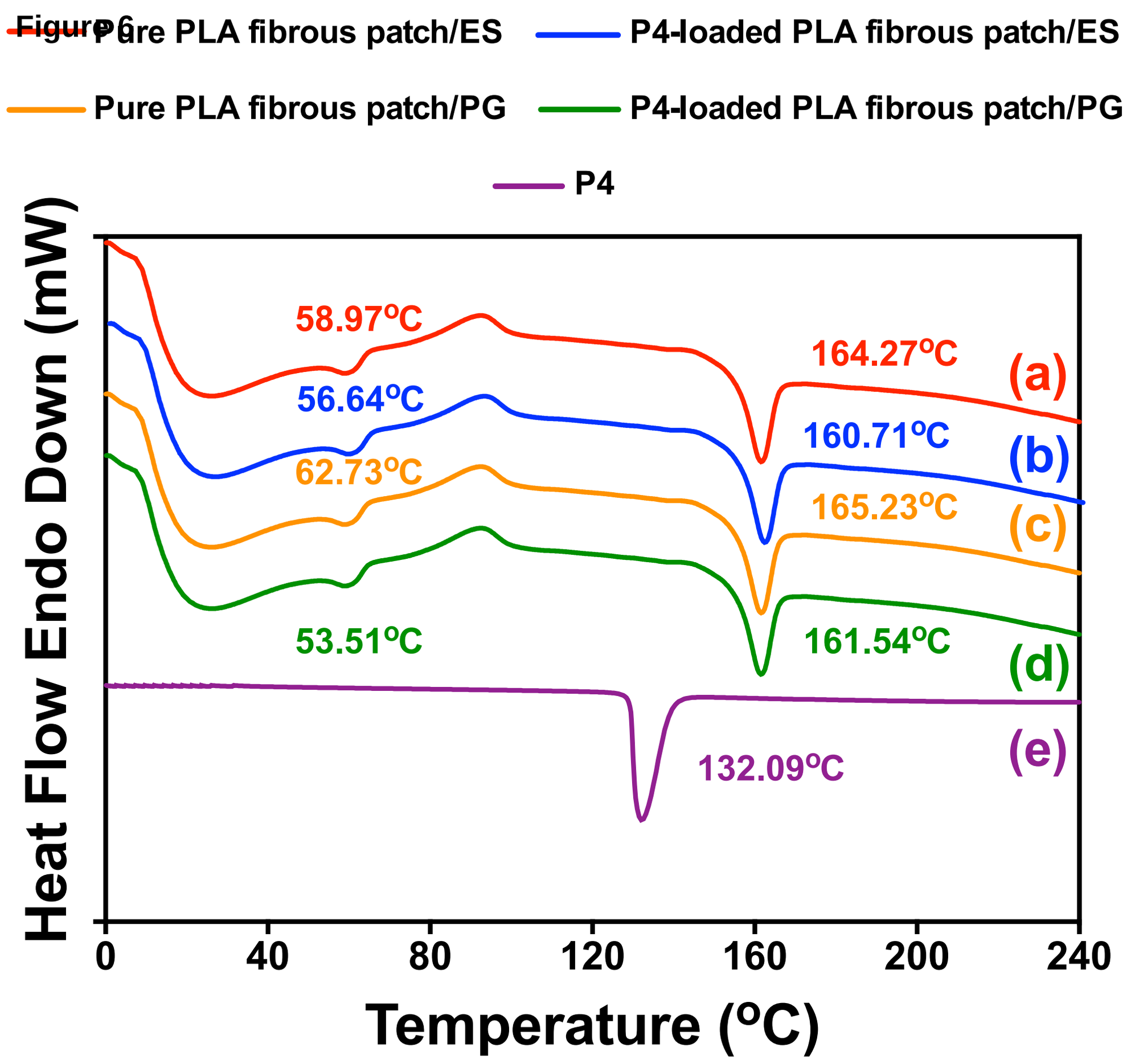
Pure PLA fibrous patch/ES
P4-loaded PLA fibrous patch/ES
Pure PLA fibrous patch/PG
P4-loaded PLA fibrous patch/PG
P4
Heat Flow Endo Down (mW)
58.97°C
164.27°C
(a)
56.64°C
160.71°C
(b)
62.73°C
165.23°C
(c)
53.51°C
161.54°C
(d)
132.09°C
(e)
0
40
80
120
160
200
240
Temperature (°C)

Figure 7A

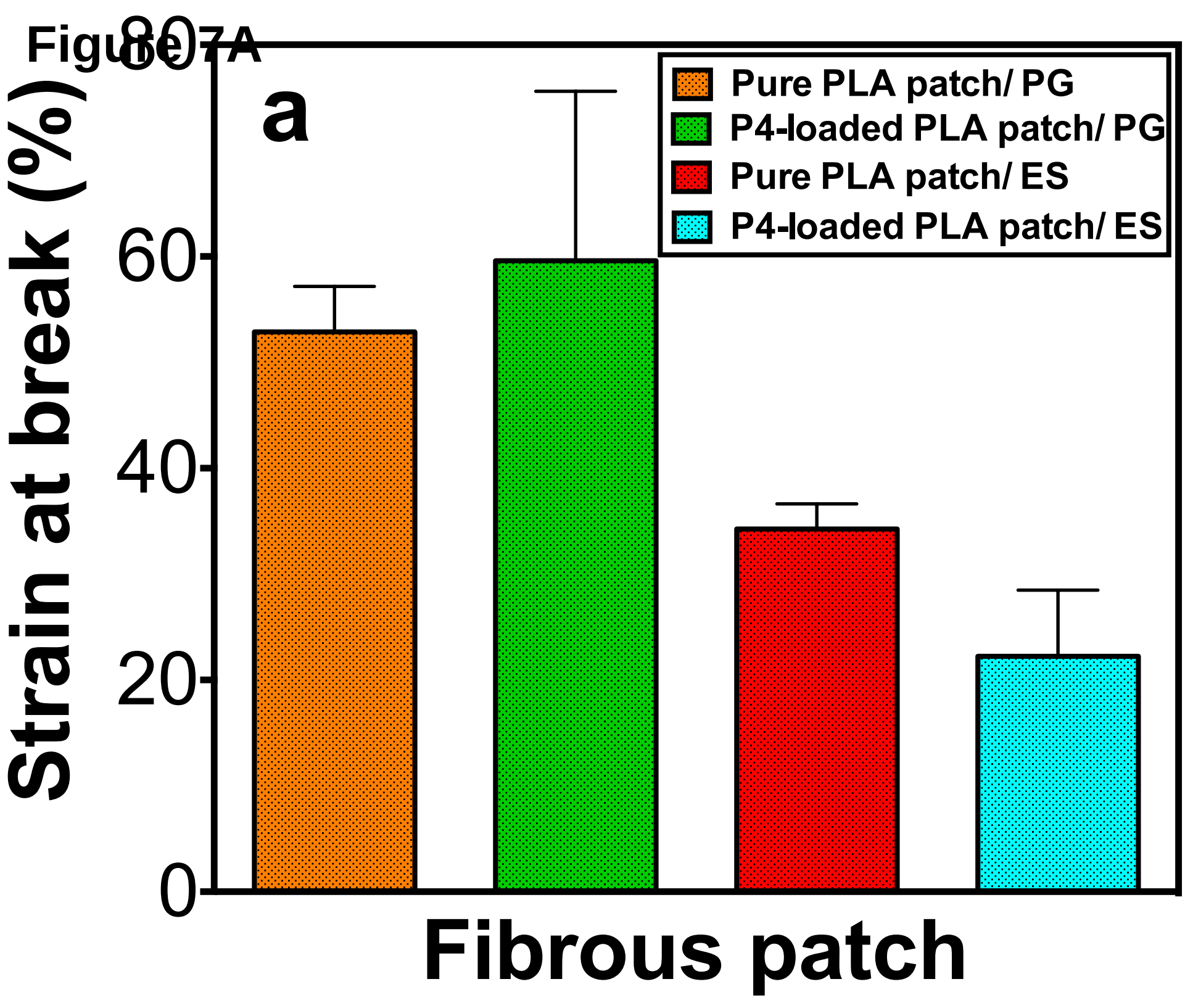
a
Pure PLA patch/ PG
P4-loaded PLA patch/ PG
Pure PLA patch/ ES
P4-loaded PLA patch/ ES
Strain at break (%)
80
60
40
20
0
Fibrous patch

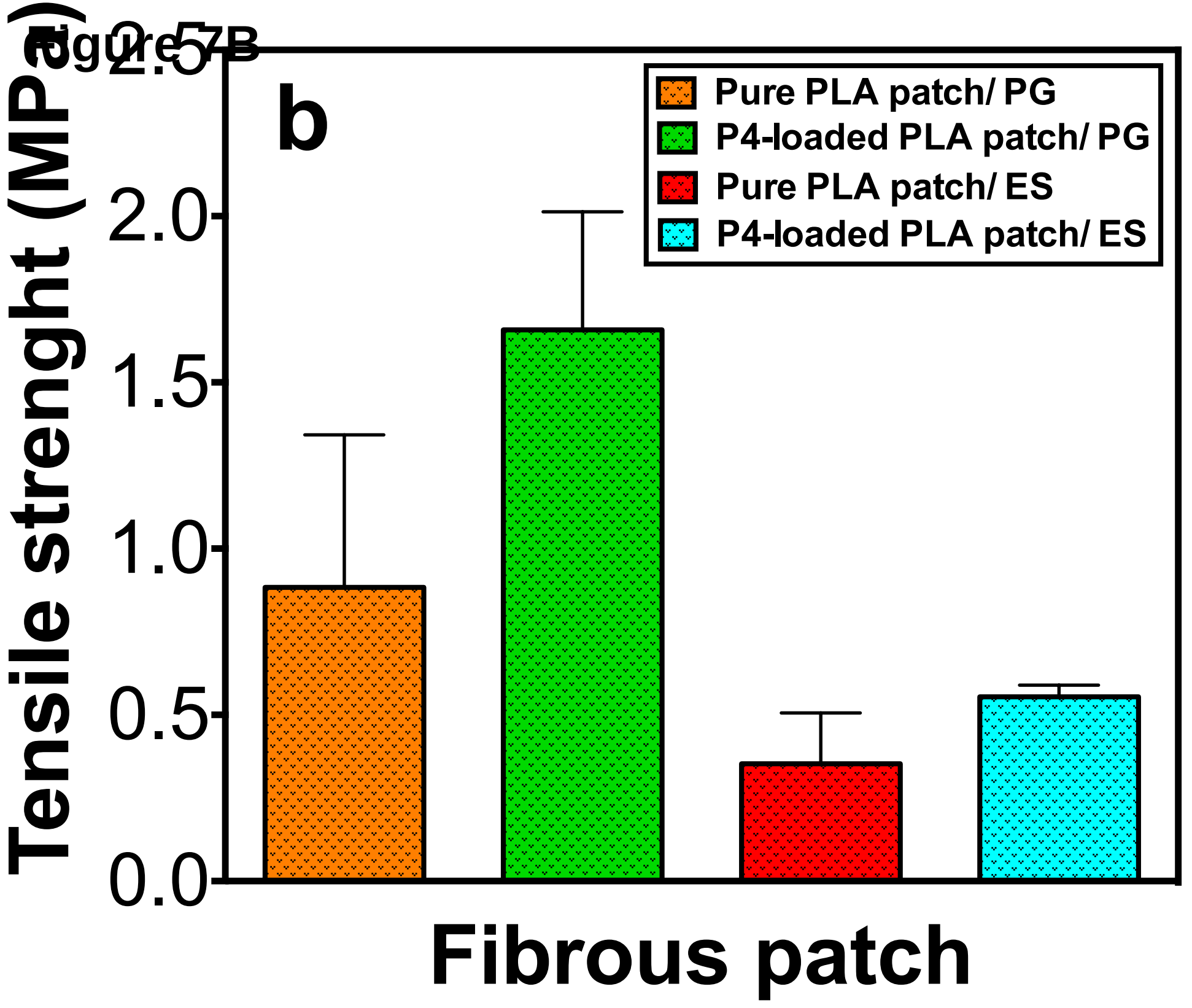
Figure 7B
b
Pure PLA patch/ PG
P4-loaded PLA patch/ PG
Pure PLA patch/ ES
P4-loaded PLA patch/ ES
Tensile strenght (MPa)
2.5
2.0
1.5
1.0
0.5
0.0
Fibrous patch

Figure 8

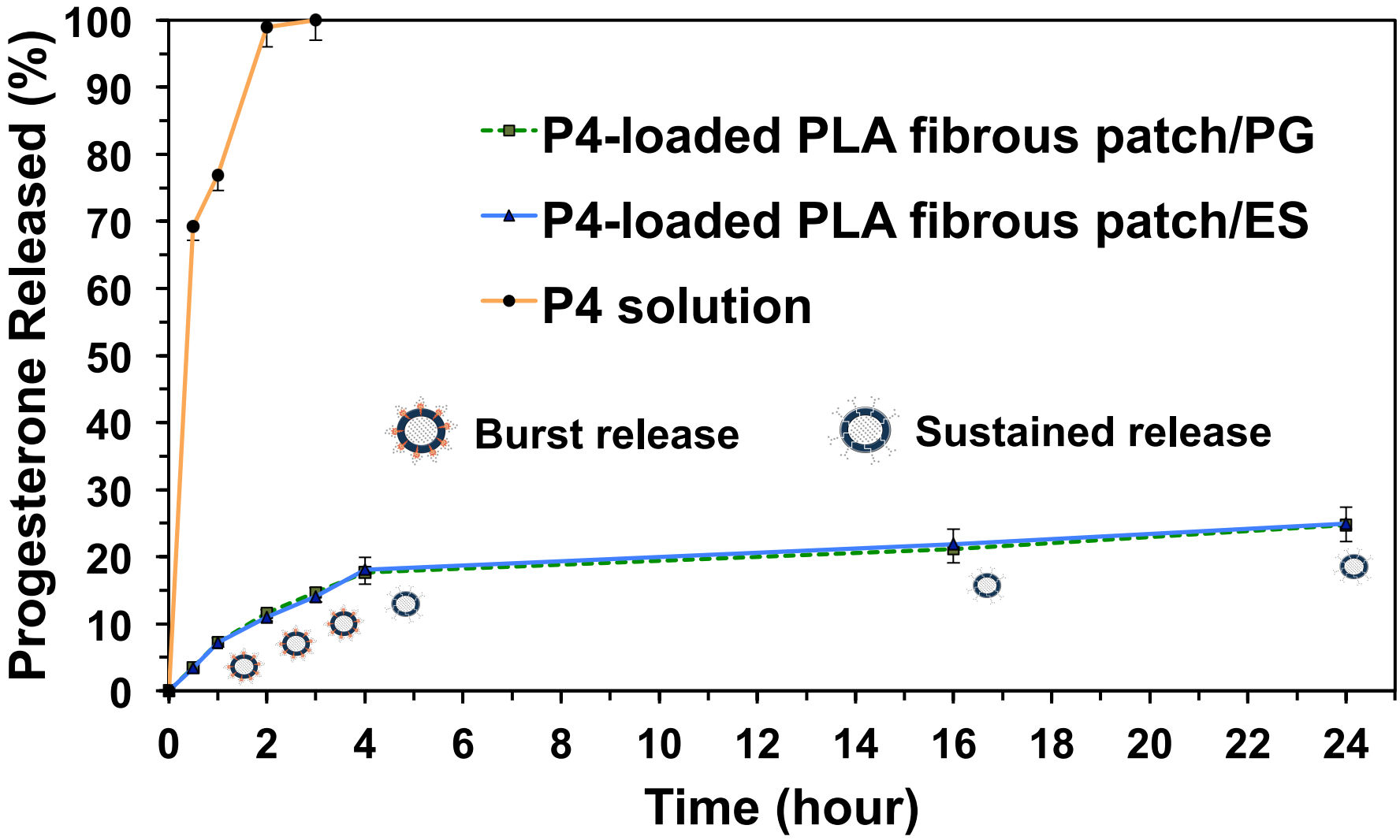
Progesterone Released (%)
100
90
80
70
60
50
40
30
20
10
0
0
2
4
6
8
10
12
14
16
18
20
22
24
Time (hour)
P4-loaded PLA fibrous patch/PG
P4-loaded PLA fibrous patch/ES
P4 solution
Burst release
Sustained release

Figure 9

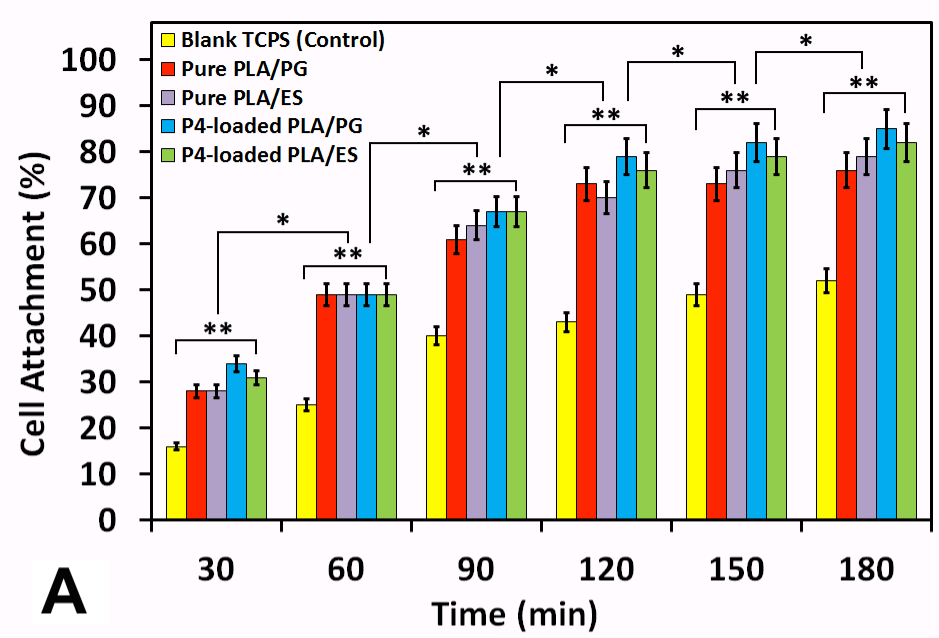
Blank TCPS (Control)
Pure PLA/PG
Pure PLA/ES
P4-loaded PLA/PG
P4-loaded PLA/ES
Cell Attachment (%)
Time (min)
30
60
90
120
150
180
A

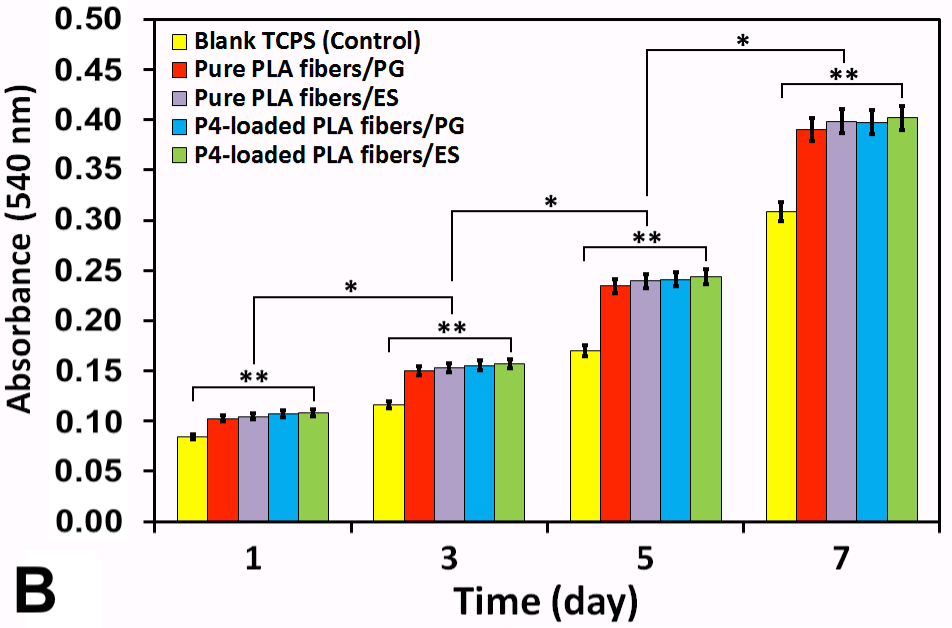
Blank TCPS (Control)
Pure PLA fibers/PG
Pure PLA fibers/ES
P4-loaded PLA fibers/PG
P4-loaded PLA fibers/ES
Absorbance (540 nm)
Time (day)
1
3
5
7
B

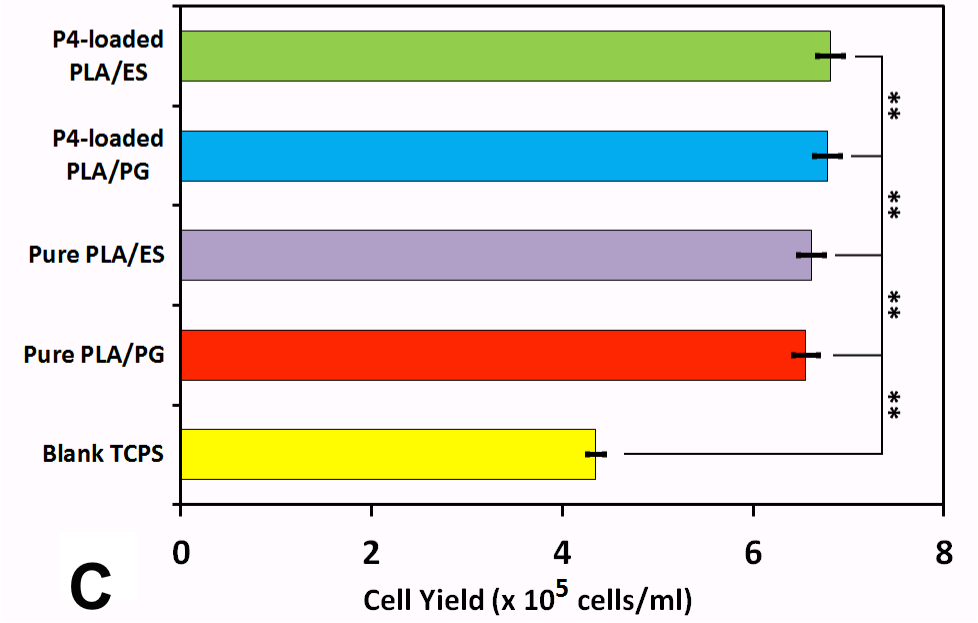
P4-loaded PLA/ES
P4-loaded PLA/PG
Pure PLA/ES
Pure PLA/PG
Blank TCPS
Cell Yield (x 10^5 cells/ml)
C

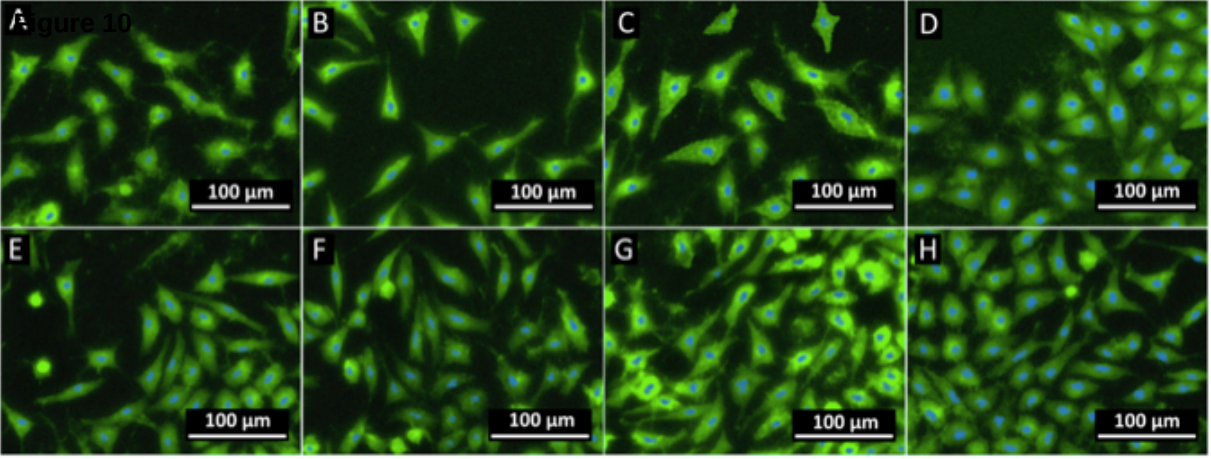
A
B
C
D
E
F
G
H
100 µm

Figure 14A

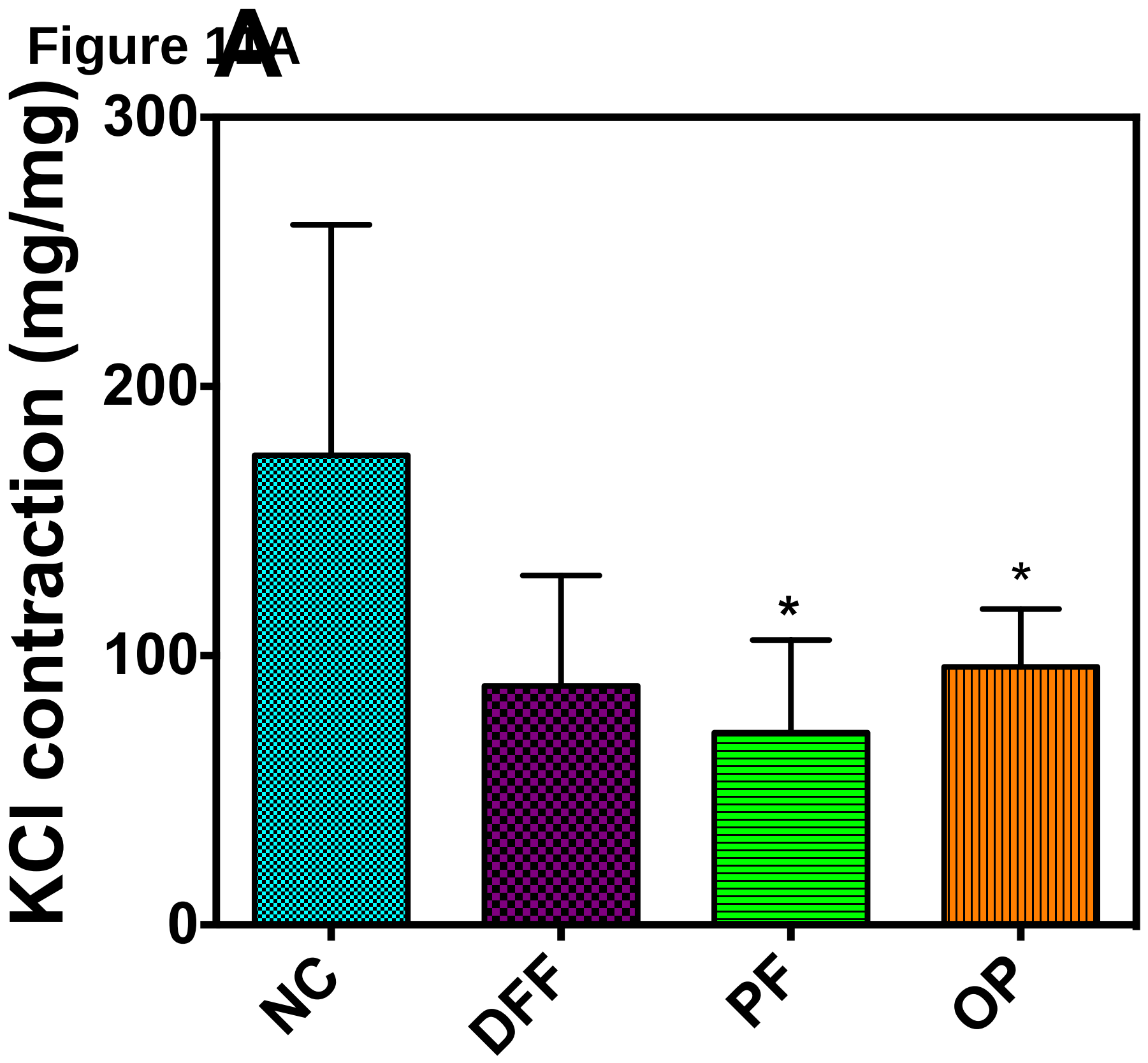

Figure 1B

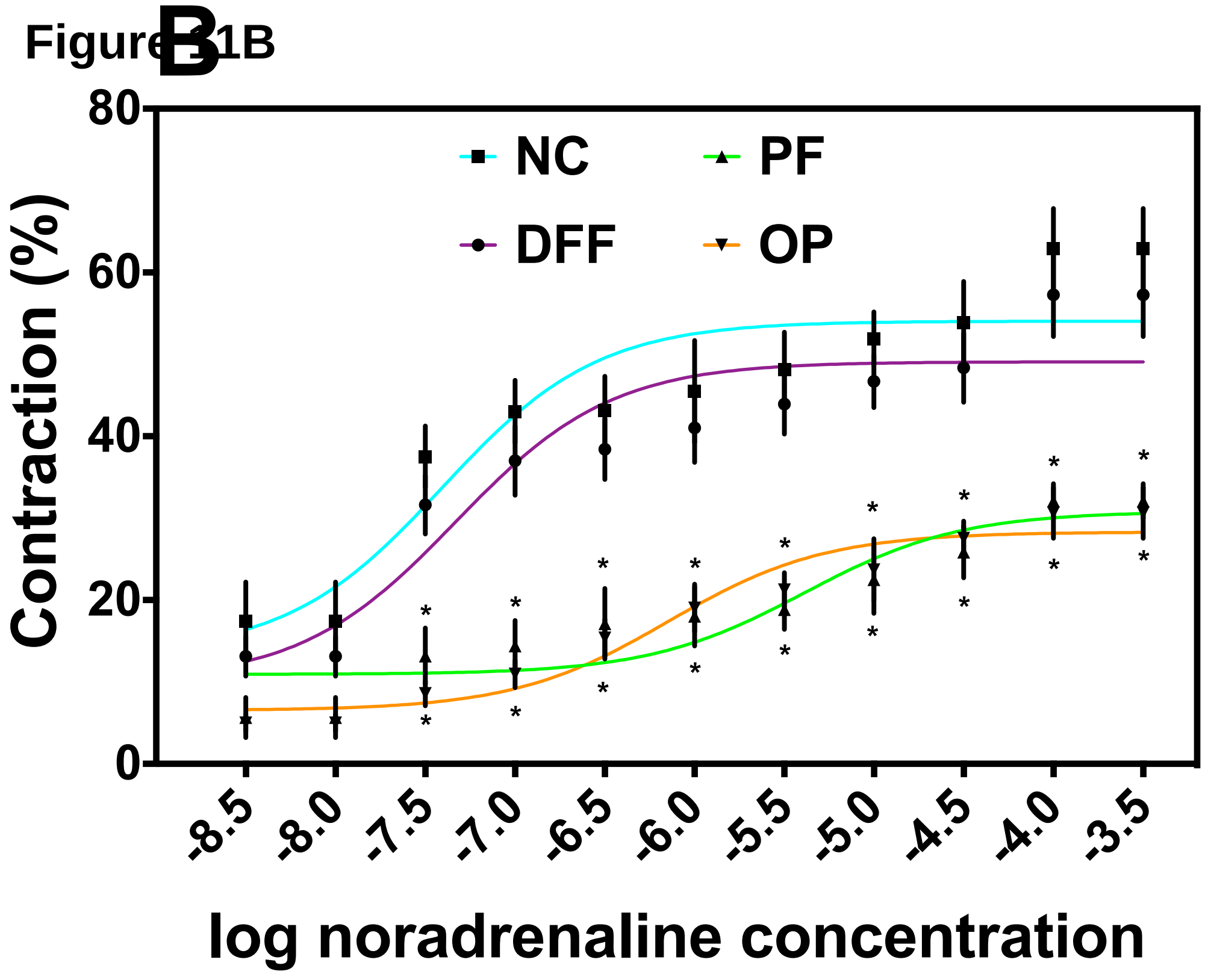
B
80
60
40
20
0
Contraction (%)
NC
PF
DFF
OP
-8.5
-8.0
-7.5
-7.0
-6.5
-6.0
-5.5
-5.0
-4.5
-4.0
-3.5
log noradrenaline concentration

Figure 11C

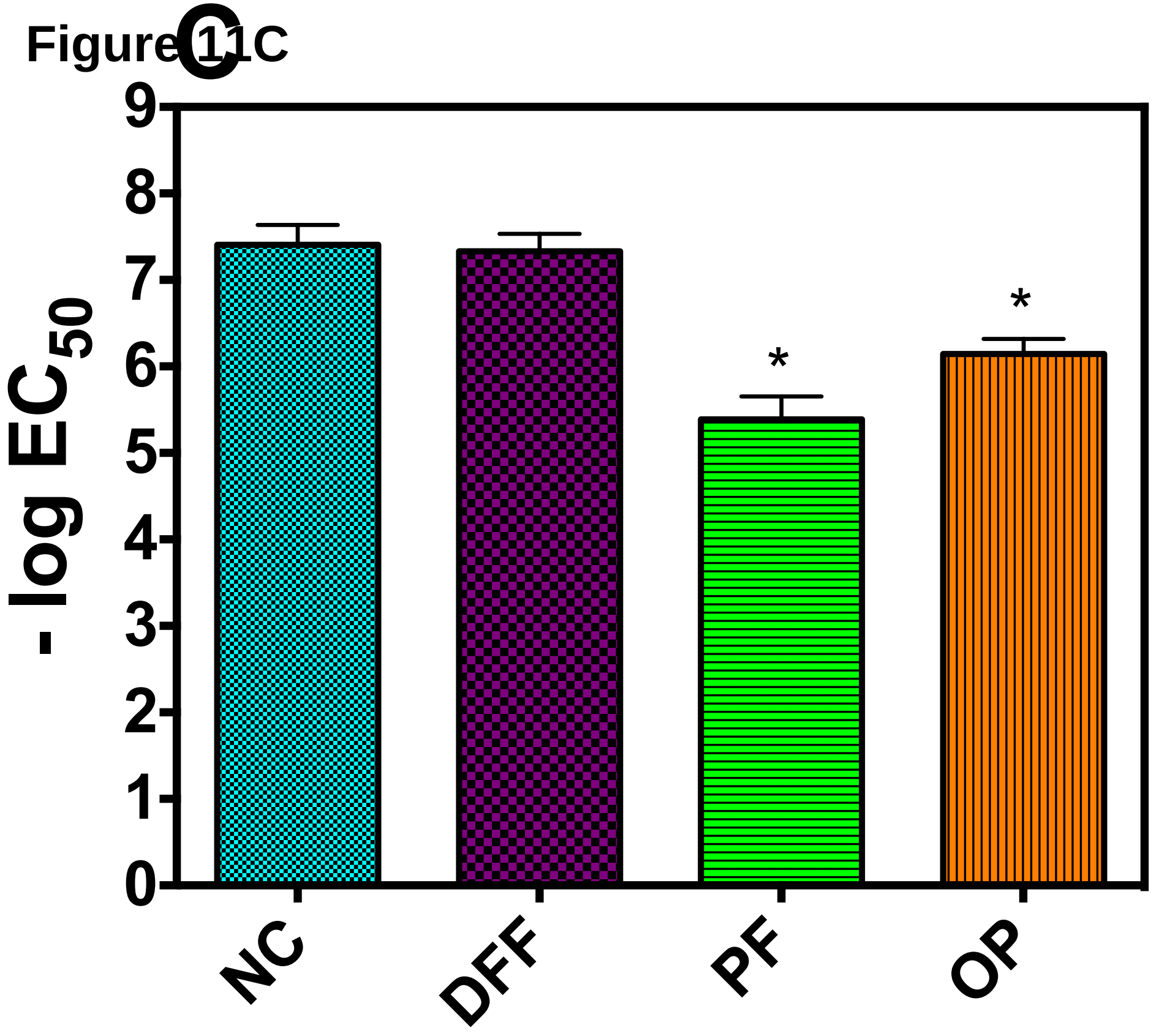

Figure 11D